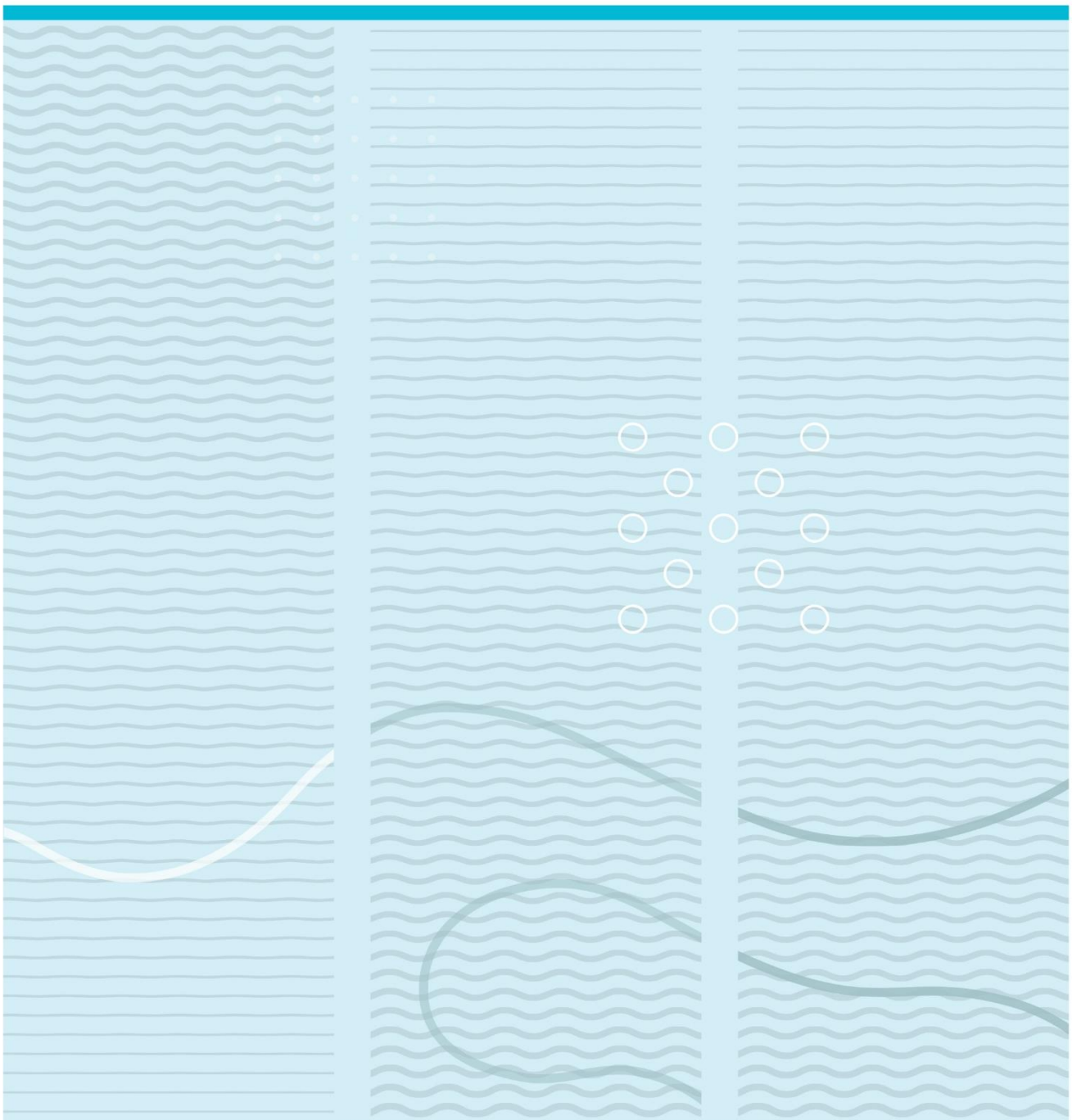


Luis Baldeon Franco

Geo-spatial analysis of stormwater runoffs from a highway in the catchment of the lake Brusdalsvatnet in Ålesund



Luis Baldeon Franco

**Geo-spatial analysis of stormwater runoffs from a highway
in the catchment of the lake Brusdalsvatnet in Ålesund**

University of South-Eastern Norway
Faculty of Technology, Natural Sciences and Maritime Sciences
Department of Natural Sciences and Environmental Health
PO Box 235
NO-3603 Kongsberg, Norway

<http://www.usn.no>

© 2023 Luis Baldeon Franco

This thesis is worth 60 study points

Acknowledgments

This thesis concludes my master's degree studies in Ecology and Environmental Management at the University of South-Eastern Norway (USN).

At the very first, I would like to express my sincere thanks to my supervisors Prof. Dieu Tien and Prof. Razak Seidu, for giving me the opportunity to work with Geospatial information system (GIS), a field that interests me and for helping me to reach my goal throughout the guidance, support, and valuable discussions.

I would like to extend my gratitude to MSc. Lam Van Nguyen a PhD student at the Norwegian University of Science and Technology (NTNU), for his close guidance throughout the technical part of this thesis.

I would also like to acknowledge my sincere gratitude to Prof. Mona Sæbø, Master Coordinator at USN, for her support and interest during the process of my thesis.

Further, I'm very grateful to NTNU and Ålesund Municipality for giving me the opportunity to be part of the project Smart Water Management which allowed me to acquire more experience and knowledge related to (GIS).

Lastly, I want to express my deepest thanks to my family for their support, especially to my mother, Ms. Isabel Franco Pacheco, for her support during these five years of hard work.

Abstract

Climate change is leading to rising temperatures as well as increasing the number of extreme rainfall events. This is a matter of concern in Norway, given that it increases the runoff volume from impervious surfaces and can potentially lead to pollutant load increment. Pollutants such as heavy metals (HMs) are commonly found in areas traversed by high-trafficked roads. Heavy metals can be transported through runoff to drinking water sources, causing adverse effects on the environment and human health. Likewise, these pollutants have been associated with cancer.

This thesis aims to model runoff from Highway E-39, located in the catchment of Brusdalsvatnet in Ålesund, accounting for present and future rainfall regimes. To achieve the aim of the thesis, three objectives were identified and pursued i) Develop an interactive geospatial map of the runoff flow paths within the catchment of Brusdalsvatnet. ii) Quantify the volume of runoff that flows from the catchment, crossing Highway E-39 and reaching Brusdalsvatnet, accounting for present and future rainfall scenarios. iii) Quantify Heavy Metals load associated with runoffs, accounting for present and future rainfall scenarios. This thesis was undertaken using a quantitative approach, considering Geo-referenced data such as terrain data (DTM), road network, hydrological network, rainfall data, and the RCP8.5 projection emission scenario.

The thesis includes three emission scenarios. The model Gage 1 considers current emissions while Gage 2 and Gage 3 account for future emission scenarios. The delineation of runoff pathways was engineered using ArcGIS Pro, whereas the computation of runoff volume and pollutants load was carried out using SWMM (Storm Water Management Model) and SWAT (Soil and Water Assessment Tool).

The results show that there is a close relationship between rainfall intensity and runoff volume, being the main driven factors Impervious surface, low infiltration capacity, and to a lesser extent, steep gradient. Moreover, a close interaction was observed between runoff volume and pollutant washoff loading. The amount of pollutant loading increases significantly in the subcatchments that are close to developed areas. Furthermore, it is projected that a noticeable runoff volume will increase; thus, pollutant loading will increase in future rainfall regimes. These findings indicate that climate change negatively affects factors such as rainfall, runoff, and pollutant loading, increasing runoff volume and, subsequently, pollutant loading.

At last, according to the projections presented in this study, the Zinc loading will increase up to 45% for the period from 2060 to 2100. It represents a threat to drinking water sources, hence to human health. The results of this study confirm that it is necessary to take mitigating and preventive measures to reduce the effects of climate change on natural patterns and protect the environment and human health. However, it should be noted that the dataset used in this study has certain limitations. For example, it doesn't consider important variables such as soil type, temperature, evaporation rates, sewer network, and wind speed. To enhance the accuracy of the model, future studies should consider incorporating some of these variables.

Sammendrag

Vi ser at klimaendringene fører til både stigende temperaturer samt tiltakende ekstrem nedbørshendelser. Dette gir grunn til bekymring i Norge, siden det øker avrenningsvolumet som ikke naturlig absorberes grunnet ugjennomtrengelig overflater, og til slutt medfører til en økt forurensningsbelastning.

Forurensende stoffer som tungmetaller finnes ofte i områder som krysses av sterkt trafikkerte veier. Tungmetaller kan transporteres gjennom avrenning til drikkevannskilder og forårsake negative virkninger på miljøet og menneskers helse. Disse miljøgiftene har senere blitt satt i forbindelse med kreft forekomster.

Denne avhandlingen tar sikte på å modellere avrenning fra riksvei E-39 i nedslagsfeltet til Brusdalsvatnet i Ålesund ved å ta hensyn til nåværende og fremtidige nedbørsscenarier. Målet med oppgaven ble videre delt inn i tre delmål

- i) Utvikle et interaktivt geospasialt kart over avrenningsstrømmene i nedbørsfeltet til Brusdalsvatnet.
- ii) Kvantifisere volumet av avrenning som strømmer fra nedbørsfeltet, krysser E-39 og når Brusdalsvatnet, med hensyn til nåværende og fremtidige nedbørsscenarier.
- iii) Kvantifisere tungmetallbelastningen forbundet med avrenning, med hensyn til nåværende og fremtidige nedbørsscenarier. Denne oppgaven ble utført ved hjelp av en kvantitativ tilnærming, med tanke på georefererte data som høydedata (DTM), veinettverk, hydrologisk nettverk, nedbørsdata og utslippsscenarioet RCP8.5.

Avhandlingen omfatter tre utslippsscenarioer, der modellen Gage 1 tar hensyn til dagens utslipp, mens Gage 2 og Gage 3 tar hensyn til fremtidige utslippsscenarioer. Avgrensningen av avrenningsveier ble konstruert ved hjelp av ArcGIS Pro, mens beregningen av avrenningsvolum og forurensningsbelastning ble utført ved hjelp av SWMM og SWAT.

Resultatene viser at det er en nær sammenheng mellom nedbørsintensitet og avrenningsvolum, og at de viktigste faktorene er ugjennomtrengelig overflate, lav infiltrasjonskapasitet og, i noe mindre grad, bratt gradient.

Videre ble det observert et nært samspill mellom avrenningsvolum og forurensningsbelastning. Mengden forurensende stoffer øker betydelig i delnedbørfelt som ligger nær bebygde områder.

Det forventes en merkbar økning i avrenningsvolumet og dermed i forurensningsbelastningen i fremtidige nedbørsscenarier. Disse funnene indikerer at klimaendringene påvirker faktorer som nedbør, avrenning og forurensningsbelastning negativt, noe som øker avrenningsvolumet og dermed forurensningsbelastningen. I tillegg vil sinkbelastningen øke med opptil 45 % i perioden fra 2060 til 2100, ifølge prognosene som presenteres i denne studien. Dette utgjør en trussel mot drikkevannskildene og dermed mot menneskers helse.

Resultatene av denne studien bekrefter at det er nødvendig å iverksette avbøtende og forebyggende tiltak for å redusere virkningene av klimaendringer på naturlige mønstre, samt for å beskytte miljøet og menneskers helse. På den annen side har datasettet som er brukt i denne studien sine begrensninger, ettersom det ikke tar hensyn til relevante data som jordsmonn, temperatur, fordampning, kloaknett og vindhastighet. For å styrke modellen i fremtiden, bør noen av dataene nevnt ovenfor vurderes, til tross for begrensningene.

Table of Contents

| | |
|--|------------|
| Acknowledgments | i |
| Abstract | ii |
| Sammendrag | iv |
| List of Figures | ix |
| List of Tables | xi |
| Abbreviations | xii |
| 1 Introduction | 1 |
| 1.1 Background..... | 1 |
| 1.2 Research questions and objectives | 3 |
| 1.2.1 To assess it, the following specific objectives must be addressed: | 3 |
| 1.2.2 Expected answers and outcomes:..... | 4 |
| 1.3 Significance and contributions of the study | 4 |
| 1.4 Thesis Structure | 4 |
| 2. Literature review | 6 |
| 2.1 Main factors affected due to climate change..... | 6 |
| 2.1.1 Temperature | 6 |
| 2.1.2 Precipitation | 6 |
| 2.1.3 Evaporation and evapotranspiration..... | 7 |
| 2.1.4 Runoffs from impervious surfaces | 7 |
| 2.2 Pollutants' sources, behavior, and convey..... | 9 |
| 2.3 Heavy metals..... | 10 |
| 2.4 Previous research on stormwater runoff from highways and catchments..... | 11 |
| 2.5 Geospatial Analysis (ArcGIS Pro)..... | 13 |
| 2.6 Soil and Water Assessment Tool (SWAT) | 13 |
| 2.7 Storm Water Management Model (SWMM) | 14 |

| | |
|---|-----------|
| 2.8 Future rainfall scenarios..... | 14 |
| 3 Study area and data | 16 |
| 3.1 Description of the study area | 16 |
| 3.2 Data | 18 |
| 3.2.1 Data Collection | 18 |
| 3.2.2 Notation of data..... | 18 |
| 3.2.3 Data processing..... | 20 |
| 4. Methodology | 23 |
| 4.1 Objective 1: Geospatial interactive map on the runoff flow pathways within the catchment of Brusdalsvatnet..... | 23 |
| 4.1.1 Computing runoff pathways..... | 23 |
| 4.1.2 Building the Geospatial interactive map..... | 25 |
| 4.2 Objective 2: Quantify the volume of runoff to Brusdalsvatnet from Highway E-39, accounting for present and future rainfall scenarios | 28 |
| 4.2.1 Computing the Basin, watershed, and subcatchments of the study area..... | 28 |
| 4.2.2 Watershed delineation and projection of future rainfall scenarios..... | 28 |
| 4.2.3 Water runoff modelling..... | 33 |
| 4.2.4 Emissions scenarios justification | 34 |
| 4.3 Objective 3: Quantify Heavy Metals load associated with runoffs, accounting for present and future rainfall scenarios | 35 |
| 4.3.1 Heavy Metals samples | 35 |
| 4.3.2 Water Quality Analysis..... | 36 |
| 4.3.3 Water quality modelling..... | 37 |
| 5. Results and Analysis | 37 |
| 5.1 Geospatial map..... | 40 |
| 5.2 Geospatial Tool for Calculating Runoff Flow | 40 |
| 5.3 SWMM model's simulation reliability | 41 |

| | |
|---|-----------|
| 5.4 Stormwater runoff entering Brisdalsvatnet from Highway E-39 | 41 |
| 5.5 Heavy Metals load associated with runoffs | 50 |
| 5.5.1 Relationships and trends | 59 |
| 6. Discussion..... | 61 |
| 6.1 Geo-spatial map at Brisdalsvatnet..... | 61 |
| 6.2 Runoff Flow Calculator Geo-spatial tool..... | 62 |
| 6.3 Precipitation-Runoff relationship..... | 62 |
| 6.4 Runoff-Washoff relationship | 66 |
| 7. Conclusion and further work..... | 68 |
| 7.1 Conclusion | 68 |
| 7.2 Further work..... | 70 |
| References..... | 71 |
| Appendix A | 75 |
| Appendix B | 76 |
| Appendix C: Subcatchment Runoff Summary Gage 1..... | 77 |
| Appendix D: Subcatchment Runoff Summary Gage 2..... | 78 |
| Appendix E: Subcatchment Runoff Summary Gage 3..... | 79 |

List of Figures

| | |
|--|----|
| Figure 1: Study area at Brusdalsvatnet in Ålesund municipality. ArcGIS Pro. | 17 |
| Figure 2: Extracting the DTM to the study area extent. ModelBuilder workflow. | 20 |
| Figure 3: Clipping the Building footprint data to the study area extent. ModelBuilder workflow. | 21 |
| Figure 4: Applying symbology to AR50 Landuse. ModelBuilder workflow. | 21 |
| Figure 5: Hydrograph of Ålesund Municipality for the year 2021. HEC-HMS. | 22 |
| Figure 6: Flow paths Feature Class symbology. ArcGIS Pro. | 25 |
| Figure 7: Runoff Flow Calculator Geo-spatial tool. ArcGIS Pro. | 26 |
| Figure 8: Geoprocessing tool showing ModelBuilder's workflow. ArcGIS Pro. | 27 |
| Figure 9: Subcatchments, Outfalls and Gages overview at Brusdalsvatnet lake. SWMM. | 29 |
| Figure 10: Slope and Area computing process. ModelBuilder workflow. ArcGIS Pro. | 30 |
| Figure 11: Setting up suitable interval values to Slope. ArcGIS Pro. | 31 |
| Figure 12: Landuse areal computation. ModelBuilder workflow. ArcGIS Pro. | 32 |
| Figure 13: Subcatchments parameters window. SWMM. | 33 |
| Figure 14: Precipitation intensity related to the frequency of the events. Gage 1. SWMM. | 38 |
| Figure 15: Runoff volume related to the frequency of the events. Gage 1. SWMM. | 39 |
| Figure 16: Runoff flow at Brusdalsvatnet, Ålesund municipality. | 40 |
| Figure 17: Close Rainfall- Runoff relationship. Ålesund 2021. Gage 1. SWMM. | 42 |
| Figure 18: Runoff Coefficient (C) at Brusdalsvatnet, Ålesund. SWMM. | 44 |
| Figure 19: Percentage Imperviousness at Brusdalsvatnet, Ålesund. SWMM. | 45 |
| Figure 20: Subcatchments Slope at Brusdalsvatnet, Ålesund. SWMM. | 46 |
| Figure 21: Subcatchments Total Runoff volume at Brusdalsvatnet, Ålesund. SWMM. | 47 |
| Figure 22: Relationship between Total Runoff and Impervious surface. Gage1. | 48 |
| Figure 23: Subcatchments impervious surface impact in pollutants load. Gage 1. | 50 |
| Figure 24: Subcatchments Total runoff- Pollutants washoff interaction. Gage 1. | 51 |

| | |
|---|----|
| Figure 25: Heavy Metals load at Brusdalsvatnet. Gage 1..... | 52 |
| Figure 26: Heavy Metals load at Brusdalsvatnet. Gage 2..... | 53 |
| Figure 27: Heavy Metals load at Brusdalsvatnet. Gage 3..... | 53 |
| Figure 28: Impact of future rainfall scenarios on runoff volume and heavy metals load. Site NE1..... | 54 |
| Figure 29: Impact of future rainfall scenarios on runoff volume and heavy metals load. Site Agric. | 55 |
| Figure 30: Impact of future rainfall scenarios on runoff volume and heavy metals load. Site NW1. | 56 |
| Figure 31: Impact of future rainfall scenarios on runoff volume and heavy metals load. Site NE3..... | 57 |
| Figure 32: Index of Zinc concentration at the subcatchments of Brusdalsvatnet. Gage 1..... | 58 |
| Figure 33: Index of Zinc concentration at the subcatchments of Brusdalsvatnet. Gage 2..... | 58 |
| Figure 34: Index of Zinc concentration at the subcatchments of Brusdalsvatnet. Gage 3..... | 59 |
| Figure 35: Total Runoff volume-% impervious surface relationship. Gage 1..... | 60 |
| Figure 36: Runoff volume-Zinc loading trend. Gage 1, Gage 2 and Gage 3..... | 61 |
| Figure 37: Impact of Highway E-39 on Impervious surfaces increase. Gage 3..... | 65 |
| Figure 38: Impact of Highway E-39 on the total Runoff at Brusdalsvatnet. Gage 3..... | 66 |
| Figure 39: The impact of Slope on Total runoff volume. Gage 1..... | 67 |

List of Tables

| | |
|--|----|
| Table 1: Summary of the data used in this study. | 18 |
| Table 2: Locations and heavy metals measurements in water. | 22 |
| Table 3: Locations and heavy metals measurements in soil. | 23 |
| Table 6: Concentration levels of heavy metals in water (Seidu, 2021, p. 14)..... | 35 |
| Table 7: Concentration levels of heavy metals in soil (Seidu, 2021, p. 17)..... | 35 |
| Table 9: Runoff assessment data..... | 42 |
| Table 10: Runoff Coefficient analysis of the subcatchments with the higher impervious surface percentage at Brusdalsvatnet. Using Gage 3 rainfall scenario..... | 43 |
| Table 11: Pervious and Impervious areas showing the Total volume of runoff and the volume of runoff originating in Highway E-39. Using the <i>Gage 3</i> rainfall scenario..... | 49 |

Abbreviations

AR6: The Sixth Assessment Report.

As: Arsenic.

Cd: Cadmium.

Cr: Chromium.

Cu: Copper.

DTM: Digital Terrain Model.

EMC: Event-Mean Concentration washoff.

GHGs: Greenhouse gases.

GIS: Geographic information system.

HBCDD: Hexabromocyclododecane.

Hg: Mercury.

HMs: Heavy metals.

IPCC: Intergovernmental Panel on Climate Change.

MET Norway: The Norwegian Meteorological Institute.

NaCl: sodium chloride.

NCCS: Norwegian climate service Center.

Ni: Nickel.

NOAEL: Non-Observed Adverse Effect Limit.

NTNU: Norwegian University of Science and Technology.

NVE: Norges vassdrags- og energidirektorat.

PAHs: Polycyclic Aromatic Hydrocarbons.

Pb: Lead.

POW: Power Function.

RCP: Representative Concentration Pathway.

S1: Subcatchment number one. There are in total 22 subcatchments.

SMC: Site Mean Concentration.

SRES: The Special Report on Emission Scenarios.

SSPs: Shared Socio-economic Pathways.

SWAT: Soil and water assessment tool.

SWMM: The EPA Storm Water Management Model.

UN Environment: The United Nations Environment Programme.

US EPA: U.S. Environmental Protection Agency.

WHO: The World Health Organization.

WMO: The World Meteorological Organization.

ZN: Zinc

1 Introduction

1.1 Background

Over the last century and a half, anthropogenic activities have increased substantially, affecting the environment, human health, and the economy leading to climate change (Kazemi Garajeh et al., 2023, p. 2; Ortiz-Bobea et al., 2021, p. 306). Even though it is not possible to establish an exact date when climate change started, 1976 is generally accepted as the beginning of the “climate shift”(Meehl et al., 2007). As a consequence of the “Climate shift”, temperatures began to rise mainly due to the greenhouse effect meaning the accumulation of greenhouse gases (GHGs) in the atmosphere (Beldring et al., 2008; Ortiz-Bobea et al., 2021, p. 306; Trenberth et al., 2007, p. 238).

During the last 100 years, it has been observed an increase in land surface temperature of about 1 °C during the period 1906–2005 (Beldring et al., 2008, p. 439; Ortiz-Bobea et al., 2021; Skaland et al., 2022, p. 539; Trenberth et al., 2007, p. 237). According to the last report of the Intergovernmental Panel on Climate Change (IPCC), temperatures have risen 0.99 °C in the range of (0.84 to 1.10) for the period from 1850–1900 to 2001–2020 and 1.09 °C in the range of (0.95 to 1.20) for the period from 1850–1900 to 2011–2020. Moreover, in high CO₂ emission scenarios, the average global surface temperature can rise to 5.7 °C for the period from 1850–1900 to 2081–2100 (Arias et al., 2021, p. 59).

Furthermore, the IPCC Sixth Assessment Report state that due to the increase of anthropogenic activity, and consequently, increment of greenhouse gases (GHGs), the following effects were reported: “warming to the troposphere and upper troposphere humidity changes since 1979, cooling of the lower stratosphere, precipitation increment, global mean sea level rise since 1971, Arctic Sea ice loss since 1979, reduction in Northern Hemisphere spring snow cover since 1950, the retreat of glaciers, and increased of atmospheric CO₂ since the early 1960s”. In sum, it causes “warming of the global climate system since pre-industrial times” (Arias et al., 2021, p. 65).

The impact of climate change is well-known globally, and Norway is no exception. Furthermore, in Norway, this phenomenon leads to higher temperatures, increasing precipitation and runoff, extreme rainfall, poor water quality, and extreme weather conditions. (Hanssen-Bauer et al., 2017; Kazemi Garajeh et al., 2023, p. 2; Skaland et al., 2022, p. 539). As a consequence of this, increasing precipitation and runoff could potentially have adverse effects on raw and drinking water quality

due to the amount of nutrients such as Nitrogen and Phosphorous that the water could contain. Moreover, in Norway, the consequences of climate change have materialized very quickly, being noticeable as floods, quick clay landslides, infrastructure deterioration, nutrient loss, and death (Greipsland, 2016, p. 1; Nikel, 2019).

Several studies (Arias et al., 2021; Beldring et al., 2008; Greipsland, 2016; Hanssen-Bauer et al., 2017; Meehl et al., 2007; Skaland et al., 2022; Trenberth et al., 2007) have concluded that precipitation and temperature are the main factors that climate change will affect. Due to the consequences of global warming, we it is essential to understand better climate change and its impact on nature, environment, and society. In order to make a proper assessment, it is relevant to carry out studies in natural and social science, taking into account phenomena such as “rainfall discharge, energy fluxes to the ocean, heat fluxes, glacier mass balance, snow cover, and permafrost conditions”(Pickering, 1996), because they have a direct effect on global climate (Arias et al., 2021; Beldring et al., 2008, p. 439; Hanssen-Bauer et al., 2017). Since these factors are influenced by land surface hydrological conditions, it is essential to consider variations such as “changes in temperature mean values, seasonal variability, extremes of water availability including snow, subsurface moisture conditions, and runoff” (Arias et al., 2021; Beldring et al., 2008, p. 439; Hanssen-Bauer et al., 2017).

Given that the main manifestations of climate change are predicted to be more noticeable in temperature and precipitation, it is vital to take into consideration that the annual average temperature is directly related to the annual average precipitation (Beldring et al., 2008; Greipsland, 2016, p. 1; Skaland et al., 2022, p. 539). According to projections of future scenarios, global warming will lead to extreme temperatures with heat waves that last longer, are more frequent, and are more intense. In addition, the cold periods will be shorter with warmer temperatures during the day worldwide and with frost periods that last less both in the mid and high latitudes (CH 10-4 1-1-3 Hanssen-Bauer et al., 2017; Meehl et al., 2007).

According to (Hanssen-Bauer et al., 2017; NCCS, 2022) and based on results from the Fifth Assessment report by the Intergovernmental Panel on climate change (IPCC, 2013), the annual average temperature in Norway for the period from 1971–2000 to 2071–2100 will increase by ca. 4.5 °C within an interval between 3.3°C and 6.4°C. Alike, the rising temperatures in western Norway will be less severe, with an annual average precipitation of about 3.7 °C. Moreover, the

heat will traverse Norway from the south to the north throughout the mainland, and the northern part is the one that will get warmer on average. Likewise, the temperatures will increase from the coast to inland. Consequently, the warm air that contains more moisture will increase the probability of precipitation. It is predicted an increase of 18% in the annual average precipitation inland in Norway in a range from 7% to 23 %. Besides, during the period 1971–2000, the mean annual precipitation for the mainland was 1600 mm. Accordingly, the highest annual precipitation level was registered in Western Norway with 3500 mm, and the lowest level was registered in south-eastern Norway with 300 mm of precipitation. Moreover, the season that registered a remarkable precipitation increment was the spring, given that from 1900 it registered an increment of 27%. On the contrary, the summer season registered the smallest precipitation increase.

Precipitation is part of the Hydrological cycle and runoff, which is one of the several pathways that water can follow to reach the oceans or evaporate and start the cycle again. In the bargain, the precipitation-runoff interaction has, as a result, more runoff if the amount of precipitation increases. However, the relationship between precipitation-runoff is not proportional. It is likely because warmer temperatures lead to more evapotranspiration. Consequently, these interactions are related to the runoff volume in Norway, which had a mean annual runoff of 1100 mm during the period (1971-2000). Likewise, “The annual average runoff varies from 400 mm in the upper part of the valley Gudbrandsdalen and interior parts of Finnmark to 5000 mm at the glacier Ålfotbreen in western Norway” (Hanssen-Bauer et al., 2017, pp. 27-29).

1.2 Research questions and objectives

Goal: *This work aims to model runoff from Highway (E-39) located in the catchment of Brusdalsvatnet in Ålesund, accounting for present and future rainfall regimes.*

1.2.1 To assess it, the following specific objectives must be addressed:

1. Develop an interactive geospatial map of the runoff flow paths within the catchment of Brusdalsvatnet, Ålesund, Norway.
2. Quantify the runoff volume to Brusdalsvatnet from Highway E-39, accounting for present and future rainfall scenarios.

3. Quantify Heavy Metals load associated with runoffs, accounting for present and future rainfall scenarios.

1.2.2 Expected answers and outcomes:

1. Map the flow-path runoff within the catchment of Brusdalsvatnet.
2. Quantify the volume of runoff from Highway E-39 to Brusdalsvatnet.
3. Present projections of future runoff volumes.
4. Quantify the HMs load at Brusdalsvatnet.
5. Present projections of Heavy metals load in future rainfall scenarios.

1.3 Significance and contributions of the study

The increase in rainfall intensities caused by global climate change, as well as the expansion of impervious urban surfaces, pose several challenges, such as the rising volume of runoff on impervious surfaces and the resulting high pollutant load from the washoff. Furthermore, these processes are especially dangerous when pollutants such as heavy metals (HMs) reach drinking water sources, given that they are carcinogenic. Unfortunately, there is not yet a complete understanding of the connection between climate change and intense rainfall. Likewise, it is limited information about how infrastructures such as highways can affect the environment and how the contaminants transported on these infrastructures can affect water bodies (Beldring et al., 2008).

This study will try to shed some light on extreme rainfall's effects on runoff volume and pollutant loading. Furthermore, to what extent are impervious surfaces affecting the runoff volume and pollutants washoff.

1.4 Thesis Structure

Section 2.

This section laid the foundation for understanding the current global warming situation and how the authorities worldwide try to develop sustainable solutions to the problem at hand. In this pursuit, by working on model projections, the authorities and scientists are trying to understand better what natural patterns can be affected by climate change and analyze its consequences.

Therein, use the gathered knowledge to predict what could happen in the future and what kind of preventive and mitigation measures should be taken in order to reverse the climate change effect.

Section 3

This section describes the study area and gives detailed information about the pre-processing data. Moreover, aspects such as model calibration, simulation model reliability, and the justification of the chosen emission scenarios are explained in detail.

Section 4, 5

Section 4 on ArcGIS Pro, SWAT, and SWMM lays the framework for the set of tools and methods used in this thesis. Section 5 presents the results of the thesis, and these results are presented by using figures, tables, maps, and graphs. Moreover, the most relevant outcomes related to the three objectives of the thesis are presented and summarized.

Section 6,7

The results presented in Section 5 are discussed in depth in Section 6. Section 7 presents the main findings, conclusion, and further work.

Appendix

Appendix A, in Section 4, presents the Classification levels of heavy metals in water from Miljødirektoratet 2020. Hence, the water samples used in this thesis can be compared with the Norwegian standards.

Appendix B, in Section 4, shows the Classification levels of heavy metals in soil from Miljødirektoratet 2020. As such, the soil samples used in this thesis can be compared with the Norwegian standards.

Appendix C, D, and E present the Subcatchments Runoff summary of the rainfall scenarios Gage 1, Gage 2, and Gage 3, respectively.

2. Literature review

2.1 Main factors affected due to climate change

2.1.1 Temperature

As stated by the IPCC Sixth Assessment Report 2021, global warming is unequivocally an effect of greenhouse gases GHGs and is influenced by human activity. Accordingly, the IPCC has a high level of confidence in their projection due to the inclusion of a broader range of indicators to assess the effect of anthropogenic activity and GHGs emissions on climate change. At last, the report yielded that in the worst-case scenario (SSP5-8.5), it will be an increase in the average global surface temperature of 4.4°C for the period from 1850–1900 to 2081–2100.

As reported by The Norwegian climate service Center (NCCS) report no. 1/2017, in Norway, temperatures have varied with warming and cooling periods. Given that, during the period (1900-1938), it registered an increment of about +0.32 °C, whereas, during the period of 1976-2014, temperatures rose to +0,50 °C. Moreover, between those periods (1938-1976), the temperature decreased by about -0,04 °C. Likewise, the mean average temperature in mainland Norway showed an increment of about 1 °C in the period 1900-2014. Trøndelag and Norland-Troms were the regions that showed the most significant temperature increase (Hanssen-Bauer et al., 2017, pp. 13-16). Rising temperatures are leading to more precipitation, thus runoff volume and washoff increment, which are the main factors studied in this research.

2.1.2 Precipitation

Anthropogenic-caused climate change has had a noticeable impact on the water cycle both at global and regional scales since 1950, having a faster global land precipitation increment since 1980. Also, it occurred particularly in high altitudes in the Northern Hemisphere (Arias et al., 2021). According to the SSPs projections, the precipitation increment will be proportional to the temperature rising. Likely by 2–3% per °C, and as stated by IPCC, it will continue at least until 2100. Regarding extreme weather events such as extreme precipitation or extreme heat, the water cycle variability will be more noticeable on extreme changes than on mean changes. As such, it is predicted under all model projections worldwide. Alike, according to the projections published by IPCC Sixth Assessment Report 2021, the global annual mean precipitation over land is projected to increase by 2.4% under SSP1-1.9, 4.6% under SSP2-4.5, and 8.3% under SSP5-8.5 from the

period 1995–2014 to 2081–2100. Moreover, the report claims that the precipitation increments, and precipitation extremes will be related to runoff increment, particularly in northern high latitudes (Arias et al., 2021, pp. 85-87). Since patterns such as precipitation are changing due to climate change, modeling their future behavior is essential to environmental management to plan and take preventive measures.

2.1.3 Evaporation and evapotranspiration

Evaporation and evapotranspiration are part of the hydrological cycle directly affected by climate change. Furthermore, these changes will be noticeable globally, as it is predicted to increase evaporation over the ocean. Moreover, evapotranspiration will probably increase over land, mainly depending on future mean surface temperatures (Arias et al., 2021, p. 85). Notably, in Norway, the mean annual evapotranspiration for the period 1971-2000 was about 500 mm, with an uncertainty of 25% (Hanssen-Bauer et al., 2017, p. 27). The amount of precipitation depends among other factors of evaporation and evapotranspiration, also affecting patterns such as runoff volume and, to a lesser extent, washoff.

2.1.4 Runoffs from impervious surfaces

In general terms, rainfall positively affects flora and fauna, but when it rains intensely and for long periods, the consequences can be negative. Moreover, the soil has a natural capacity to contain water through infiltration. However, when it reaches its maximum capacity, the soil is saturated, meaning it cannot infiltrate or contain more water. Hence, pervious surfaces are an essential resource for infiltration, but their natural capacity is reduced due to rapid urbanization. In fact, the expansion of impervious surfaces such as buildings, roads, and infrastructure does not allow water to soak through the ground leading to rainfall runoff (Xiao et al., 2016, p. 162).

Runoff is a common consequence of impervious surface development and the increment of precipitation extremes. Besides, rainfall-runoff is a phenomenon that is occurring more frequently due to climate change. Therefore, it has become an important subject of study. Accordingly, when the soil is saturated, water starts to accumulate on the ground surface, and then, rainwater runoff starts to flow, transporting substances such as pollutants that are contained on the surface. Likewise, surface runoff pollution is the main element of highway runoff pollution. Rainwater runoff from highways contains various pollutants, including hydrocarbons, heavy metals (HMs), and de-icing chemicals such as sodium and chloride (commonly used in countries with cold

climates. As well as sedimented and leached pollutants from the vehicle's exhaust (Folkesson et al., 2009, pp. 109,113; Wang et al., 2016, pp. 814-817).

Highway runoff pollution can highly affect vulnerable areas such as drinking water sources and quality ecosystems. Following that, when a highway is built near a water body or the hydrological system, it can transport pollutants through its network, increasing the probability of contamination in vulnerable areas. Furthermore, vulnerable areas can be polluted, among other reasons, due to traffic accidents that lead to oil spillage, vehicle exhaust sedimentation and filtration, de-icing salt, and microplastic (Rutledge et al., 2022; Senduran et al., 2018, p. 336). In countries such as Norway, which experience long periods of cold weather, it is common practice to use large quantities of sodium chloride (NaCl) on roads to maintain their functionality. Therefore de-icing can be considered a source of pollution both to groundwater and surface water (Enhuus et al., 2020, pp. 4-5). Moreover, according to ((Wang et al., 2016, p. 814), when the number of vehicles on the countryside roads exceeds 30.000 per day, it directly affects the water bodies of the surrounding areas, having water pollution as well the main consequence.

The rainwater runoff process can be divided into two phases. Firstly, the washoff takes most of the substances from the roads and other surfaces with a high sewage content, suspending solids and hydrocarbons. More specifically, as stated by the Europe design standard and the Australian environmental protection department, the initial rainwater runoff is categorized as about 8~16 mm. On the other hand, the second phase of rainwater-runoff usually contains cleaner water with less precipitation intensity. The first phase, called initial rainwater, contains highly polluted water that cannot be released directly into the water bodies. Instead, it must be transported through the sewer network to a water treatment plant to be processed and then released into the river.

As a result, initial rainwater must undergo strict treatment processes, including solids settlement, oil separation, and sand filtration, before being discharged into the sewage pipe (Folkesson et al., 2009, p. 14). Rainwater from the second phase, which is relatively clean, can be released directly into the water body. In accordance with this, the first phase of rainwater, which is the initial runoff, washes away most of the pollutants on the surface. It first removes small particles and soluble pollutants, followed by the removal of larger, immobile, and insoluble pollutants (Wang et al., 2016, p. 818).

2.2 Pollutants' sources, behavior, and convey

Runoff and washoff pollution from impervious urban surfaces mainly consist of pollution from roofs and roads. Therefore, this document will focus on pollution from roads and how it can impact vulnerable areas. Accordingly, pollutants from urban impervious surfaces can be divided into two: particulate pollutants and dissolved pollutants. However, there is more feasible to find available information about particulate pollutants than dissolved pollutants (Xiao et al., 2016, p. 162).

Different factors are essential to consider concerning the pollutant's transportation and spread. Factors such as pollutants' physical and chemical properties, the intensity and duration of rainfall, and soil roughness. Moreover, pollutants that are exposed to intense rainfall on the smooth ground tend to get washed away quickly, reducing the pollutant's concentration time and increasing the pollutant's transportation rate (Xiao et al., 2016, pp. 162-165).

Rainwater runoff from heavily trafficked roads is the primary source of pollution. According to Folkeson et al. (2009), this type of road has five sources of pollution “traffic and cargo, pavement and embankment materials, road equipment, maintenance and operation, and external sources”. Additionally, the amount of pollutants a traffic road can generate depends on “road design, road materials, road maintenance and operation, types of fuel used and traffic characteristics such as volume of light and heavy vehicles, speed, and driving behavior”.

Pollution spreads mainly by being transported on the road's surface and by aerial transport. Moreover, the polluted rainwater flows on the road's surface, and only a low percentage of this water can infiltrate through the pavement or cracks. Alike, most of the polluted water is infiltrated when it reaches the ground or the drainage ditch on the sides of the road. Additionally, rainwater pollutants such as HMs, organics, PAHs, and de-icing salt stay close to the road polluting plants, animals, and soil. In fact, these pollutants disturb the biological processes of vegetation, animals, and microorganisms and potentially contaminate surface water and groundwater (Folkeson et al., 2009, pp. 109,114,120; Wang et al., 2016, p. 814).

Due to the negative impact that road surface pollutants and rainfall runoff have on the environment, road planners and engineers are taking measures to prevent pollutants from spreading quickly. As such, these measures are usually taken during the early stages of road planning since the current legislation effectively protects the water bodies. Once the road is built, the responsibility rests on

the road's operators, being the most challenging part of offering exemplary service to the community without contaminating the environment (Folkson et al., 2009, pp. 107-109).

2.3 Heavy metals

Heavy metals (HMs) such as Zinc (Zn), nickel (Ni), copper (Cu), chromium (Cr), lead (Pb), arsenic (As), mercury (Hg), and cadmium (Cd) are matter of concern to governments worldwide due to their presence in drinking water. Besides, HMs are difficult and expensive to remove from the environment due to their properties since they are stable, non-biodegradable, and accumulative (Yan et al., 2018, p. 2). These pollutants are present in nature, but they have become a problem mainly due to the excessive amount of waste that is currently necessary to store and process. Moreover, industrial, agricultural, and household waste deposits are the primary source of drinking water sources contamination. As such, the leaching of metals from metal deposits is a common pathway HMs take to reach the hydrological system and pollute drinking water sources.

Furthermore, another pathway these pollutants take is impervious surfaces when they get washed away from road surfaces through runoff. Land use and traffic volume are the main parameters of generating and distributing pollutants such as lead (Pb) and mercury (Hg). Various studies claim that the amount of HMs in stormwater-runoff can exceed the threshold recommended for recreational and drinking water, representing a risk to human health. Hence, drinking water quality is important (Chowdhury et al., 2016, pp. 477-479; Ma et al., 2017, pp. 593,599).

Several studies, i.e., (Chowdhury et al., 2016; Ma et al., 2017; Yan et al., 2018), claim that HMs have negative consequences on human health. For instance, in Bangladesh, according to a study carried out in 2011, more than 40 million people were affected due to exposure to HMs. It was demonstrated that exposure to these pollutants through drinking water could lead to chronic and sub-chronic health effects. Furthermore, there is a total of 23 HMs that represent a risk to human health. Among them, inorganic arsenic (As) and cadmium (Cd) are classified as cancerogenic. Moreover, arsenic is also related to skin damage, cadmium is related to kidney damage, and mercury (Hg) represents a high health risk. According to (Smith et al., 1992), drinking 1 liter of water a day containing 50 µg/L organic arsenic could develop liver, lung, kidney, or bladder cancer in 13 per 1000 persons. Being exposed to high amounts of organic arsenic through drinking water is likely capable of causing between 200.000 and 270.000 deaths (Chowdhury et al., 2016, pp. 77-80; Yan et al., 2018, p. 8).

Due to the risk that exposure to HMs represents to human health, it is essential to identify the high-risk areas considering all factors mentioned before in order to make a proper assessment. Subsequently, developing a strategic plan to take preventive and mitigating measures is important. In this pursuit, regulatory health agencies such as US EPA and The World Health Organization (WHO) have given guidelines based on the non-observed-adverse-effect limit (NOAEL). These guidelines give an insight into maximum concentrations of HMs in drinking water, including pollutants such as As, Cd, Cr, Hg, Pb, Se, and Sb, since they have been linked to cancer development and other diseases (Chowdhury et al., 2016, p. 481; Ma et al., 2017, p. 599).

In Norway, the situation regarding water quality is much better than in other parts of the globe due to its governmental policy. Nonetheless, the quality of raw water is still the object of concern, but regarding drinking water, it has been remarkable improvements in the last 20 years. Accordingly, the waterworks have to be approved by the Norwegian Institute of Public Health, so 9 out of 10 Norwegians receive water from waterworks. Furthermore, according to the authorities of this country, water sources in Norway are well protected against pollution. Moreover, they state that the level of pesticides, HMs, and other pollutants in water is low (Steinberg, 2017). However, isolated events could change the conditions and affect the water quality. Therefore, continuous monitoring of drinking water sources is recommended.

2.4 Previous research on stormwater runoff from highways and catchments

According to Sytsma et al. (2020), there is not yet a good understanding of how to account for runoff that originates from impervious surfaces. Moreover, the study states that most of the methods for quantifying connected impervious areas are based on assumptions about the meaning of “connection”. This study developed a new conceptual model that tries to solve these issues by using PySWMM and ArcGIS.

Furthermore, Martin et al. (2019), used Geographic Information System (GIS) to build a TPP risk map. This study aimed to develop a geospatial model capable of predicting the contribution that thermal energy has to surface runoff in an urban catchment. Moreover, this study developed a specific theoretical methodology that integrates the thermal potential of landuse, and thermal decay. This methodology was applied to a case study watershed in Blacksburg, Virginia. The result is that the Geospatial method applied is reliable and can be used in future research related to the TTP risk map of thermal pollution management.

On the other hand, SWMM has recently developed a new approach regarding urban stormwater management. Since launching Low Impact Development (LID), several studies have developed engineering models applying this approach. For example, this new tool was used by Baek et al. (2020) to assess the performance of LID in Yongin, a small-Medium city in South Korea. As such, applying this approach yields that it is necessary to adjust the method since it oversimplifies the LID-associated numerical models. These challenges were overcome by modifying the water quality model of LID. As a result, the modified model is reliable and thus will be applicable to future research while designing LID facilities and a guideline for LID installation.

It is essential to highlight that LID is not the only feature that SWMM has regarding stormwater management. SWMM has developed applications that help analyze the impact of the “sponge city concept” on runoff volume derived from stormwater. Accordingly, sustainable drainage systems (SuDS) and Green stormwater infrastructure (GSI) have become widely used in stormwater control. According to a study conducted by (Dell et al., 2021) in the city of Fort Collins-USA, the use of SWMM and its different methods make it feasible to build models which permit analyze the impact of green-good practices on stormwater runoff as well as their effect on the sewer network.

Tuomela et al. (2019) applied SWMM to shed some light on using constant source concentrations while modelling pollutant loading. The study was conducted in Southern Finland and was based on the event mean concentrations (EMC) function. This function was applied to different landuses and considered on-site rainfall and discharge data. However, the simulated pollutant load results were widely different from the samples, given that the results vary depending on the EMC data source, weather conditions, and rainfall intensity. Lastly, the study states that the use of SWMM is recommendable while performing modelling of stormwater pollutants loads and can provide helpful information to decision-makers regarding stormwater management.

The discussed papers presented different applications of GIS, hydrological modelling to geospatial analysis, and stormwater management. This thesis will be focused on the delineation of the runoff pathways as well as on the computation of runoff volume and pollutant loading. Besides, future rainfall scenarios will be modelled using the RCP8.5 approach.

2.5 Geospatial Analysis (ArcGIS Pro)

Geospatial models, also known as GIS models, can be utilized for various applications, including stormwater management, making them a valuable tool. Moreover, GIS with various spatial analysis tools has become essential in the last decades while managing stormwater runoff from urban areas, for instance, in cases when the runoff can potentially reach drinking water sources. In accordance with that, GIS's ability to collect data, analyze data, data management, develop predictive models, and digital visualization of the studied phenomena has turned GIS into an accurate and reliable analysis geospatial tool (Mapscaping, 2022).

Regarding this thesis, GIS presents the possibility of computing an accurate and comprehensive data analysis from sources such as digital terrain model (DTM), soil, and landuse. Likewise, these inputs are used to develop a comprehensive understanding of the runoff pathways within the catchment at Brusdalsvatnet, and to route runoff from Highway E-39 to the water body. Additionally, this approach can help to identify areas with high runoff potential and develop appropriate preventive and corrective measures. Furthermore, Geospatial models can be a key tool regarding disaster management due to their capacity to develop predictive models which permit the manager to simulate the impact of different stormwater strategies enabling the possibility of always being a step forward (Esri, 2023).

At last, the GIS approach is cost-effective, enabling analyzing different stormwater scenarios without the cost and time that the fieldwork entails. Besides, GIS can produce high-quality visualizations, which gives a closer perception of the runoff pathways and, thus, the potential damage to the drinking water source. Furthermore, using GIS allows interaction with other programs due to its capacity to transform the outcomes in different file types (Esri, 2023).

2.6 Soil and Water Assessment Tool (SWAT)

The Soil & Water Assessment Tool (SWAT) is a geospatial analysis tool that enables users to model projections of the quality and quantity of groundwater and surface water. Likewise, SWAT has become a vital tool while undertaking studies about soil erosion control, non-source pollution control, and climate change effects on natural patterns and landuse (SWAT, 2023).

On the other hand, given that SWAT has been on the market for about 20 years, it has allowed modifying and refining the tool over the years. Even though SWAT is a complex geospatial

analysis tool that can overwhelm the user initially, its use is recommended (SWAT, 2012). When said, the use of SWAT is recommendable given that its results are reliable and have high accuracy, enabling the user to present reliable results to the decision makers (Texas University, 2023).

2.7 Storm Water Management Model (SWMM)

The EPA Storm Water Management Model (SWMM) is a dynamic rainfall-runoff simulation model. Moreover, using SWMM enables the user to model the generation and transport of runoff and compute runoff volume. This approach permits the computation of the pollutant loads derived from the runoff (S.L. NEITSCH, 2000, pp. 14-16). The principal capabilities of this engine are its capacity to process up to 10 different pollutants, four buildup models, and three washoff models, enabling use as a planning and design tool. Nevertheless, SWMM has some limitations, the most relevant in its inability to account for pollutant interaction, lack of accuracy in process replication, and absence of uncertainty analysis (Wijesiri et al., 2020, p. 4).

2.8 Future rainfall scenarios

Global warming and its consequences have forced governmental institutions and scientists to actively work on solutions to change the course of the greenhouse effect. Therefore, it is crucial to understand the global warming phenomena deeply to take adequate preventive and mitigating measures. With that in mind, scientists worldwide have been working on developing climate models which can give insight into how the future could look with different emission scenarios.

According to global and scaled climate projections, a substantial increase in temperatures is expected in the 21st century in an interval from 3.3 °C to 5.7 °C in the worst-case scenario (Arias et al., 2021, p. 63; Beldring et al., 2008, p. 439; Hanssen-Bauer et al., 2017, p. 6; CH 10-3 I.13-17 Meehl et al., 2007). As a result, institutions have been established to assess, plan, and implement preventive and mitigating measures related to the impacts of climate change. Institutions such as the Intergovernmental Panel on Climate Change (IPCC), which was created by the United Nations Environment Programme (UN Environment) and the World Meteorological Organization (WMO) in 1988 (IPCC, 2023).

In 2000 the IPCC published the Special Report on Emission Scenarios (SRES). Moreover, in 2014 they published a new approach to emission scenarios called Representative Concentration Pathway (RCP) system. Lastly, in 2021 the IPCC published the last approach regarding emission scenarios

called Shared Socio-economic Pathways (SSPs) (Arias et al., 2021, p. 52). These future emission scenarios projections are based on the emission of anthropogenic greenhouse gases over time and high-CO₂ emissions pathways. Likewise, something that all scenarios have in common, regardless of the variables taken into consideration, is that temperatures will rise continuously. Nonetheless, depending on the model's approach, the temperature increment varies from 1 °C to 6.7 °C (Mark B, 2020; I. Hanssen-Bauer & Sandven, 2015; Literacy, 2015; CH 10-3 1.38-41 Meehl et al., 2007).

The SRES emission scenarios are based on storylines records that consider socioeconomics, demographics, and technological and policy change factors. As well as how these factors can affect the emission of anthropogenic greenhouse gases in the future. Furthermore, this data makes it possible to model future emission scenarios. (Literacy, 2015). Likewise, the most critical SRES scenario is the A1F1, also called “business as usual”, in which it is estimated that intense use of fossil fuel in the future having as result in the highest emission values with a projection of global warming in the range of 3.5°C to 5.8°C in 2100. Furthermore, graphic patterns show that the northern latitude will be the most affected with a temperature increase of approximately double the global average temperature (Literacy, 2015; CH 10-3 1.45-46 Meehl et al., 2007; Nebojsa Nakicenovic et al., 2000).

The next generation of model emission was the Representative Concentration Pathway (RCP) system. This system has four possible scenarios RCP2.6, RCP4.5, RCP6.0, and RCP8.5. These scenarios are named after their radiative forcing values, meaning the difference between the sunlight absorbed by the earth and the sunlight reflected into space. Besides, The Representative Concentration Pathway (RCP) system is the approach the Norwegian authorities used for their emission model projection in 2015 (Mark B, 2020; I. Hanssen-Bauer & Sandven, 2015; Literacy, 2015).

The ultimate update from IPCC regarding climate change scenarios is the five illustrative scenarios exposed in the Sixth Assessment Report (AR6). Furthermore, this new approach is based on the Shared Socio-economic Pathways (SSPs), which consider the analysis of observations, paleoclimate information, models, chemical & biological processes, and climate system components. These emission scenarios are called SSP1-1.9, SSP1-2.6, SSP2-4.5, SSP3-7.0, and SSP5-8.5. This approach is the most relevant as it achieves higher accuracy and includes a wider variety of greenhouse gases (GHGs) and air pollutants, as well as accounting for high-CO₂

emissions without considering mitigation measures and new low-CO₂ emission pathways. This represents an improvement over earlier WMO reports.

The Norwegian white paper on climate adaptation (Meld. St. 33 (2012–2013)) suggests that “to be precautionary, the government wants risk assessments of climate change to be based upon the high climate projections”. In this context, RCP8.5 and SSP5-8.5 are the worst-case scenarios. As such, RCP8.5 projects an increment in fossil fuel use and no renewable energy sources, characterized by the high emission of greenhouse gases into the atmosphere. This approach is based on current and historical emissions patterns (Mark B, 2020; Hanssen-Bauer et al., 2017; Literacy, 2015). On the other hand, SSP5-8.5 more accurately represents the current changes, e.g., air pollution control and climate change mitigation stringency. Accordingly, these mitigation measures will affect the influence of anthropogenic GHGs effect on climate change (Hanssen-Bauer et al., 2017).

Regarding which is the best approach to future emission scenarios and which measures must be taken, it is something that we will not discuss in this document. However, it is essential to highlight that it is quite a disagreement among scientists about how the emission patterns will look in the future (Nexus, 2021).

3 Study area and data

3.1 Description of the study area

The study is a part of the Smart Water Management project, which aims to develop a comprehensive system for monitoring, modelling, and simulating water and sewage systems. The project is a collaborative effort between the Municipality of Ålesund and the Norwegian University of Science and Technology (NTNU) (United Future Lab Norway, 2021).

The focus of this research is on Brisdalsvatnet, a lake located on Uksenøya in the municipalities of Ålesund and Skodje in Møre and. Covering a total area of 7.52 square kilometers and sitting at an elevation of 25.96 meters above sea level, Brisdalsvatnet has a volume of approximately 300 million cubic meters (Åge Brabrand, 2013, p. 10). Brisdalsvatnet, the focus of this study, is situated in Ålesund municipality and has a total area of 7.52 square kilometers. The lake's outlet is located on the west side and flows from east to west through Lillevatnet and Spjelkavikelva before ending at Åsfjorden. Brisdalsvatnet and Spjelkavikelva represent the largest watercourse

in Ålesund municipality, and in the northern part of the lake, the E-136 road and E-39 highway run alongside. The lake has been the primary source of drinking water for Ålesund since 1980, but high levels of environmentally toxic brominated flame retardants (HBCDD) were discovered in 2009. However, subsequent studies carried out by the sanitary authorities concluded that the levels of pollutants in the water were not harmful to human health (Seidu, 2021).

The catchment area of Brusdalsvatnet covers a total area of 8.09 square kilometers. It is particularly steep in the central part, with a maximum slope value of 66.2% and a minimum slope value of 16.5%. The altitude of the catchment ranges from 25.2 meters above sea level to 351.39 meters above sea level.

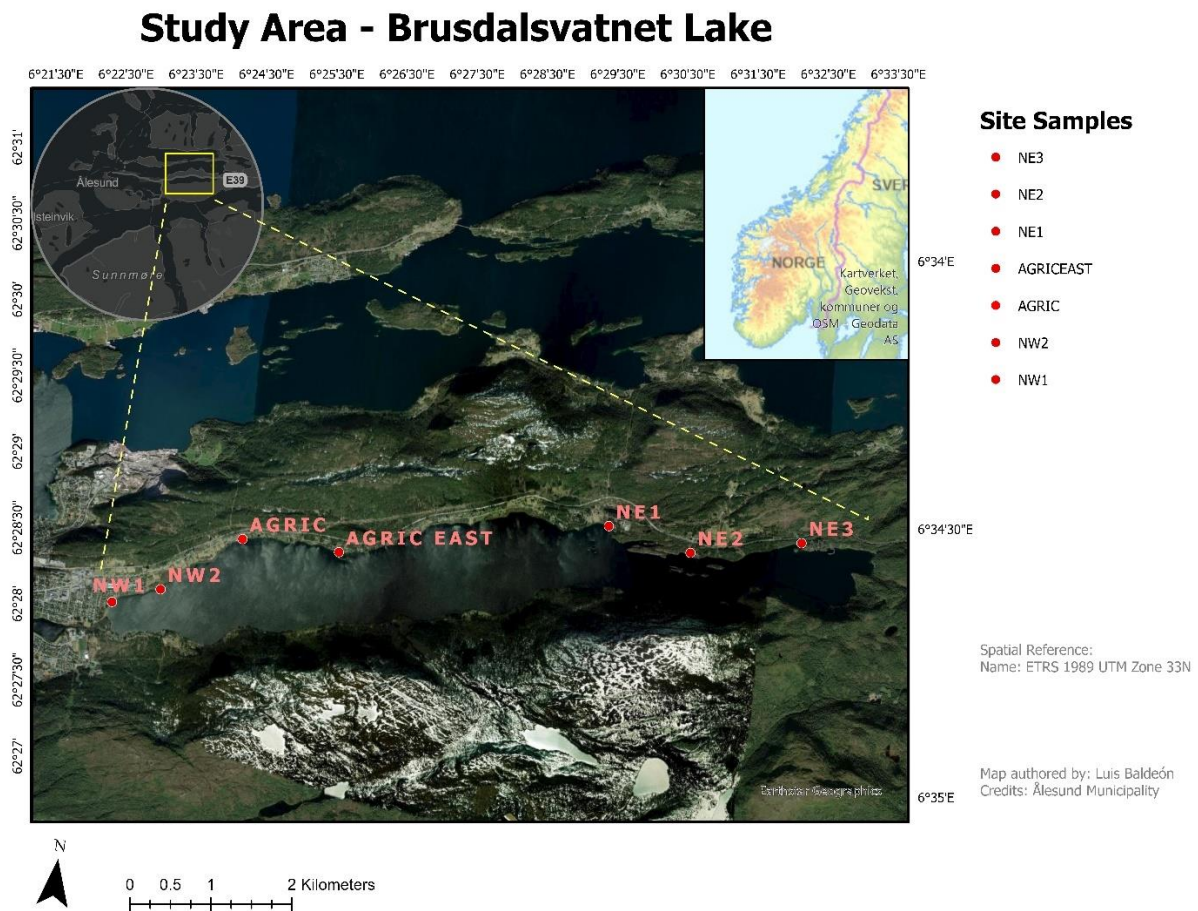


Figure 1: Study area at Brusdalsvatnet in Ålesund municipality. ArcGIS Pro.

3.2 Data

3.2.1 Data Collection

In order to assess the impact that intense rainfall has on runoff volume and pollutants load at Brusdalsvatnet, this study considered rainfall data from period 01.01.2021 to 31.12.2021 provided by (MET Norway). Additionally, using Storm Water Management Model (SWMM), the volume of runoff flow from the catchments through the highway is calculated. Further, continuing with the process, the pollutant load that flows from the catchment into the lake will be computed to assess water quality.

The data was provided by the Norwegian University of Science and Technology (NTNU) as part of the development of the Smart Water management project. The dataset includes is presented in Table 1.

Table 1: Summary of the data used in this study.

| Data | Spatial resolution | GIS data type | Data source |
|----------------------------------|--------------------|---------------|-----------------------|
| Digital Terrain Model (DTM) | 1 m x 1 m | GRID | Høydedata.no |
| Boundary of Ålesund Municipality | 10 m x 10 m | Polygon | NTNU |
| Landuse | 1 m x 1 m | Polygon | Geonorge.no |
| Road network | 1 m x 1 m | Line | Geonorge.no |
| Hydrological network | 1 m x 1 m | Line | NVE.no |
| Building area | 1:5000 | Polygon | NTNU |
| Rainfall | - | - | MET Norway |
| Climate scenarios | - | - | Klimaservicesenter.no |
| Heavy metals samples | - | - | NTNU |

3.2.2 Notation of data

AR50: Landuse classification in Norway AR50 adapted to a scale from 1:20.000 to 1:100.000. This dataset provides information at an overview level (Eva Solbjørg Flo Heggem, 2019).

Area Imperviousness-Perviousness (%): Area's imperviousness is given in percentage.

C: Runoff coefficient. For the range from 0.35 to 0.95.

C1: Maximum buildup possible.

C2: Build-up rate constant.

C3: Time exponent.

C_{3emc} : Washoff coefficient (M/L^3).

CMS: Unit of measure for runoff volume. Minimum-Maximum event mean value.

Exceedance frequency (%): the probability of precipitation/runoff occurs.

Grid_code: Used as a unit of measure. Raster layer data.

Hectares (ha): The subcatchments area is given in hectares.

m^3 : Volume of water in the study area.

mm/hr: Unit of measure for precipitation intensity. Minimum-Maximum events mean value.

ModelBuilder: “ Visual programming language for building geoprocessing workflows” (ArcGisPro, 2022d).

Parameter (P): Parameter in the Geoprocessing tool of ArcGIS Pro.

Pollutants water samples (ug/l): Water samples were measured in micrograms per liter.

Pollutants soil samples (mg/Kg TS): Soil samples were measured in milligrams per kilogram dry.

Precipitation/rainfall (mm): rainfall volume.

Temp ($^{\circ}C$): Mean temperature.

Slope (%): Area’s slope value is given in percentage.

W_{emc} : Amount of washoff (M/L^3).

Weight : It is described as TS tørrstoff in Norwegian since the samples were analyzed in Norway.

Width (m): The width of runoff flow was given in meters.

X-Y unit (m): The Latitude of the study area was set to meters.

Z-unit (m): The Altitude of the study area was set to meters.

3.2.3 Data processing

ArcGIS Pro 3.0.1 was used to process the data for this thesis using the *ModelBuilder tool*. The dataset provided by NTNU needed to be processed before it could be used as input in the methods discussed in Section 4.

The DTM and hydrological network of the study area were used to delineate the flow pathways, using features such as elevation or slope. Further, the road network was used to snap Highway E-39. Lastly, the raster layer building footprint was used to identify the developed areas within the study area.

Firstly, the DTM, landuse, road network, hydrological network, and building footprint were clipped to the extent of the study area. *Extract by mask* was used to clip the DTM. The mask used was a polygon of the Ålesund municipality area *Ålesund boundary*. Further, it was snapped using the *Create features* tool. The workflow is shown in Figure 2. Besides, landuse, road networks, hydrological networks, and building footprints were clipped using the *Clip* tool, and the same mask was used. Process shown in Figure 3.

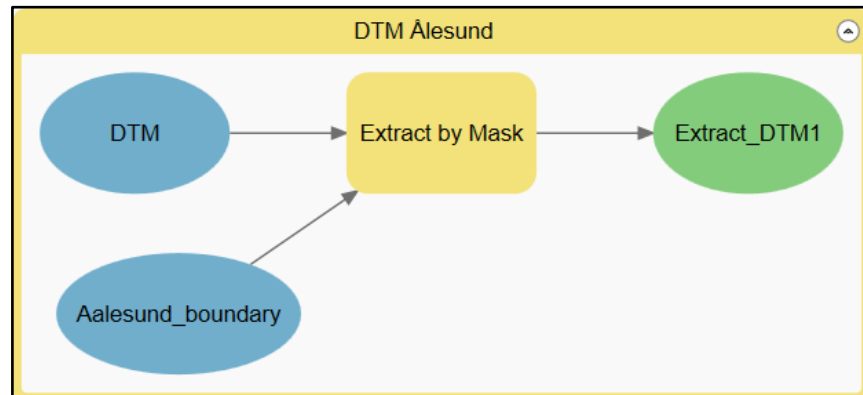


Figure 2: Extracting the DTM to the study area extent. ModelBuilder workflow.

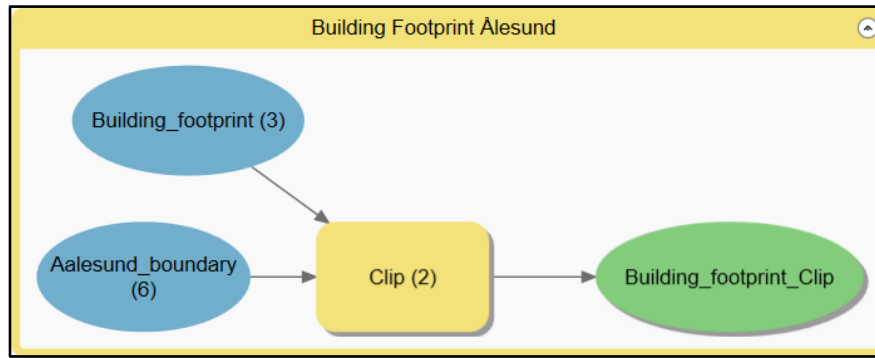


Figure 3: Clipping the Building footprint data to the study area extent. ModelBuilder workflow.

Next, the landuse data provided by Georange.no was based on the Norwegian AR50 Landuse classification, which does not take specifically into account road network.

Therefore, in order to calculate impervious and pervious surfaces, it was created a polyline representing Highway E-39 and added to AR50 Landuse classification. Process shown in Figure 4.

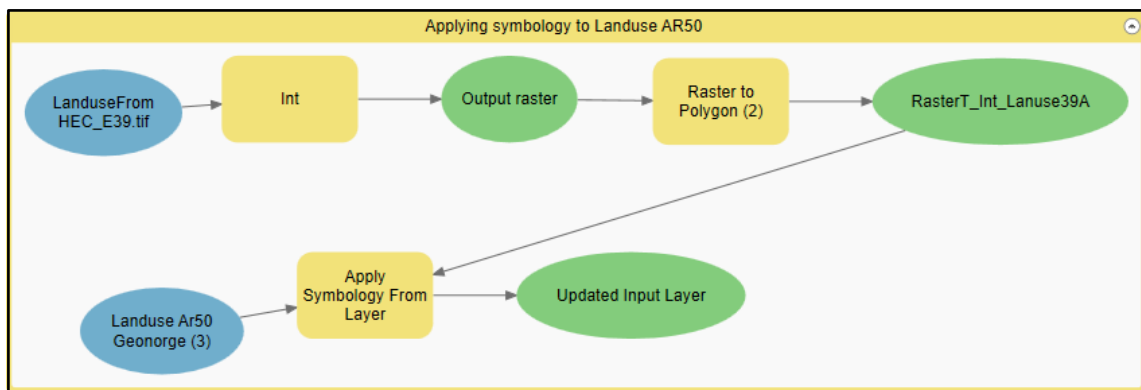


Figure 4: Applying symbology to AR50 Landuse. ModelBuilder workflow.

Also, the rainfall data was in Excel format; therefore, in order to use the data as input in SWMM, it was necessary to transform the data file from .xlsx to .csv and then to .dat. Given that, this is the file format allowed to use in SWMM. The same procedure was applied to future climate scenarios data for periods 2031-2060 and 2060-2100, with a precipitation increase of 20% and 30%, respectively. Figure 5 shows a hydrograph of the rainfall volume in Ålesund municipality during the year 2021.

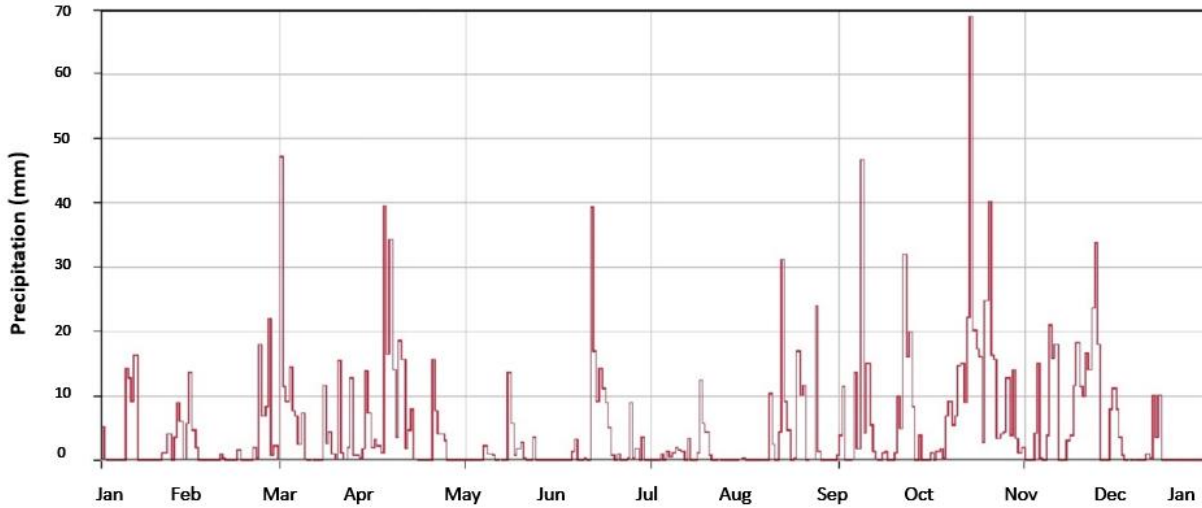


Figure 5: Hydrograph of Ålesund Municipality for the year 2021. HEC-HMS.

Lastly, the measurements of heavy metals were provided by NTNU. Moreover, the values were taken from the NTNU report “*Concentration of heavy metals in the catchment Brusdalsvatnet, 2021*”, the values are shown in Table 2 and Table 3 (Seidu, 2021).

Table 2: Locations and heavy metals measurements in water.

| Pollutants | NE1 | NE2 | AGRIC | NW1 | NW2 |
|-------------------|------------|------------|--------------|------------|------------|
| Zinc (ug/l) | 32 | 19 | 34 | 3.9 | 8.6 |
| Lead (ug/l) | 1.4 | 2.3 | 4 | < 0.20 | < 0.20 |
| Cadmium (ug/l) | 0.053 | 0.01 | 0.06 | 0.01 | < 0.010 |
| Chromium (ug/l) | 2.1 | 2.6 | 4.8 | < 0.50 | < 0.50 |
| Copper (ug/l) | 6 | 4.2 | 13 | 1 | 1.3 |
| Nickel (ug/l) | 1.9 | 3.2 | 4.4 | < 0.50 | < 0.58 |

Table 3: Locations and heavy metals measurements in soil.

| Pollutants | NE1 | NE2 | NW1 | NW2 | NE3 | AGRIC | AGRIC EAST |
|-------------------|------------|------------|------------|------------|------------|--------------|-----------------------|
| Zinc (ug/l) | 43 | 46 | 38 | 55 | 70 | 81 | 42 |
| Lead (ug/l) | 8.4 | 8.3 | 6 | 9.2 | 11 | 11 | 12 |
| Cadmium (ug/l) | <0.20 | <0.20 | <0.20 | <0.20 | <0.21 | <0.20 | <0.20 |
| Chromium(ug/l) | 18 | 16 | 28 | 19 | 41 | 20 | 21 |
| Copper (ug/l) | 19 | 20 | 14 | 21 | 37 | 57 | 23 |
| Nickel (ug/l) | 14 | 14 | 16 | 14 | 34 | 42 | 21 |

4. Methodology

The methodology aimed to achieve three objectives; (i) The runoff flow paths within the catchment were calculated and delineated. This process was engineered using ModelBuilder in order to develop the Geospatial interactive map. (ii) The catchment was divided into 22 subcatchments to calculate the volume of runoff, whereas the scenarios were calculated and projected. (iii) The load of heavy metals was computed from the runoff volume previously calculated, accounting for present and future scenarios.

4.1 Objective 1: Geospatial interactive map on the runoff flow pathways within the catchment of Brusdalsvatnet

ArcGIS Pro version 3.0.1 was used to engineer the necessary procedures to accomplish the first objective. Moreover, ModelBuilder was used to execute the workflow.

4.1.1 Computing runoff pathways

The raster layer DTM was corrected using the Fill spatial analysis tool, which fills sinks in the raster to improve the data by removing small imperfections. The z-limit is the parameter that determines which sinks will be filled and which ones will not (ArcGisPro, 2022b). After executing the tool, the final DTM was generated, and it was used as input to calculate the flow direction using the Flow Direction tool. The resulting layer was named FlowDirBrus. Subsequently, the Watershed, Basin, and Flow Accumulation tools were used to compute the study area's watershed, basin, and flow accumulation, respectively, for each computation.

To compute the Brusdalsvatnet watershed, it was necessary to establish the Pour Point. This point was located at a natural outlet within the study area and created using the Create Feature tool, resulting in the feature class Pourpoint. Next, FlowDirBrus and Pourpoint were used as inputs in the Watershed tool, generating the raster Watershed_Brusdalsvatnet as an output. The Grid_code values of the Flow Accumulation output Flow_ACCum were then segregated to only have representative values. This was achieved using the Con tool with the expression "Where the value is greater than or equal to 4000", since the Grid_code values were too coarse and ranged from 1 to 297023. The value of 4000 was chosen after evaluating the most suitable value from the Flow_ACCum raster's Attribute table.

The outcome of this computation was Segwater_ways. Then, Segwater_ways was used as an input in the Divide spatial analysis tool to compute the amount of flow that will not be accounted for as runoff flow but instead will be accounted for as water loss through infiltration, evaporation, evapotranspiration, and sewer network, resulting in the Flow_amount. In addition, to calculate the flow paths within the catchment of the lake, the Stream to feature spatial analysis tool was utilized with FlowDirBrus and Flow_amount as inputs and the Flow_paths feature class layer as the final. Lastly, the symbology was set to refine the outcome and create a visually friendly layer, as shown in Figure 6.

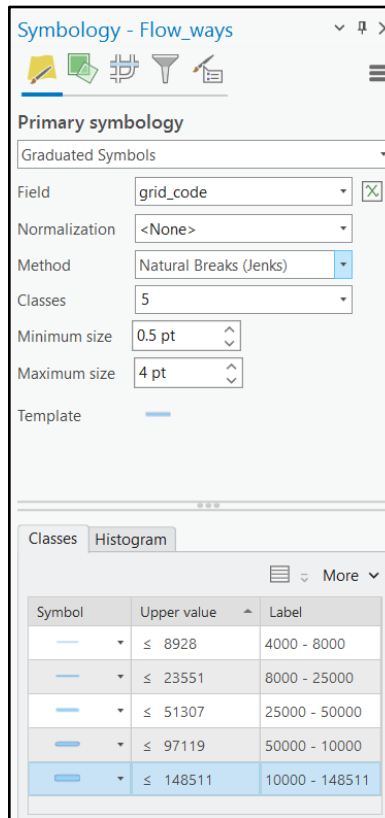


Figure 6: Flow paths Feature Class symbology. ArcGIS Pro.

4.1.2 Building the Geospatial interactive map

To create an interactive geospatial map, a geoprocessing tool named Runoff Flow Calculator was developed using ModelBuilder. The first step was to design the workflow model in ModelBuilder, as shown in Figure 8. Next, the model's parameters (P) were set. The variables that were set as parameters will appear in the geoprocessing tool, allowing for different inputs such as data, values, and expressions. This makes it possible to create an interactive geospatial map with varying inputs. (ArcGisPro, 2022c).

The parameters of the Runoff Flow Calculator Geo-spatial tool include DTM, Pour point, Flow accumulation, Expression, Input raster or constant value, Segregated ways, and Flow amount. The geoprocessing tool is shown in Figure 7.

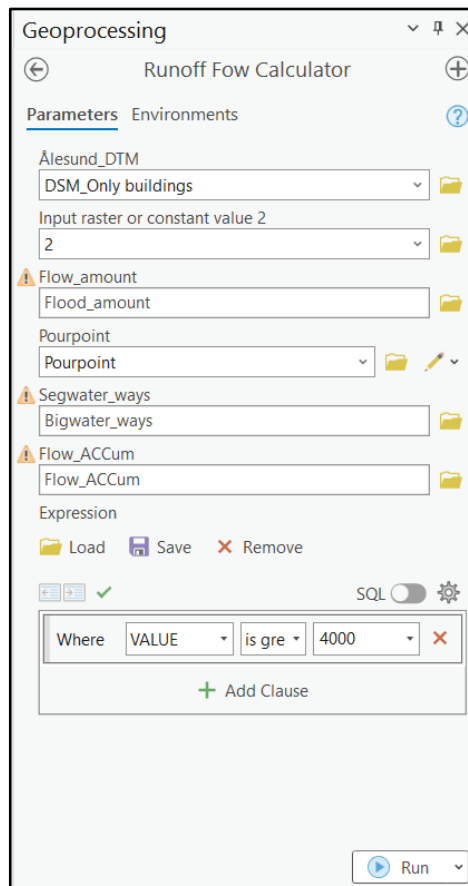


Figure 7: Runoff Flow Calculator Geo-spatial tool. ArcGIS Pro.

Runoff Flow Calculator Geo-spatial Tool

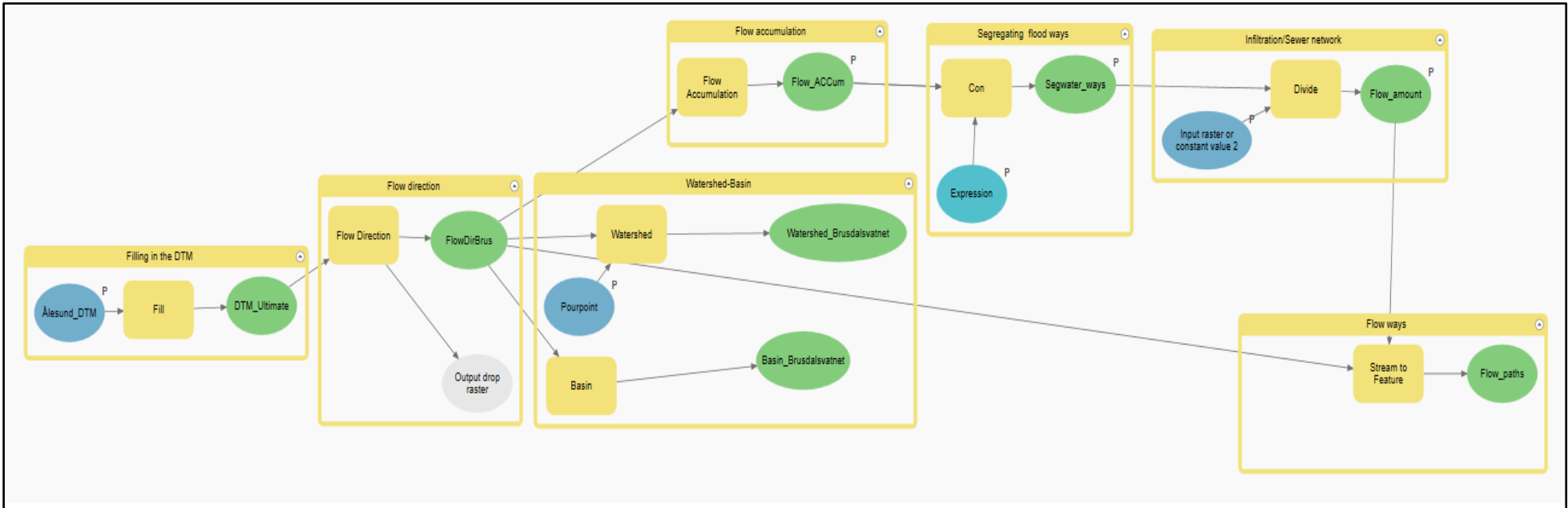


Figure 8: Geoprocessing tool showing ModelBuilder’s workflow. ArcGIS Pro.

4.2 Objective 2: Quantify the volume of runoff to Brusdalsvatnet from Highway E-39, accounting for present and future rainfall scenarios

4.2.1 Computing the Basin, watershed, and subcatchments of the study area

Soil and water assessment tool (SWAT), an application of ArcMap 10.5, was used to compute the study area's basin, watershed, and subcatchments.

Firstly, the Watershed Delineator tool was activated in order to insert the inputs and setup parameters. Subsequently, the DTM raster of the study area and the Mask were inserted, then the X-Y unit and Z-unit were set to meters (DTM projection setup). The DTM Terrain values vary in the range from -0.340 to 576.455. Besides, the mask used is a polygon feature class that was created previously and adjusted to Highway E-39. Thereafter, flow direction and flow accumulation were calculated, whereafter, the stream definition area outcome was 10 (ha). This approach seems to be the most useful since the stream definition was computed with different areas such as 2(ha), 12(ha), 15(ha), 18(ha), 25(ha), 35(ha), being the most suitable Area: 10 (ha). Next, the stream network was computed, resulting in the reaches and outlets of the study area. Using the "Edit manually" option in the Outlet and Inlet Definition tab, only the reaches and outlets related to highway E-39 were selected. After defining the outlets, the watershed was delineated, and the sub-basin parameters were calculated. The outcome of the Watershed Delineator tool was as follows: the study area basin, 22 reaches, 22 longest paths, 22 subcatchments, and 22 monitoring points (outlets), one for each subcatchment.

4.2.2 Watershed delineation and projection of future rainfall scenarios

Storm Water Management Model (SWMM) was the chosen engine to model the water runoff quantity simulations at Brusdalsvatnet.

Firstly, the Project default options were set up, with Horton as the chosen infiltration model and Dynamic wave as the routing method. Next, the previously delineated SWAT watershed image was imported as a .PNG file and used as a background to delineate the watershed and the 22 subcatchments using the Add object tool. Once the subcatchments were delineated and named (from S1 to S22), the outfalls were created (from Out 1 to Out 22). As shown in Figure 9, one outfall was designated for each.

Hydrological Model at Brusdalsvatnet

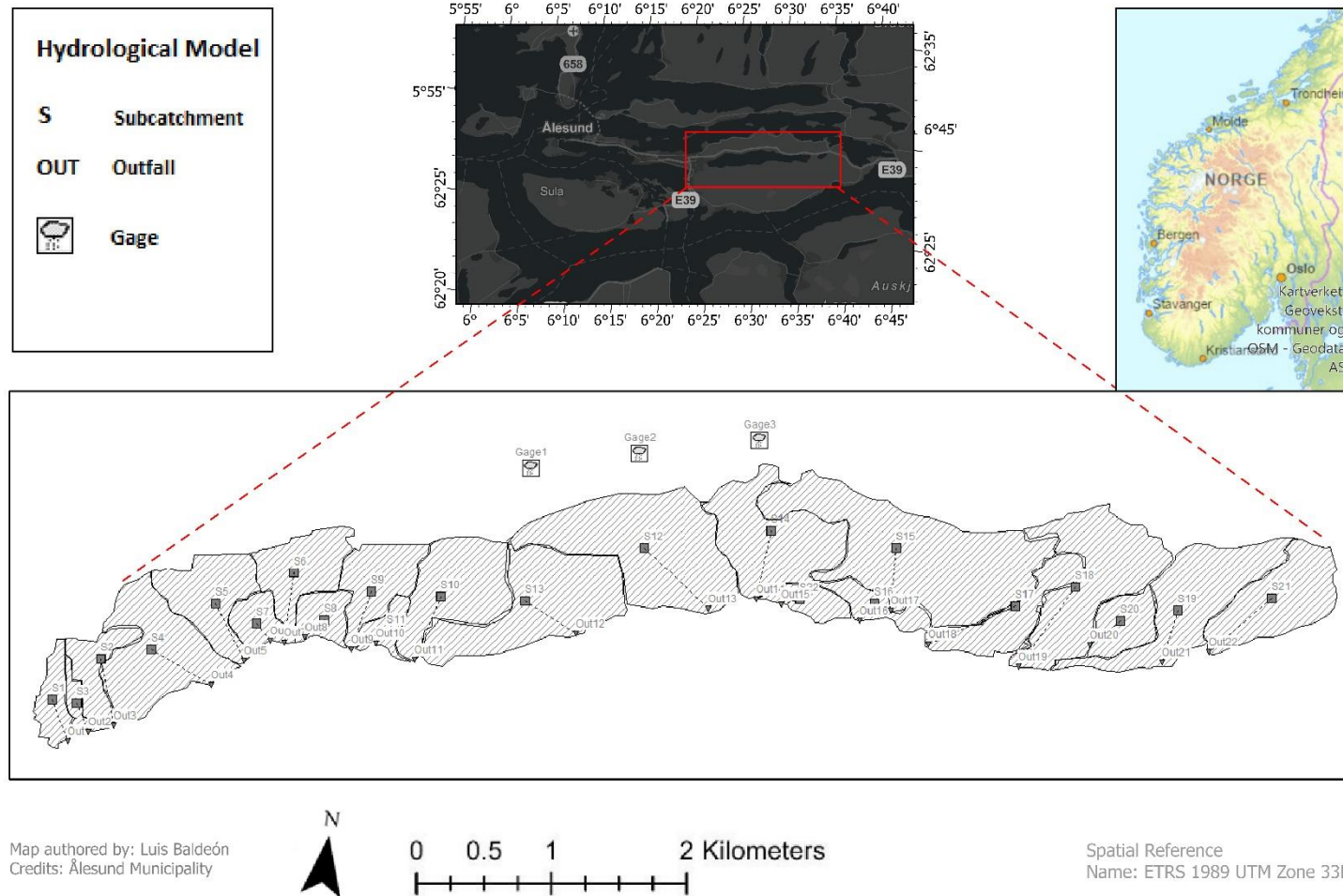


Figure 9: Subcatchments, Outfalls and Gages overview at Brusdalsvatnet lake. SWMM.

Next, the variables Area, % Slope, % Impervious Surfaces, and Width were calculated for each subcatchment. For this purpose, ArcGIS Pro (ModelBuilder) was used to calculate Area, % Slope, and % Impervious Surfaces. Width, on the other hand, was obtained from SWAT, representing the average width of tributary channels in meters. (S.L. NEITSCH, 2000). To calculate Area, the Extract by Mask tool was used, which extracts each subcatchment from the DTM of the study area using the DTM raster and the polygon feature class of the subcatchments as inputs.

Further, the Raster to Polygon tool was used to convert the raster output of the previous step (e.g., S1, subcatchment 1) to a polygon. This step is necessary in order to use the S1 feature class as input in the next tool, Dissolve (Dissolve Fields: GRIDCODE), since this tool only accepts feature layers as input. (ArcGisPro, 2022a). The Dissolve tool was used to dissolve the polygon based on the GRIDCODE field, and the output was saved as a feature class layer named S1_Dissolve. Subsequently, the area of the subcatchment was calculated from the attribute table of the S1_Dissolve layer. This same workflow was applied to each of the 22 subcatchments. It is important to note that the previous example was only for the first subcatchment (S1). The complete workflow is shown in Figure 10.

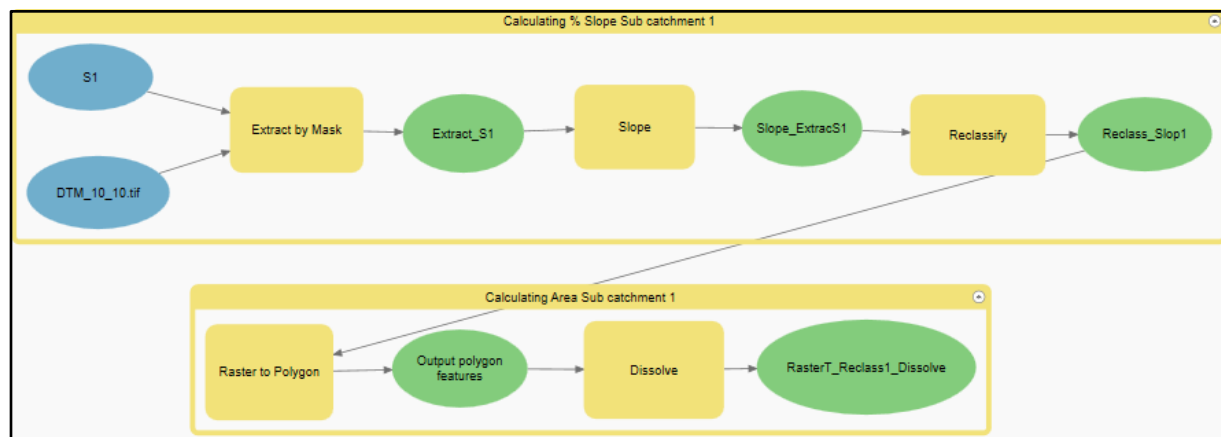


Figure 10: Slope and Area computing process. ModelBuilder workflow. ArcGIS Pro.

In order to compute the % slope for each subcatchment, the following tools were used: Extract by Mask, Slope, and Reclassify, as shown in Figure 10. The Extract by Mask tool was used to extract the DTM values for each subcatchment, the Slope tool was used to calculate the slope in degrees, and the Reclassify tool was used to assign suitable values to slope intervals, as shown in Figure 11.

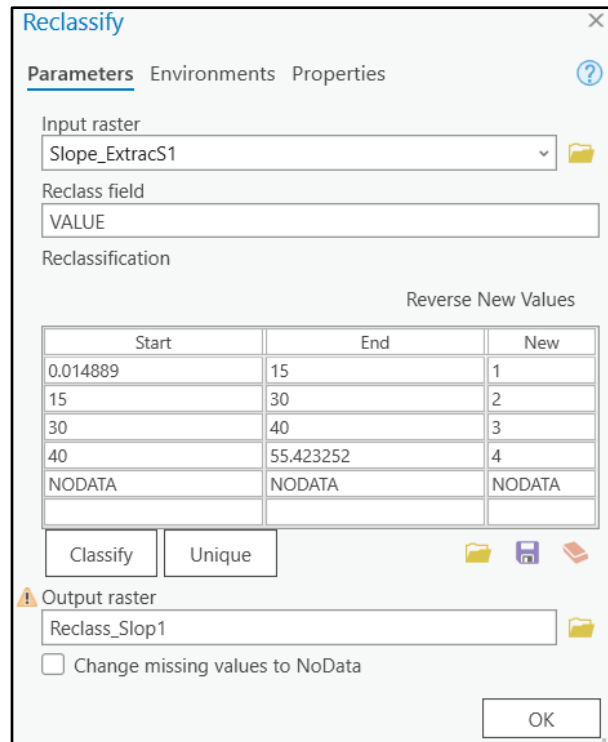


Figure 11: Setting up suitable interval values to Slope. ArcGIS Pro.

Finally, the Impervious surface percentage was computed using the Clip and Dissolve geospatial analysis tools. The Landuse E-39 feature class, which was pre-processed, was used as the input, and each subcatchment's polygon was introduced one by one as the Clip feature, resulting in LanduseS2_Clip. This was then used as the input to the Dissolve tool, with Gridcode set as the Dissolve Field. The resulting feature class layer was named LanduseS2_Clip_Dissolve, as shown in Figure 12. The landuse types were identified by checking which grid code number corresponded to each landuse type, allowing for the calculation of the area of each landuse type using the Attribute table of LanduseS2_Clip_Dissolve. The data in the Attribute table was processed in Excel to calculate the % landuse area and % Impervious/Pervious surface, as shown in Table 4.

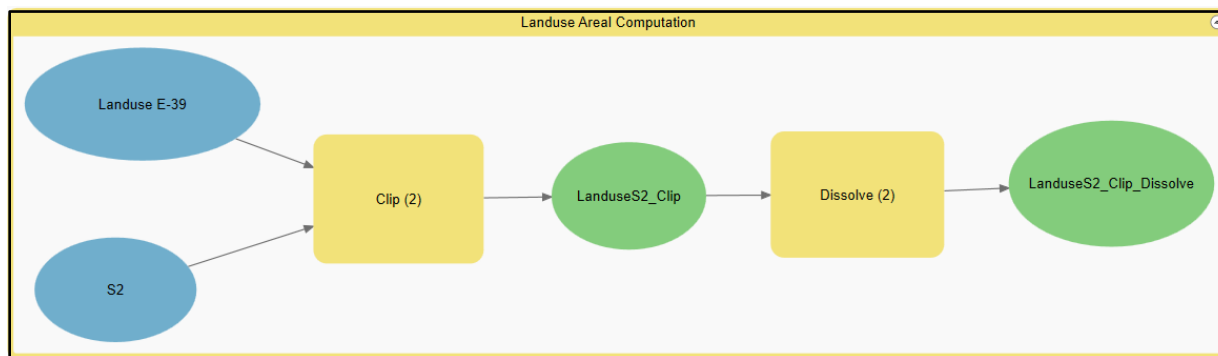


Figure 12: Landuse areal computation. ModelBuilder workflow. ArcGIS Pro

Table 4: Landuse area and Pervious-Impervious area calculation in subcatchment S2.

| AR50 Classification | Gridcode | Area (ha) | Landuse areal % | Type Surface | Impervious-Pervious Surface % |
|---------------------|--------------|-----------|-----------------|-------------------|-------------------------------|
| E-39 | 8 | 0.02 | 0.14 | <i>Impervious</i> | 25.54 |
| 10-Developed | 4 | 4.00 | 25.40 | | |
| 81-Freshwater | 6 | 0.08 | 0.51 | | 74.46 |
| 20-Agriculture | 3 | 0.87 | 5.53 | <i>Pervious</i> | |
| 30-Forest | 1 | 10.77 | 68.42 | | |
| Area S2 | Total | 15.74 | 100% | | 100% |

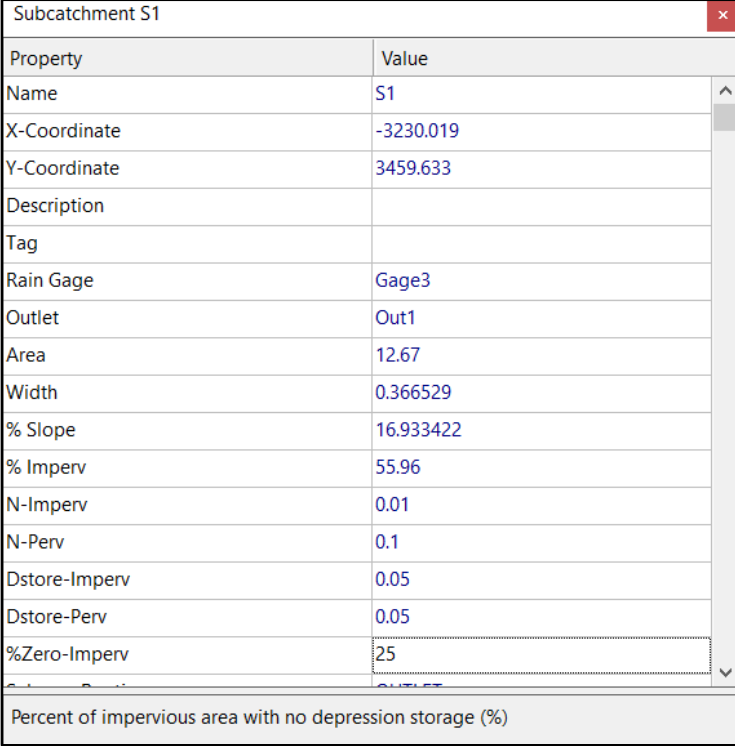
Next, rain gauges were created. Three rain gauges were used in this study and were named as follows: Gage 1, Gage 2, and Gage 3, each representing a different rainfall scenario.

Gage 1: This rain gauge used precipitation data from Ålesund in 2021, representing the first rainfall scenario. The data was provided by MET Norway.

Gage 2: This gauge is based on RCP8.5 emission scenario and represents rainfall for the period 2031-2060, with a 20% increase in precipitation projection.

Gage 3: This gauge is also based on RCP8.5 emission scenario and projects rainfall for the period 2060-2100, with a 30% increase in precipitation projection.

Then, as shown in Figure 13, rain gauges and outlets were assigned, and values for area, width, % slope, and % impervious were inserted for each subcatchment. However, the other parameters of the subcatchments have default values.



| Property | Value |
|---|-----------|
| Name | S1 |
| X-Coordinate | -3230.019 |
| Y-Coordinate | 3459.633 |
| Description | |
| Tag | |
| Rain Gage | Gage3 |
| Outlet | Out1 |
| Area | 12.67 |
| Width | 0.366529 |
| % Slope | 16.933422 |
| % Imperv | 55.96 |
| N-Imperv | 0.01 |
| N-Perv | 0.1 |
| Dstore-Imperv | 0.05 |
| Dstore-Perv | 0.05 |
| %Zero-Imperv | 25 |
| Percent of impervious area with no depression storage (%) | |

Figure 13: Subcatchments parameters window. SWMM.

4.2.3 Water runoff modelling

The last step is to analyze the performance of the model by running a simulation. To do this, it is necessary to set up the simulation options, which establish how the analysis will be carried (Lewis A. Rossman, 2022, p. 31). Therefore, in the Simulation options, on the General tab, Rainfall/Runoff was selected as the Process Model, Dynamic Wave as the Routing Model, and Horton as the Infiltration Model. Then, on the Dates tab, Start Analysis was set to 01/01/2021, Start Reporting was set to 01/01/2021, End Analysis was set to 12/31/2021, Time was set to 06:00, Start Sweeping was set to 01/01, End Sweeping was set to 12/31, and Antecedent Dry Days was set to 5. Finally, in the Time Steps tab, the Reporting Step was set to 1 day, and the Routing Step was set to 20 seconds.

This model has no calibration due to a lack of observed data. Given that, parameters such as Runoff volume, Peak runoff, and Total infiltration cannot be compared with on-site results.

For the purpose of this study, the model simulation will be validated by using the standards established in the SWMM manual. According to the manual, the results have to reflect reasonable

mass balance. Hence, “the errors represent the percent difference between initial storage + total inflow and final storage + total outflow for the entire drainage system. If they exceed some reasonable level, such as 10 percent, then the validity of the analysis results must be questioned”. The results generated by running SWMM are continuity errors for runoff, flow routing, and pollutant routing (S.L. NEITSCH, 2000, p. 158).

4.2.4 Emissions scenarios justification

Climate variables play a critical role in the hydrological processes that take place in the catchments, without neglecting the importance of the catchment’s characteristics. In accordance with that, climate variables such as temperature, precipitation, and shortwave and longwave solar radiation have to be considered. Furthermore, it has to be considered to get a better understanding of the processes that are taking place within a catchment (Mohammed et al., 2019, p. 679).

To carry out the study's second and third objectives, reliable precipitation serial data is required. In this study, the precipitation data were obtained from The Norwegian Meteorological Institute (MET Norway) for the period from 01.01.2021 to 31.12.2021. According to (Hanssen-Bauer et al., 2017), In Norway, an increment in the annual average precipitation of 18% is predicted for the period from 1971–2000 to 2071–2100. Furthermore, according to NCCS, in the worst-case scenario (RCP8.5), precipitation will increase by about 10% to 20% from the reference period 1971-2000 to 2031-2060. Whereas from the same reference period to 2071-2100, the precipitation will increase in the range of 20% to 30% in Møre and Romsdal County (CH 10-20 1.41-43 Meehl et al., 2007; NCCS, 2022). The projection computed in this study will be based on the worst-case scenario (RCP8.5), as recommended by the Norwegian government. Consequently, the highest value of the NCCS projections will be used as input in this model, as shown in Table 5.

Table 5: Rainfall scenarios based on RCP8.5 emission projection.

| Period | Emission projection | Precipitation increase % |
|-----------|---------------------|--------------------------|
| 2021 | Rainfall data | -- |
| 2031-2060 | RCP8.5 | 20 |
| 2060-2100 | RCP8.5 | 30 |

4.3 Objective 3: Quantify Heavy Metals load associated with runoffs, accounting for present and future rainfall scenarios

4.3.1 Heavy Metals samples

SWMM was used as the engine to compute the water quality analysis model. The data source for this analysis was the project report "Concentration of heavy metals in the catchment Brusdalsvatnet" by NTNU. This report presents the results of heavy metals measurements in soil and water samples taken at Brusdalsvatnet, with sampling carried out in the Northern and Southern sections of the lake from September to October 2021 (Seidu, 2021, p. 2).

The water samples were classified according to the "Classification levels of heavy metals in water" from Miljø-direktoratet 2020, as shown in Appendix A. Similarly, the soil samples were classified according to the "Classification levels of heavy metals in soil" from Miljø-direktoratet 2020, as presented in Appendix (Seidu, 2021, pp. 6,7).

The measurements used as input for SWMM were taken from the following sample points: NE1, Agric, NW1, and NE3. Soil and water samples were taken at NE1, Agric, and NW1, while only soil samples were taken at NE3. Table 6 and Table 7 present the heavy metals measurement values for each location.

Table 4: Concentration levels of heavy metals in water (Seidu, 2021, p. 14).

| Location | Zinc (ug/l) | Lead (ug/l) | Cadmium (ug/l) | Chromium (ug/l) | Copper (ug/l) | Nickel (ug/l) |
|----------|-------------|-------------|----------------|-----------------|---------------|---------------|
| NE1 | 32 | 1.4 | 0.053 | 2.1 | 6 | 1.9 |
| Agric | 34 | 4 | 0.06 | 4.8 | 13 | 4.4 |

Table 5: Concentration levels of heavy metals in soil (Seidu, 2021, p. 17).

| Location | Zinc (mg/KgTS) | Lead (mg/KgTS) | Cadmium (mg/KgTS) | Chromium (mg/KgTS) | Copper (mg/KgTS) | Nickel (mg/KgTS) |
|----------|----------------|----------------|-------------------|--------------------|------------------|------------------|
| NW1 | 38 | 6 | <0.20 | 28 | 14 | 16 |
| NE3 | 70 | 11 | <0.21 | 41 | 37 | 34 |

4.3.2 Water Quality Analysis

In order to carry out water quality analysis in SWMM, it is necessary to identify the pollutants to be analyzed. In this case, they include Zinc, Lead, Cadmium, Chromium, Copper, and Nickel (Seidu, 2021).

To begin the analysis, the Pollutant Editor window was opened, and the name of each heavy metal was entered, using composed names that include the chemical name and the location where the sample was taken. In total, there were 24 measurements with names such as ZincNE1, LeadNE1, CadmiumNE1, ChromiumNE1, CopperNE1, NickelNE1, ZincAgric, LeadAgric, CadmiumAgric, ChromiumAgric, CopperAgric, NickelAgric, ZincNW1, LeadNW1, CadmiumNW1, ChromiumNW1, CopperNW1, NickelNW1, ZincNE3, LeadNE3, CadmiumNE3, ChromiumNE3, CopperNE3, and NickelNE3. After that, the measurement unit chosen in this thesis, both for water samples and soil samples it, was (*ug/l*). In addition, the *Rain concentration* value must be entered (this process was repeated for each heavy metal measurement). After this, the landuse categories that generate these heavy metals were defined, *Residential_Impervious* and *Underdeveloped_Pervious*, the two created categories.

Next, the parameters for the Buildup and Washoff functions were set to determine the quality of runoff for each landuse category. For *Residential_Impervious*, the Max. Buildup was set to 50, Rate Constant to 1.0, Power/Sat. Constant to 1, and Normalizer to AREA. The Washoff parameter was set to Function Event-mean concentration washoff EMC, and Coefficient to 100. For *Underdeveloped_Pervious*, the Max. Buildup was set to 25, Rate Constant to 0.5, Power/Sat. Constant to 1, and Normalizer to AREA. The Washoff parameter was set to Function Event-mean concentration washoff EMC, and Coefficient to 50. These parameter values are based on SWMM's manual version 5.2 (S.L. NEITSCH, 2000, p. 43).

The chosen function for the pollutant Buildup was the Power Function (POW), which means that “Pollutant buildup (B) accumulates proportionally to time (t) raised to some power until a maximum limit is achieved,

$$B = \text{Min} (C_1, C_2 t^{C_3}) \quad (1)$$

“where C_1 = maximum buildup possible (mass per unit of area or curb length), C_2 = buildup rate constant, and C_3 = time exponent” (S.L. NEITSCH, 2000, p. 76).

Additionally, the Washoff chosen function was Event Mean Concentration (EMC).”This is a special case of Rating Curve Washoff where the exponent is 1.0 and the coefficient C_1 represents the washoff pollutant concentration in mass per liter (Note: the conversion between user-defined flow units used for runoff and liters is handled internally by SWMM). In each case, the buildup is continuously depleted as washoff proceeds, and washoff ceases when no more buildup is available” (S.L. NEITSCH, 2000, p. 77).

The formulation of Event Mean Concentration (EMC) is given as follows,

$$W_{emc} = C_{3emc} \quad (2)$$

where W_{emc} is the amount of washoff (M/L^3) and C_{3emc} is the washoff coefficient (M/L^3). The washoff coefficient C_{3emc} represents the washoff pollutant concentration in mass per liter” (Gülbaz, 2012, p. 4).

The final steps before running the simulation are, firstly, to assign a combination of landuse and percentage of area to each subcatchment. This will be based on the values previously computed in ArcGIS Pro and Excel. Secondly, the initial buildup must be defined so that it can be washed off while the event is running. Consequently, the initial buildup will be based on the number of Antecedent Dry Days for the period from August 27th, 2021, to August 31st, 2021, which is five dry days.

4.3.3 Water quality modelling

Lastly, in order to run the simulation, it is necessary to follow the same procedure specified in Section 4.2.3. Additionally, in the Simulation Options window in the General tap, the Process Model Water quality must be checked.

5. Results and Analysis

The results of this study are based mainly on rainfall data, landuse, hydrological network, and DTM from Ålesund municipality. This data is the most critical regarding the computation of outcomes and results. Besides, the rainfall data is for the period from 01.01.2021 to 31.12.2021, having antecedent dry days of *5 days*. According to the results of SWMM, during this period it was registered 44 precipitation events, with a Minimum event mean value of 0.01 mm/hr and a Maximum event mean value of 0.59 mm/hr, as well as a standard deviation of 0.18. Likewise, it

registered 21 runoff events, with a Minimum event mean value of 0.02 CMS and a Maximum event mean value of 0.17 CMS with a standard deviation of 0.04.

Figure 14 shows the precipitation intensity in the range of 0.01mm/hr to 0.15 mm/hr, having a 50 % probability of occurring during 2021. On the other hand, events with more precipitation intensity in the range of 0.5 mm/hr to 0.55 mm/hr have a 7 % probability of taking place in the same period.

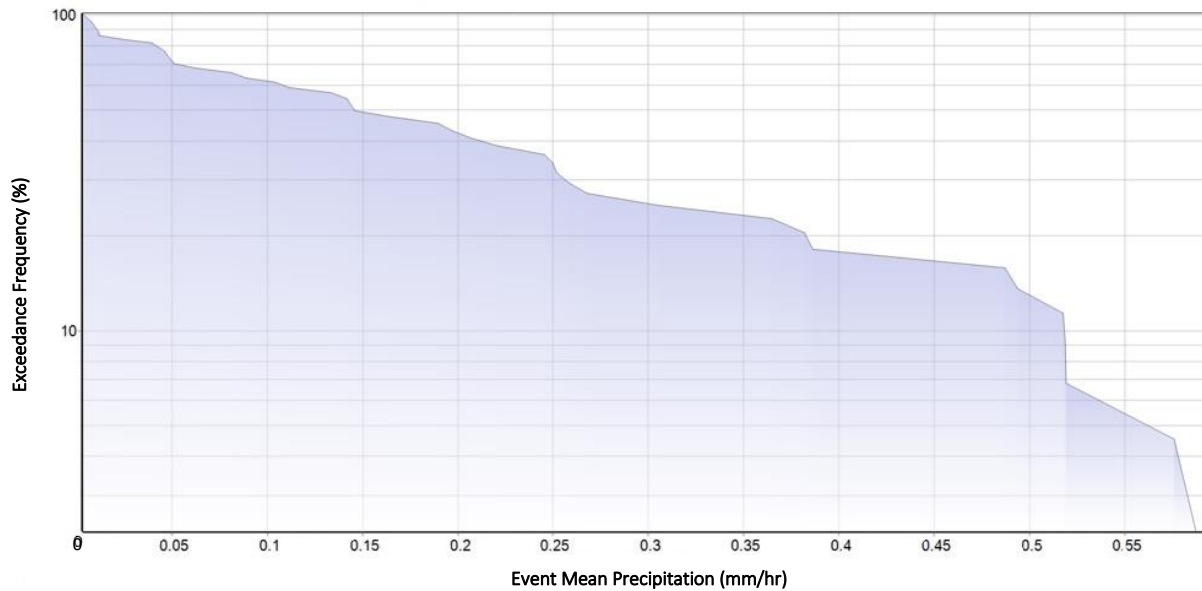


Figure 14: Precipitation intensity related to the frequency of the events. Gage 1. SWMM.

Furthermore, Figure 15 shows that there is a 65% probability of runoff events with a volume between 0.02 CMS and 0.06 CMS occurring in 2021. Conversely, events with high runoff volumes have a 10% probability of taking place during the same period.

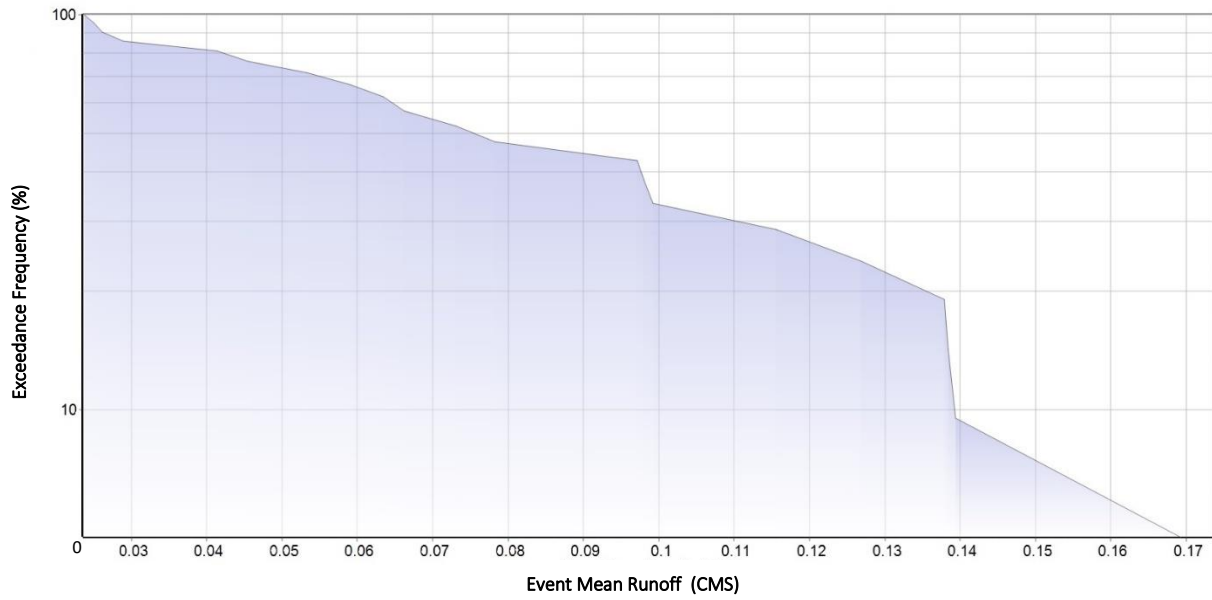


Figure 15: Runoff volume related to the frequency of the events. Gage 1. SWMM.

This study does not consider factors such as temperature, evaporation, evapotranspiration, snow melt, soil, or sewer network due to the complexity that it entails. However, the results are reliable, as shown later in this section.

5.1 Geospatial map

Runoff Pathways - Brusdalsvatnet Lake

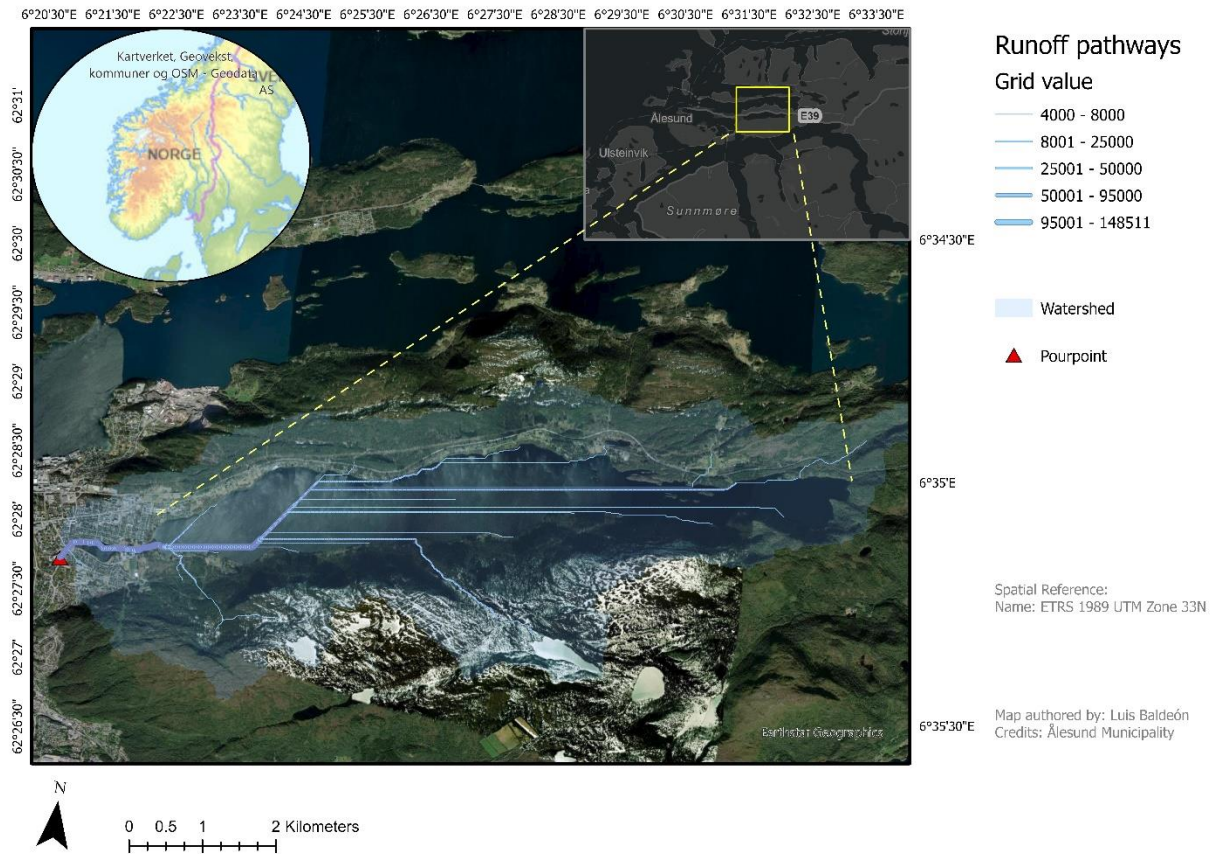


Figure 16: Runoff flow at Brusdalsvatnet, Ålesund municipality.

5.2 Geospatial Tool for Calculating Runoff Flow

The Geospatial Tool for Calculating Runoff Flow was created with the objective of allowing the same computation that was performed at Brusdalsvatnet to be conducted in different lakes, with only the DTM being required to be changed. Once the input data is entered, parameters such as flow accumulation, pour point, the expression to segregate floodways and flow amount can be adjusted to make the map interactive and adaptable. The geospatial tool is depicted in Figure 7 in Section 4.1.2.

5.3 SWMM model's simulation reliability

The results of the model simulation for both quantity and quality from Gage 1, Gage 2, and Gage 3 showed high reliability. Moreover, the results indicated good mass balance continuity errors for both runoff and routing. Additionally, regarding quality routing continuity, the pollutants showed a good balance between inflow and outflow, as shown in Table 8.

Table 8: Model simulation quality assessment.

| Model Simulation | Runoff continuity error % | Routing continuity error % | Model simulation quality |
|-------------------------|----------------------------------|-----------------------------------|---------------------------------|
| Runoff Gage 1 | -0.002 | 0.00 | Good |
| Runoff Gage 2 | -0.002 | 0.00 | Good |
| Runoff Gage 3 | -0.002 | 0.00 | Good |
| Quality routing Gage 1 | -0.001 | 0.00 | Good |
| Quality routing Gage 2 | -0.002 | 0.00 | Good |
| Quality routing Gage 3 | -0.002 | 0.00 | Good |

The Standard recommended threshold ranges from 0 % to 10 %. SWMM (S.L. NEITSCH, 2000, p. 158).

5.4 Stormwater runoff entering Brusdalsvatnet from Highway E-39

Based on the results obtained from SWMM, the rainfall volume in the source data resulted in a proportional increase in runoff at Brusdalsvatnet. This increase is mainly driven by three factors: impervious surfaces from developed areas, including Highway E-39, infiltration, and the steep gradient. Similarly, Figure 17 demonstrates a strong correlation between rainfall volume and runoff volume in Ålesund municipality during the year 2021.

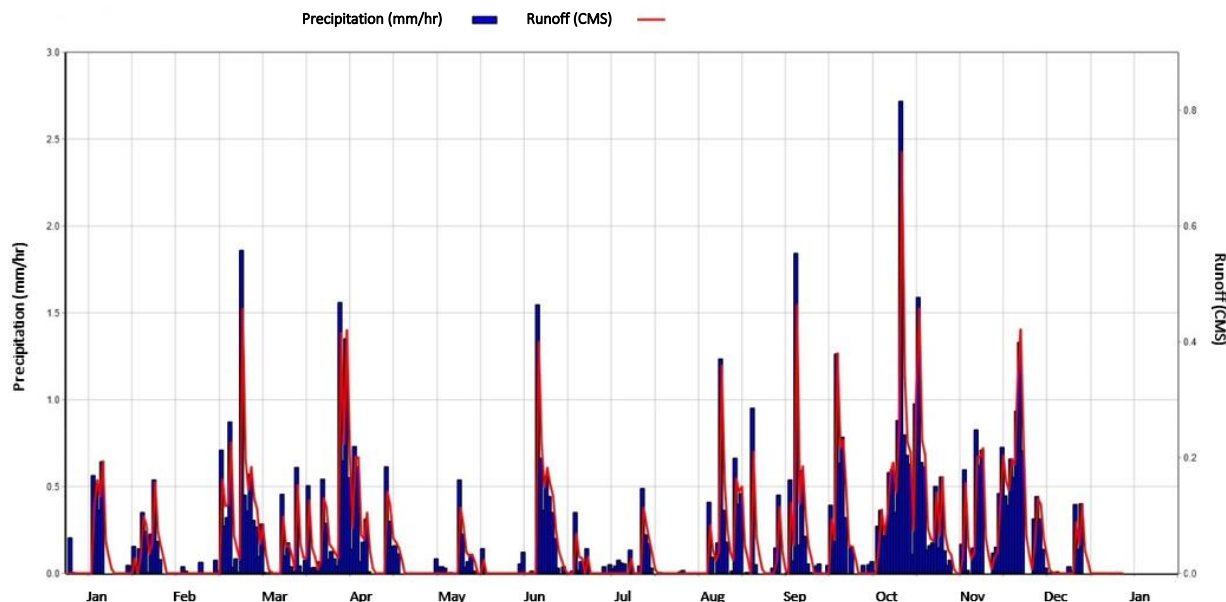


Figure 17: Close Rainfall- Runoff relationship. Ålesund 2021.Gage 1. SWMM.

The simulated runoff volume obtained from SWMM shows that all three rainfall scenarios have total runoff values that fall within the average runoff range registered in Norway in 2014 (Hanssen-Bauer et al., 2017).

Table 9 presents the most notable results of the runoff assessment data, revealing that in Gage 1, Gage 2, and Gage 3, 17%, 21%, and 23% of the total rainfall turns into runoff, respectively. Therefore, the runoff volume increases by approximately 4% and 2% in Gage 2 and Gage 3, respectively.

Table 6: Runoff assessment data.

| Model Simulation | Rainfall Scenario | Rainfall Increase (%) | Total Rainfall (mm) | Total Infiltration (mm) | Total Runoff (mm) | Runoff from rainfall (%) | Runoff Increase (%) |
|------------------|-------------------|-----------------------|---------------------|-------------------------|-------------------|--------------------------|---------------------|
| Runoff Gage 1 | 2021 | - | 1742.5 | 1454.6 | 287.9 | 17 | -- |
| Runoff Gage 2 | 2031-2060 | 20 | 2091.0 | 1654.8 | 436.2 | 21 | 4 |
| Runoff Gage 3 | 2060-2100 | 30 | 2265.3 | 1745.7 | 519.6 | 23 | 2 |

The EPA Storm Water Management Model calculates the runoff coefficient, which is a dimensionless value that relates the amount of runoff to the amount of rainfall received. The value

range varies from 0.35 to 0.95, with higher values assigned to areas with high imperviousness and steep slopes and lower values assigned to areas with high infiltration capacity, such as permeable, well-vegetated areas (Board, 2011, p. 1). Figure 18 shows the outcomes of the Runoff coefficient analysis.

Table 10 presents the subcatchments S1, S2, S3, and S7 with the highest percent imperviousness values related to Gage 3. Additionally, Figure 20 shows the highest slope values corresponding to S9 and S14, followed by S2, S5, S6, S10, and S15 with a milder slope. These outcomes can explain the Runoff Coefficient results, as the highest values are registered in subcatchments with the largest impervious surfaces Table 10. This confirms that imperviousness plays a crucial role in explaining the interaction between rainfall and runoff. Figure 22 shows a close relationship between Total Runoff and Impervious surface, further confirming the Runoff Coefficient values. In like manner, Figure 19 shows the subcatchments which present the highest impervious surface values, hence S1, S2, S3, and S7. Alike, Figure 21 confirms the robust model results showing the subcatchments that present the highest Total runoff values, S1, S2, S3, and S7, confirming the simulations' reliability.

Table 7: Runoff Coefficient analysis of the subcatchments with the higher impervious surface percentage at Brusdalsvatnet. Using Gage 3 rainfall scenario.

| Sub catchment ID | Impervious surface (%) | Slope (%) | Total Rainfall (mm) | Total Infiltration (mm) | Total runoff (mm) | Impervious runoff (mm) | Runoff Coefficient (C)* |
|------------------|------------------------|-----------|---------------------|-------------------------|-------------------|------------------------|-------------------------|
| S1 Gage3 | 55.9 | 16.9 | 2265.3 | 742.5 | 1522.6 | 1267.5 | 0.67 |
| S2 Gage3 | 25.5 | 29.4 | 2265.3 | 1289.9 | 975.4 | 578.6 | 0.43 |
| S3 Gage3 | 55.0 | 10.1 | 2265.3 | 781.8 | 1483.2 | 1245.2 | 0.66 |
| S7 Gage3 | 23.8 | 19.6 | 2265.3 | 1335.5 | 929.8 | 539.2 | 0.41 |

*Range (C)= 0.35 - 0.95 (S.L. NEITSCH, 2000).

Subcatchments - Runoff Coefficient

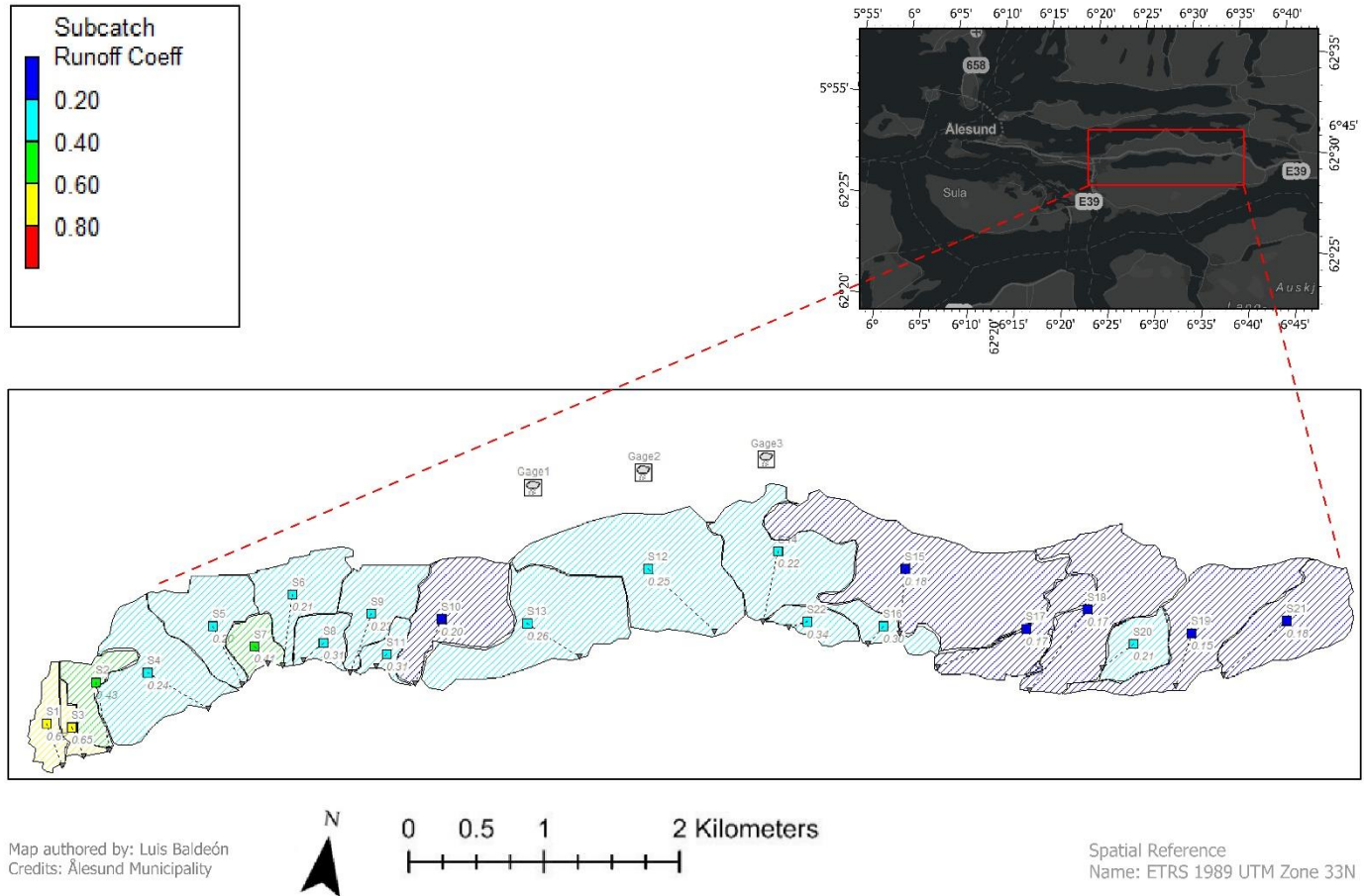


Figure 18: Runoff Coefficient (C) at Brusdalsvatnet, Ålesund. SWMM.

Subcatchments - Percentage Imperviousness

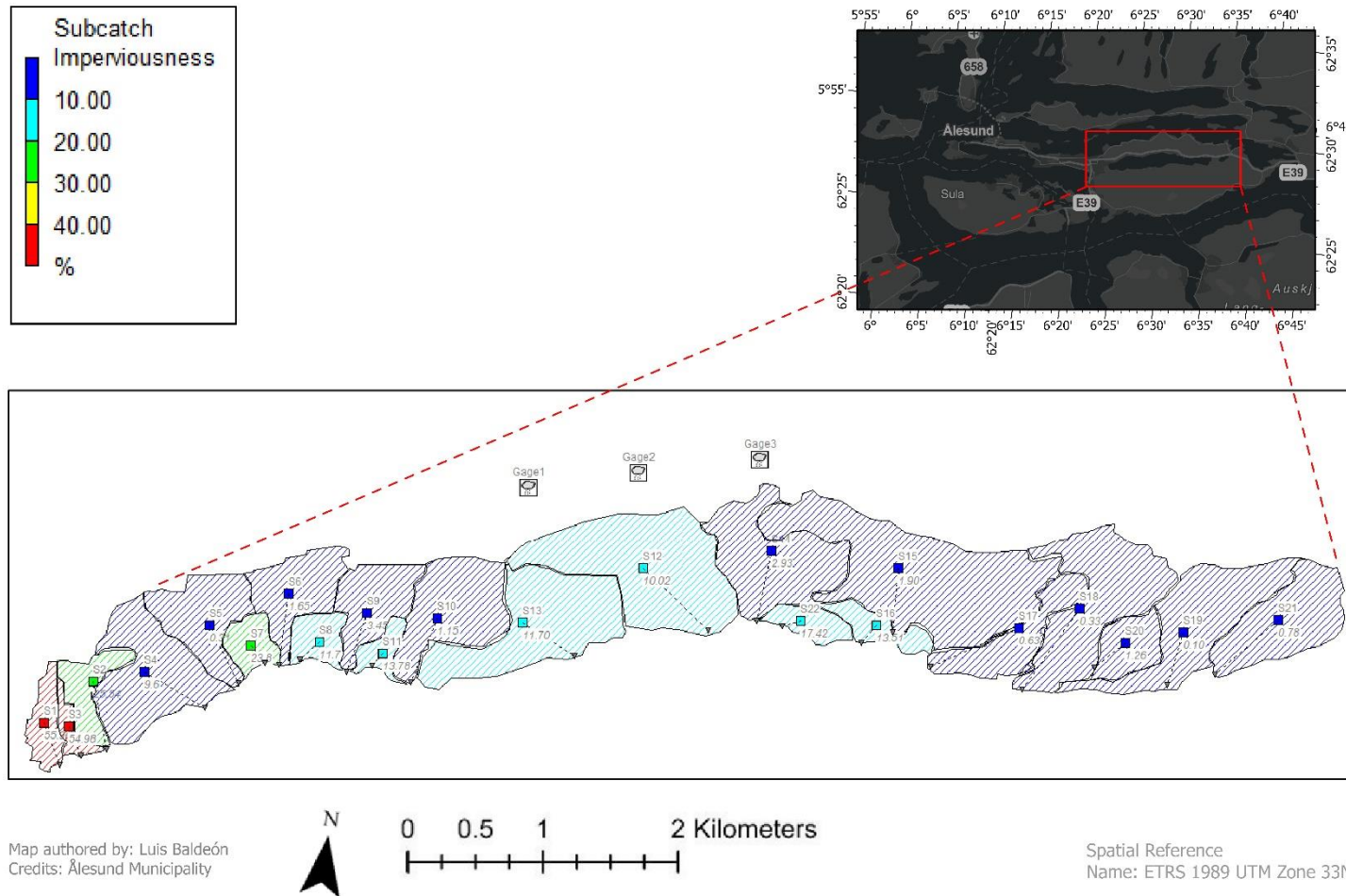


Figure 19: Percentage Imperviousness at Brusdalsvatnet, Ålesund. SWMM.

Subcatchments - Slope

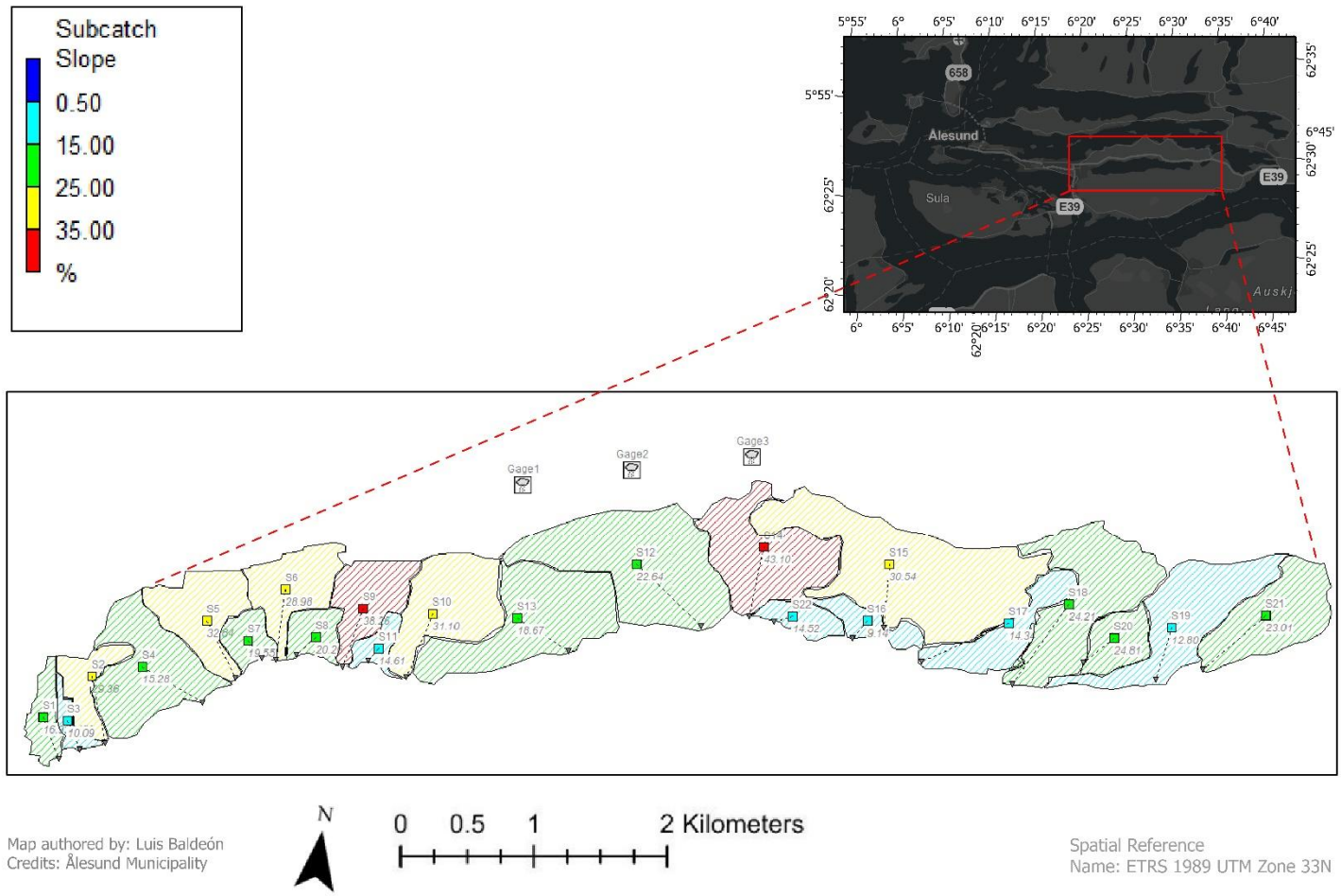


Figure 20: Subcatchments Slope at Brusdalsvatnet, Ålesund. SWMM.

Subcatchments - Total Runoff

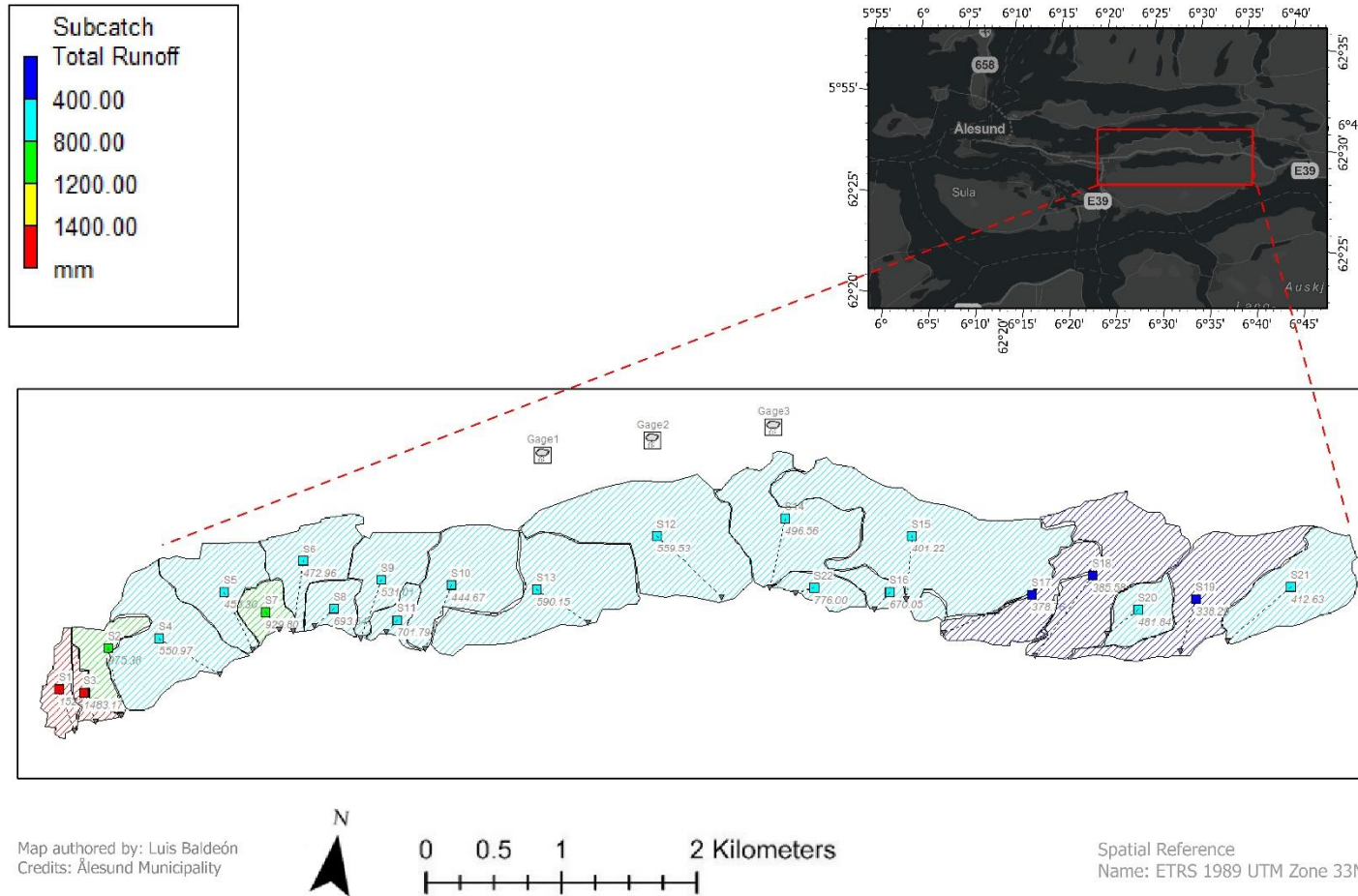


Figure 21: Subcatchments Total Runoff volume at Brusdalsvatnet, Ålesund. SWMM.

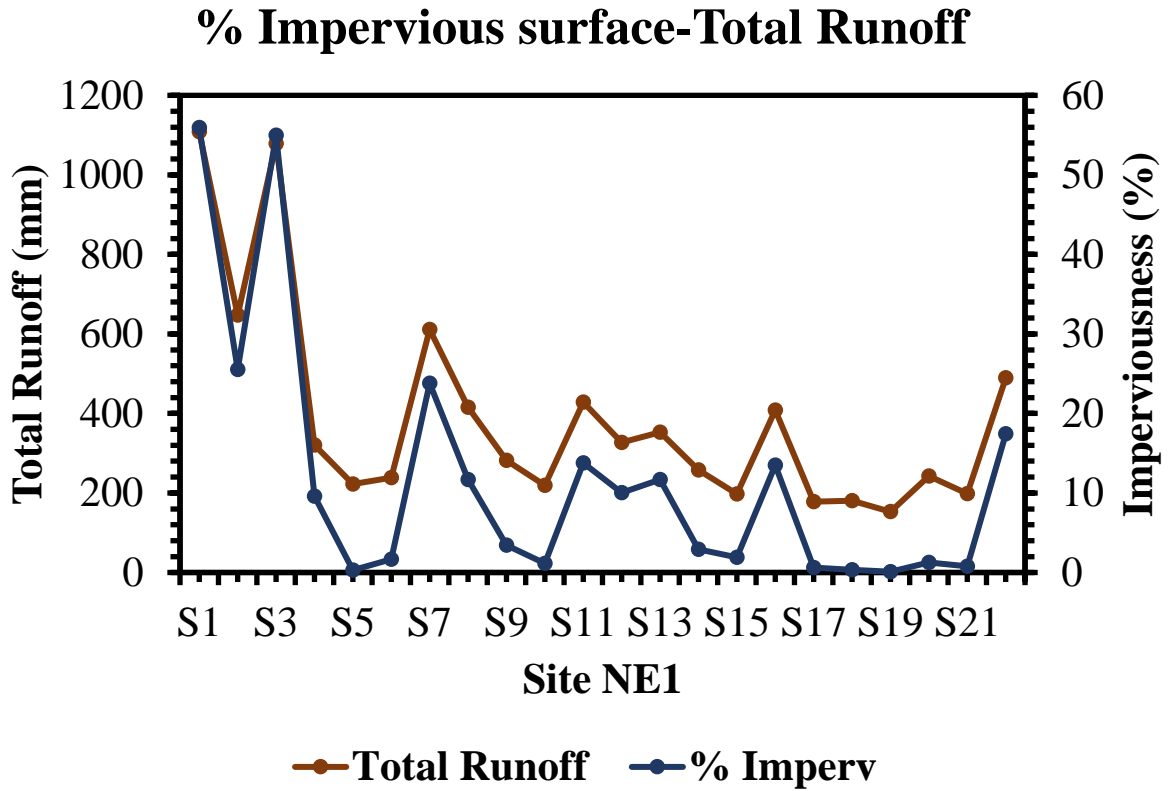


Figure 22: Relationship between Total Runoff and Impervious surface. Gage1.

Table 11 shows the extent of contribution that Highway E-39 has to the volume of runoff since this highway works as a means of runoff transport. It is possible to identify that subcatchments S1, S3, S7, and S11 have the highest runoff volume due to their paved area. Hence, they contribute the most to the increase of runoff volume and the potential transportation load of heavy metals. This will be further assessed in the next section.

Table 8: Pervious and Impervious areas showing the Total volume of runoff and the volume of runoff originating in Highway E-39. Using the *Gage 3* rainfall scenario.

| Sub catchment | Impervious surface Developed areas (%) | Impervious surface Highway E-39 (%) | Pervious surfaces Undeveloped areas (%) | Total runoff (mm) | Runoff from Highway E-39 (mm) | Sub catchment Total Area (ha) |
|----------------------|---|--|--|--------------------------|--------------------------------------|--------------------------------------|
| S1 | 55.1 | 0.9 | 44.0 | 1523 | 13.7 | 12.7 |
| S2 | 25.4 | 0.1 | 74.5 | 975 | 1.0 | 15.7 |
| S3 | 53.4 | 1.6 | 45.0 | 1483 | 23.7 | 6.8 |
| S4 | 8.7 | 0.9 | 90.4 | 551 | 5.0 | 54.6 |
| S5 | 0 | 0.3 | 99.7 | 455 | 1.4 | 31.9 |
| S6 | 1.5 | 0.2 | 98.3 | 473 | 0.9 | 30.3 |
| S7 | 22.4 | 1.4 | 76.2 | 930 | 13.0 | 12.5 |
| S8 | 10.4 | 1.3 | 88.3 | 694 | 9.0 | 12.7 |
| S9 | 3.0 | 0.5 | 96.6 | 531 | 2.7 | 28.1 |
| S10 | 0.9 | 0.2 | 98.9 | 445 | 0.9 | 43.8 |
| S11 | 12.1 | 1.7 | 86.2 | 702 | 11.9 | 7.7 |
| S12 | 9.4 | 0.6 | 90.0 | 560 | 3.4 | 75.6 |
| S13 | 10.5 | 1.2 | 88.3 | 590 | 7.1 | 69.2 |
| S14 | 2.3 | 0.6 | 97.1 | 497 | 3.0 | 52.2 |
| S15 | 1.2 | 0.7 | 98.1 | 401 | 2.8 | 110.6 |
| S16 | 13.3 | 0.2 | 86.5 | 670 | 1.3 | 13.4 |
| S17 | 0 | 0.6 | 99.4 | 379 | 2.3 | 33.2 |
| S18 | 0 | 0.3 | 99.7 | 386 | 1.2 | 64.4 |
| S19 | 0 | 0.1 | 99.9 | 338 | 0.3 | 57.3 |
| S20 | 0 | 1.3 | 98.7 | 482 | 6.3 | 18.4 |
| S21 | 0 | 0.8 | 99.2 | 413 | 3.3 | 43.5 |
| S22 | 17.4 | 0 | 82.6 | 776 | 0.0 | 11.5 |

5.5 Heavy Metals load associated with runoffs

Following the results of SWMM, there is a close relationship between the volume of runoff and heavy metals load in the study area. Furthermore, Figure 23 confirms that subcatchments' impervious surface is an important factor related to pollutants' transport and load. Figure 24 shows a close relationship between total runoff and pollutants washoff.

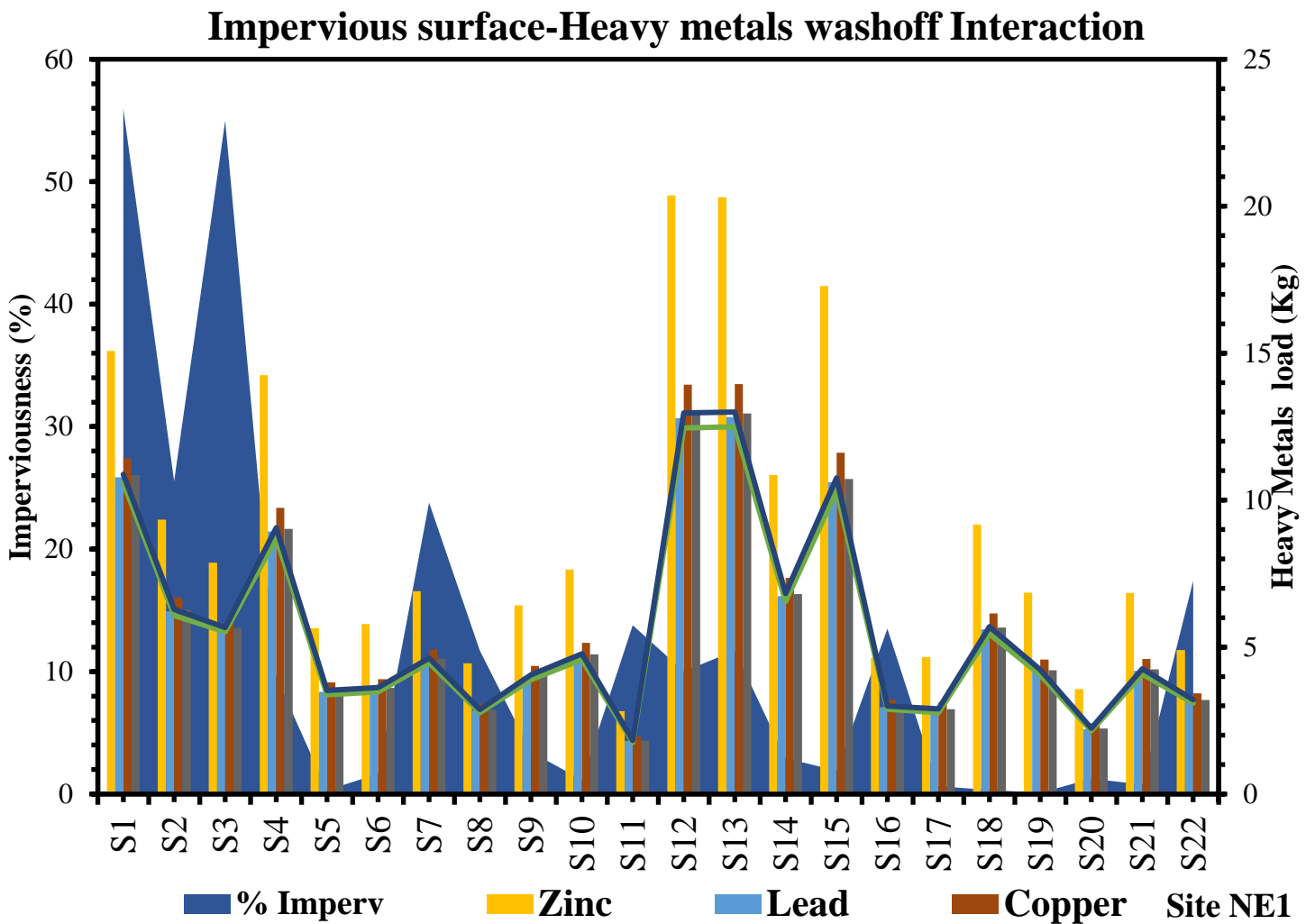


Figure 23: Subcatchments impervious surface impact in pollutants load. Gage 1.

Total Runoff-Heavy Metals Washoff

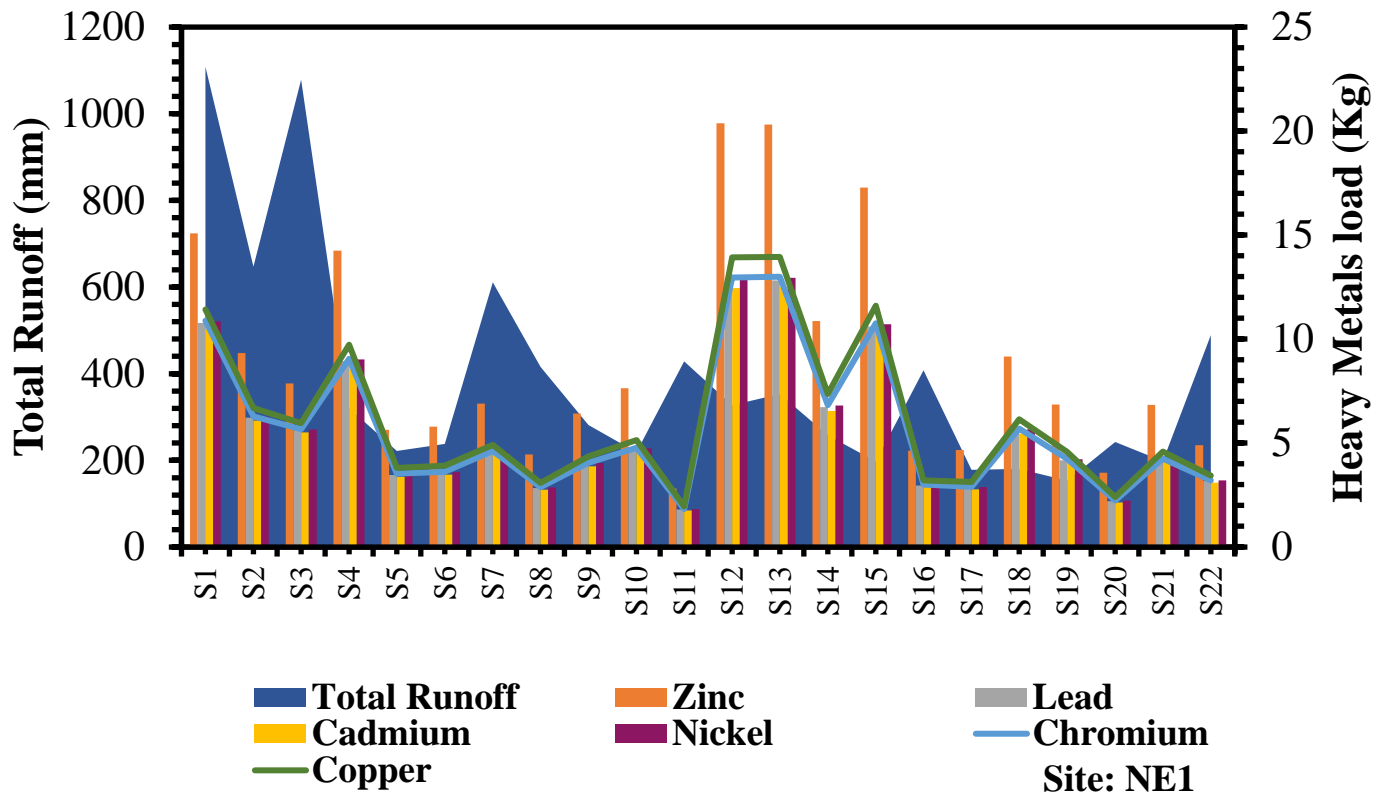


Figure 24: Subcatchments Total runoff- Pollutants washoff interaction. Gage 1.

The results of heavy metals loading confirm that intense rainfall associated with climate change directly affects the volume of runoff and, consequently, the loading of pollutants. In addition, the transport of pollutants through runoff pathways and factors such as impervious surfaces and steep gradients represents an effective means of pollutant transport that could potentially impact the quality of drinking water at Brusdalsvatnet.

According to the results of Gages 1, 2, and 3 shown in Figures 25, 26, and 27, respectively, there is a proportional increase in pollutant load in the three rainfall scenarios. This increment is closely related to the volume of runoff. Furthermore, the results show wide variation of heavy metal loads in the three systems. Zinc is the metal that presents the highest load value in all locations, followed by Chromium, Lead, Copper, Nickel, and Cadmium. Additionally, the results indicate a significant difference between heavy metal loads in water samples versus soil samples, with heavy metal accumulation being much larger in soil samples due to the higher rate of buildup during the

antecedent dry period. This leads to higher concentration values in soil samples. It should be noted that the graphs are represented in percentages. Although the load of Cadmium in soil samples is high, it is almost unnoticeable in the graphs due to its low value compared to other heavy metals. Figures 25, 26, and 27 are represented in percentages to provide a better perspective on pollutants' load, given the large load difference between water and soil samples.

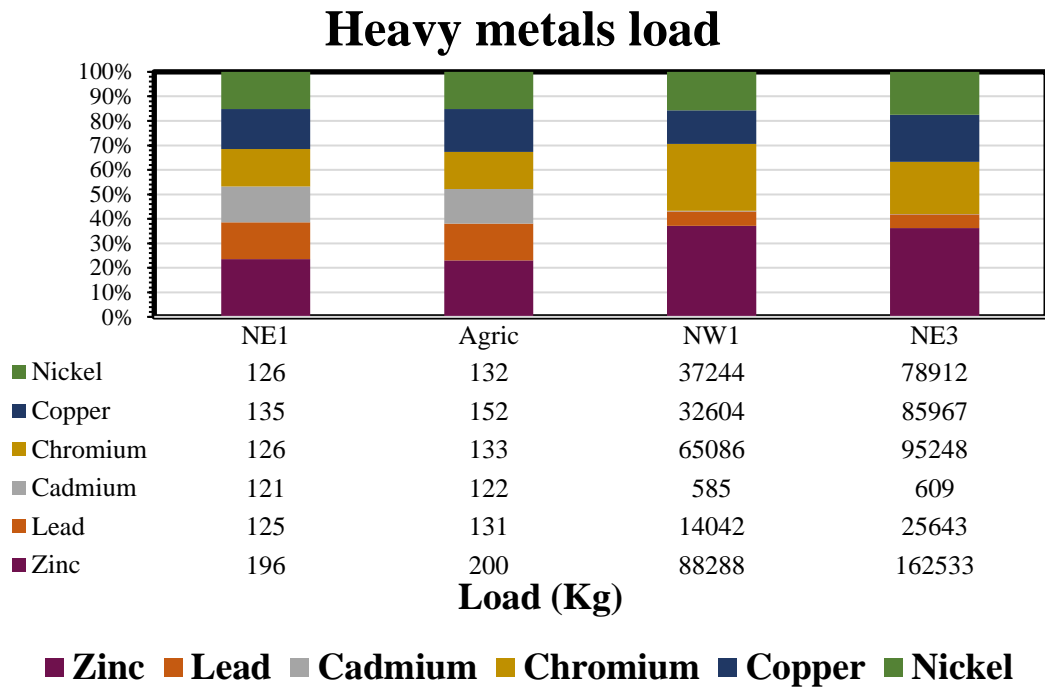


Figure 25: Heavy Metals load at Brusdalsvatnet. Gage 1.

Heavy metals load

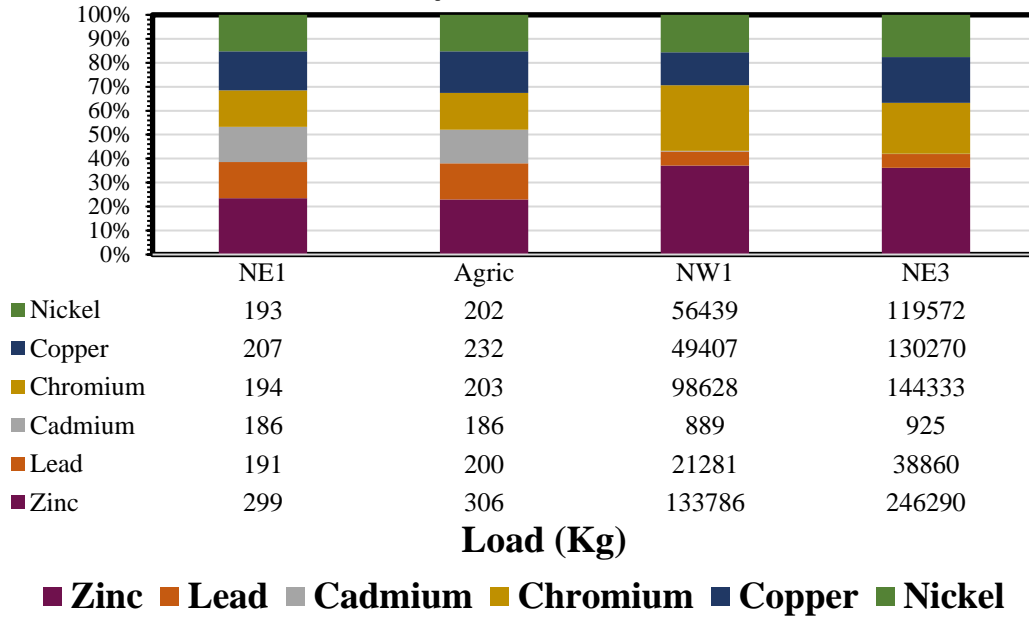


Figure 26: Heavy Metals load at Brusdalsvatnet. Gage 2.

Heavy metals Load

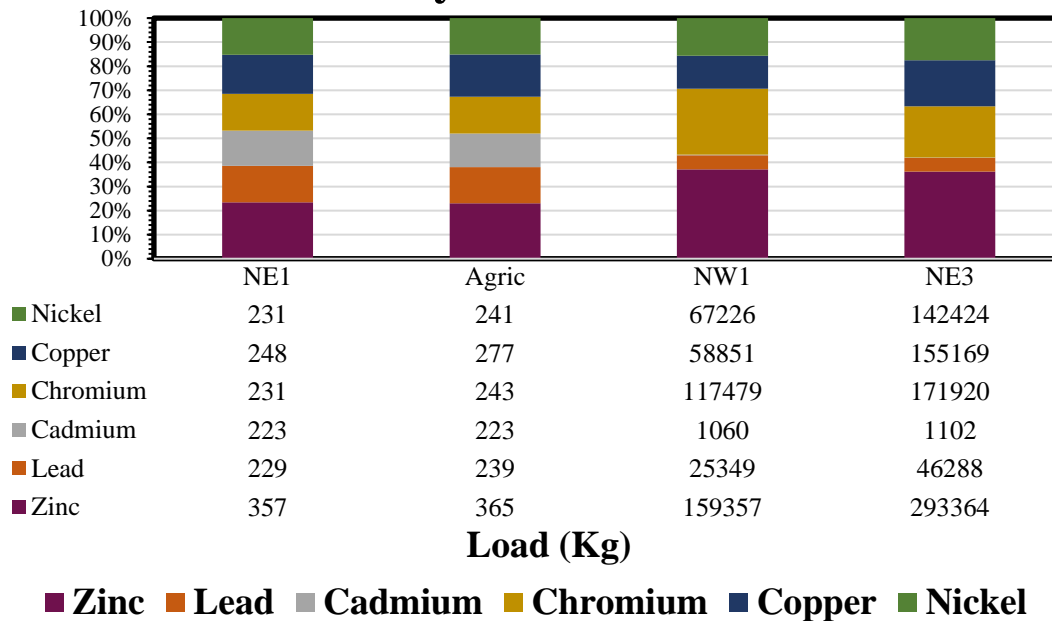


Figure 27: Heavy Metals load at Brusdalsvatnet. Gage 3.

Continuing with the trend presented by the results of SWMM, Figures 28 and 29 show that the water samples NE1 and Agric exhibit a proportional increase in pollutants load in each rainfall scenario (Gage 1, Gage 2, and Gage 3). According to the results, Gage 3 is the future rainfall scenario with the largest impact on pollutant loading, with Zinc being the pollutant with the highest washoff accumulation. On the other hand, Lead, Cadmium, Chromium, Copper, and Nickel exhibit similar loadings, even though their initial site sample values vary widely.

Rainfall-runoff-washoff interaction at system level

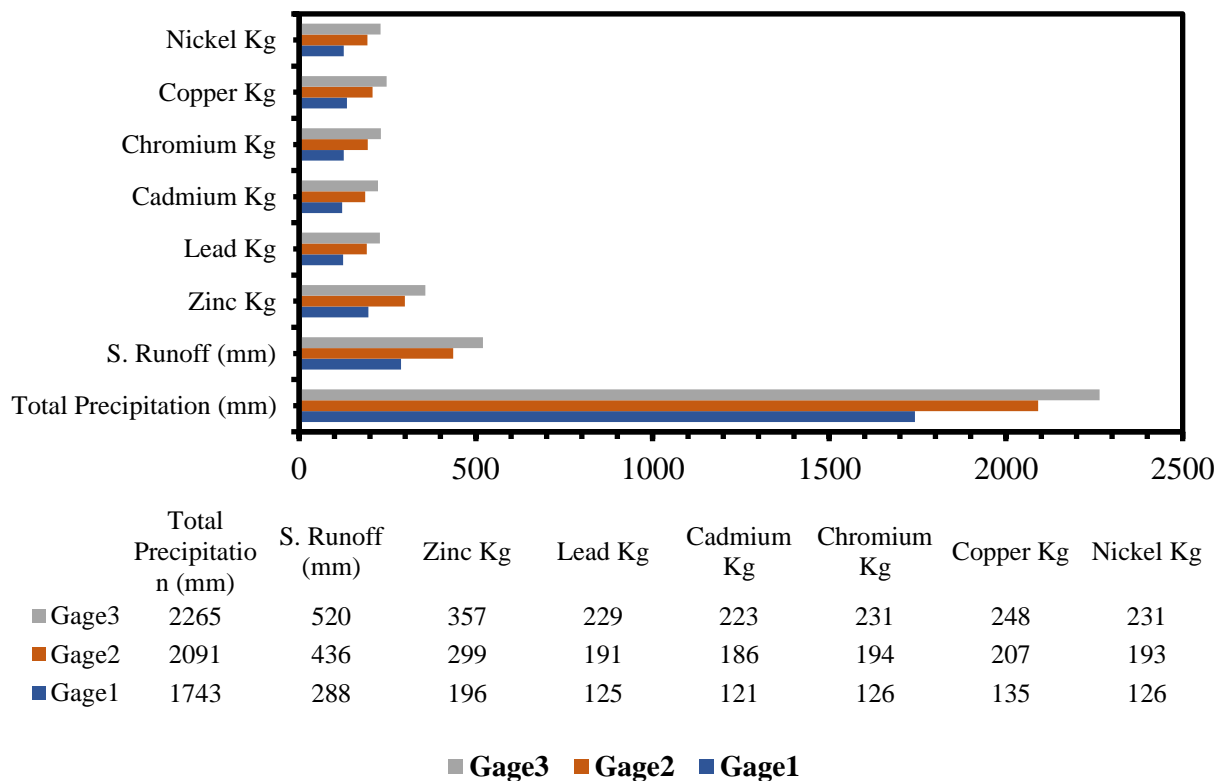


Figure 28: Impact of future rainfall scenarios on runoff volume and heavy metals load. Site NE1.

Rainfall-runoff-washoff interaction at system level

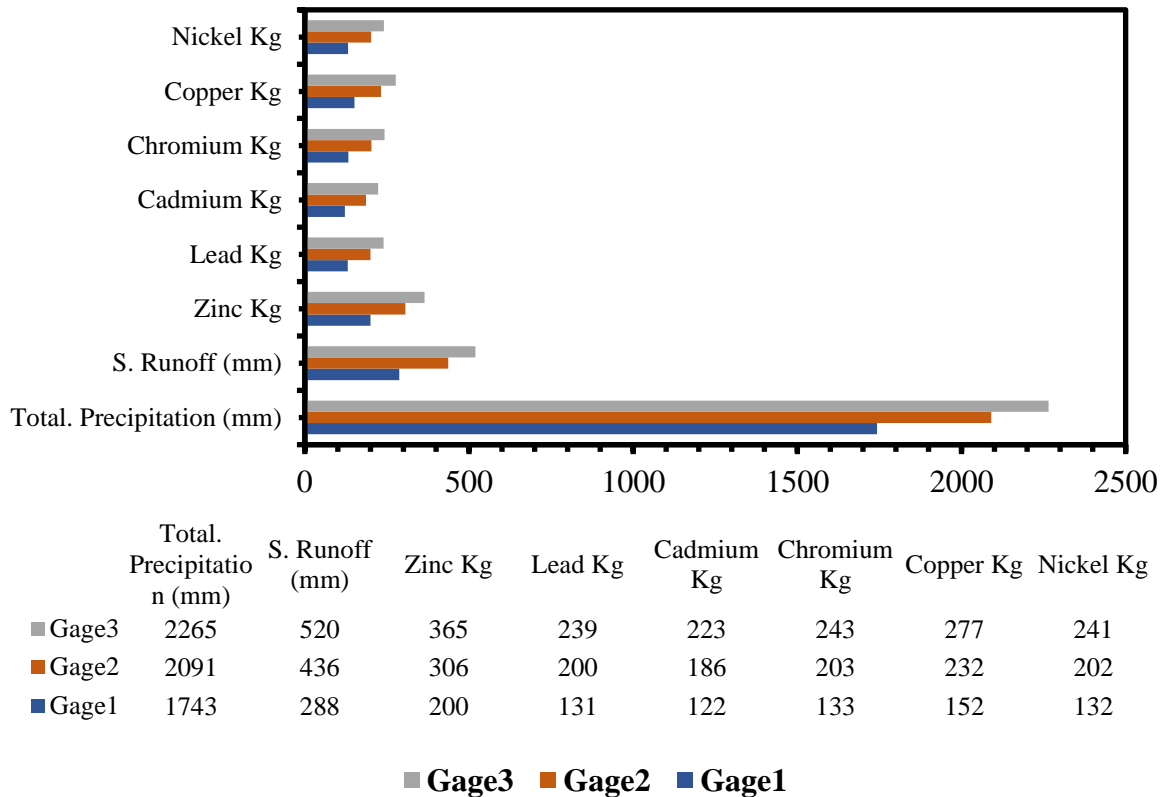


Figure 29: Impact of future rainfall scenarios on runoff volume and heavy metals load. Site Agric.

On the other hand, Figure 30 and Figure 31 demonstrate that there is much more variation in pollutant loading in soil samples, both at NW1 and NE3. The results of the NW1 system reveal that Zinc and Chromium have the highest loadings in Gage 1, Gage 2, and Gage 3, while Nickel, Copper, and Lead exhibit intermediate values. Similarly, Cadmium has the lowest pollutant loading value, and all loading values at NW1 are proportional to their initial site samples.

Rainfall-runoff-washoff interaction at system Level

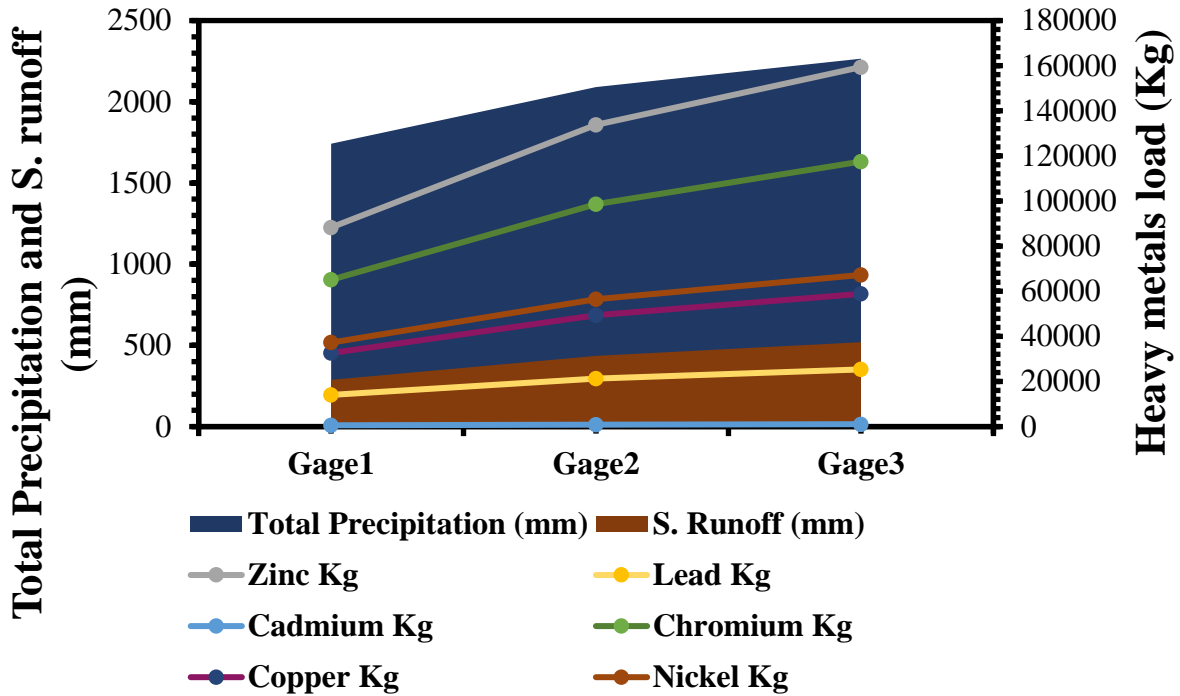


Figure 30: Impact of future rainfall scenarios on runoff volume and heavy metals load. Site NW1.

Regarding the results of the system at NE3, Figure 31 shows a wide variation in pollutant loading, with Zinc having the highest accumulation value. Additionally, Chromium, Copper, and Nickel present intermediate accumulation values that are very close to each other, differing from the results at NW1. It is also important to note that the loading of Cadmium from soil samples in Figure 31 appears insignificant compared to other pollutants at NE3. However, if this value is compared to the Cadmium loading from water samples, it appears to be much higher than any of the loading values of water samples.

Rainfall-runoff-washoff interaction at system Level

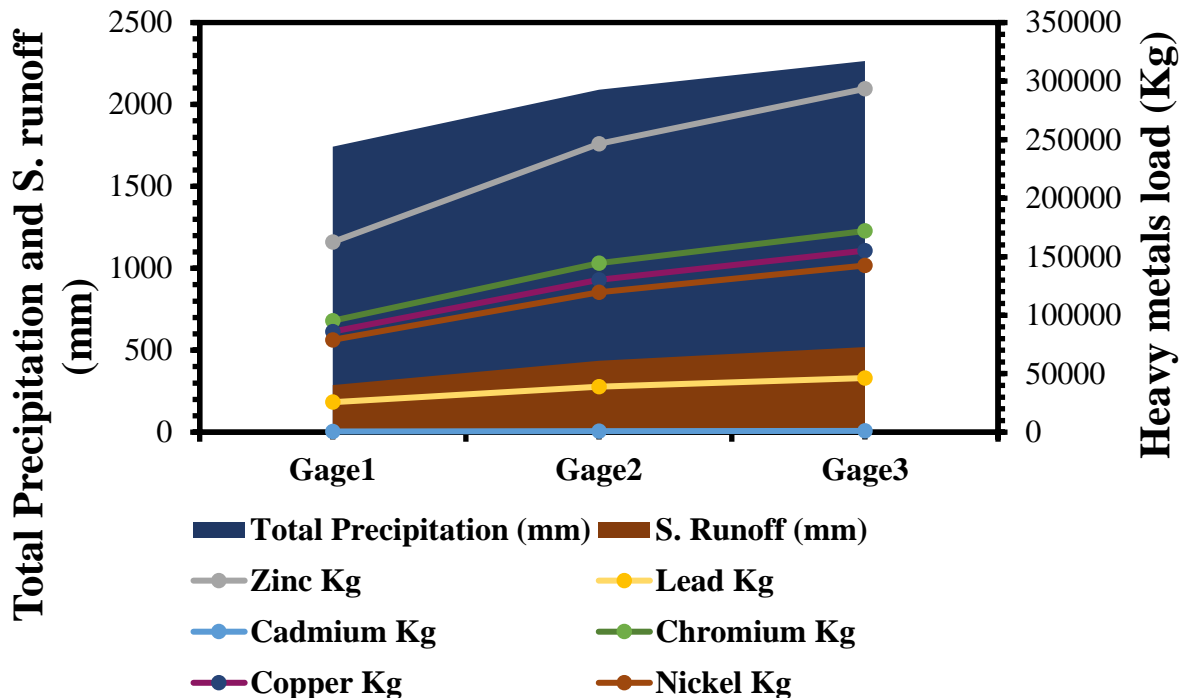


Figure 31: Impact of future rainfall scenarios on runoff volume and heavy metals load. Site NE3.

According to the results of SWMM, Zinc has the highest loading values among heavy metals due to runoff transport. In order to assess the impact of total runoff volume on Zinc loading, the average volume-weighted mean concentration will be calculated as follows: Total subcatchment load / Runoff volume. This value will be called the Site Mean Concentration index, which will be used to assess the relationship between Total runoff volume and Zinc load at the subcatchments of Brusdalsvatnet, accounting for present and future rainfall scenarios (Tuomela et al., 2019, p. 721).

According to the Site Mean Concentration index shown in Figure 32, Figure 33, and Figure 34, there is a close relationship between Total Runoff and Zinc Load at the subcatchments of Brusdalsvatnet. The trend line in Figure 32 shows that, in most subcatchments, the volume of runoff is closely related to Zinc loading. However, subcatchment S15 is an outlier, as the Zinc loading is high, but the runoff volume is low. Lastly, the results of future rainfall scenarios Gage 2 and Gage 3 presented in Figure 33 and Figure 34 show similar values, with an SMC value of 0.09, which is also an outlier.

Total Runoff-Zinc load relationship

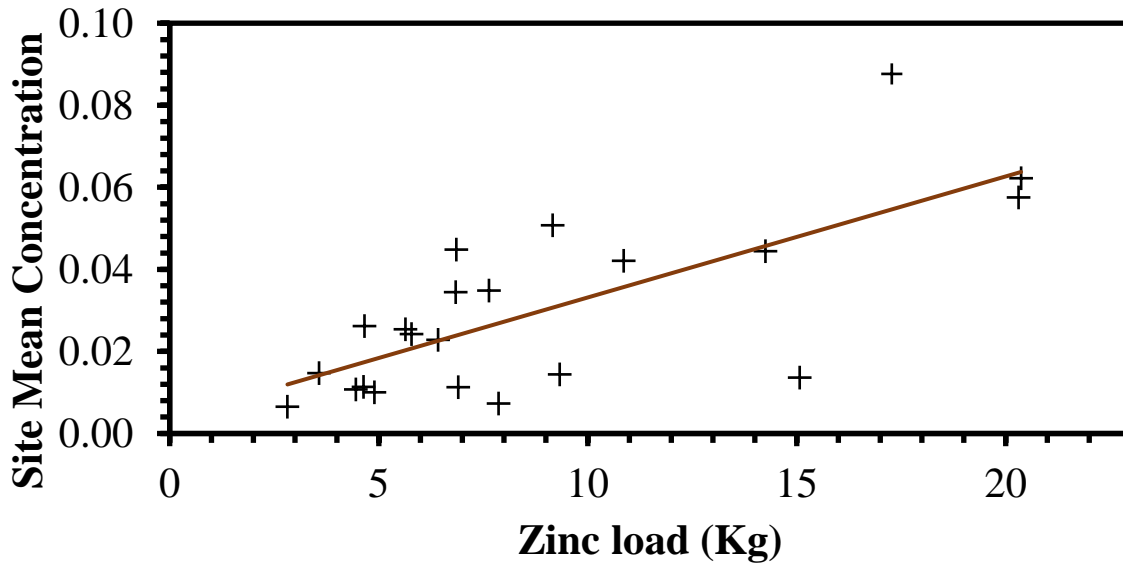


Figure 32: Index of Zinc concentration at the subcatchments of Brudalsvatnet. Gage 1.

Total Runoff-Zinc load relationship

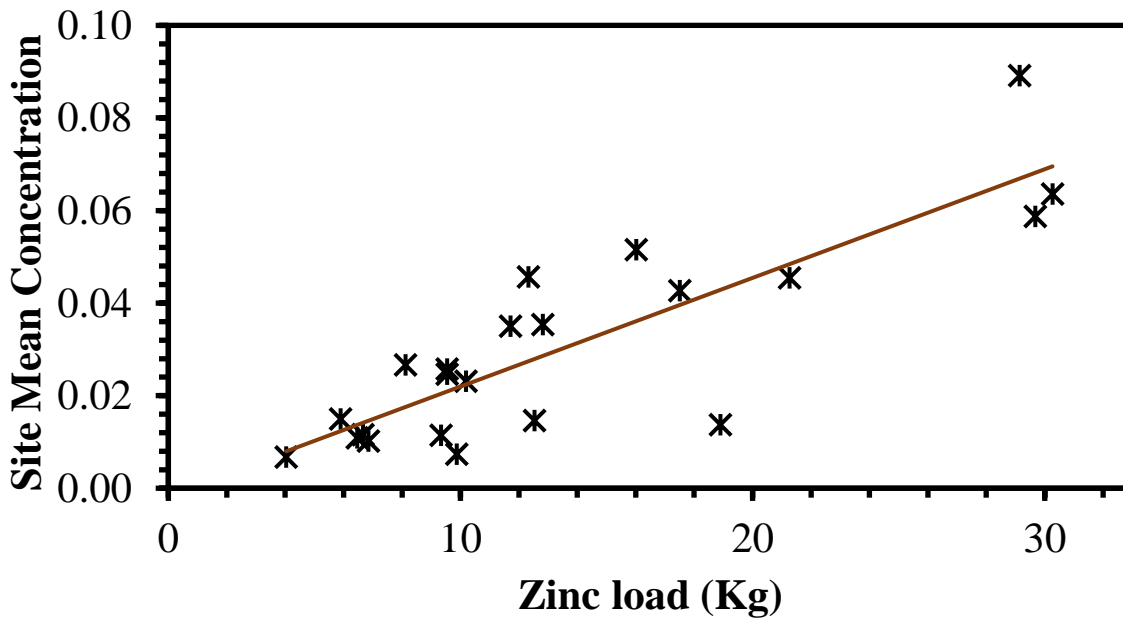


Figure 33: Index of Zinc concentration at the subcatchments of Brudalsvatnet. Gage 2.

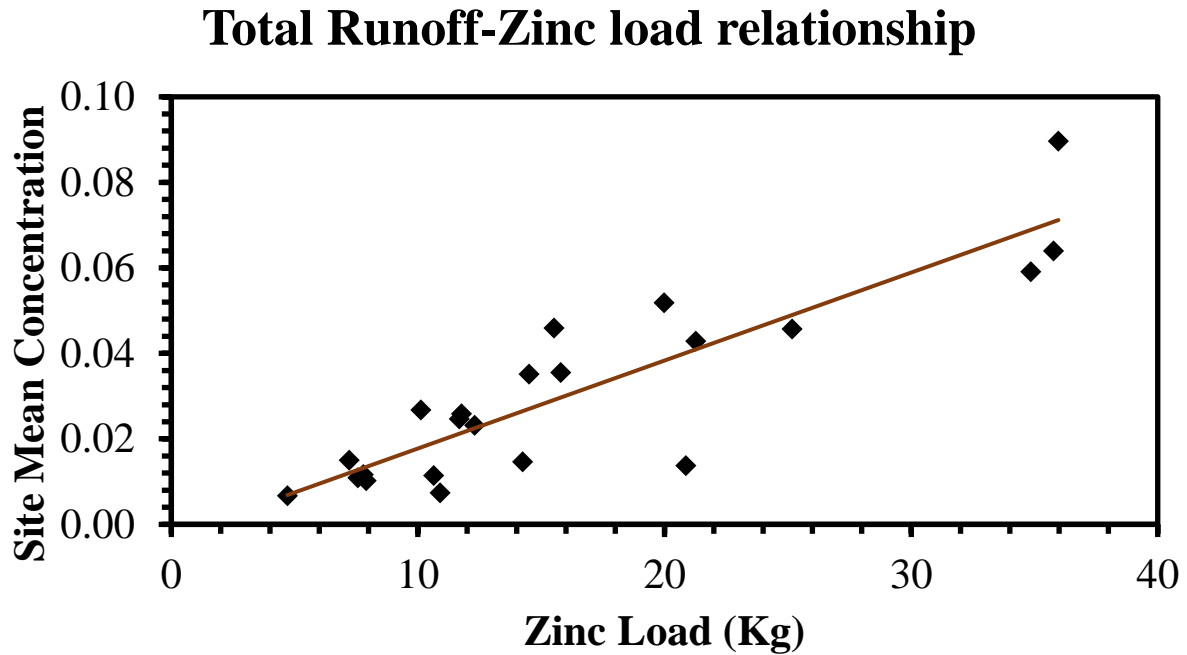


Figure 34: Index of Zinc concentration at the subcatchments of Brusdalsvatnet. Gage 3.

5.5.1 Relationships and trends

As part of the SWMM results, several trends and relationships were identified. It is essential to mention that some interactions, relationships, and trends were shown earlier in this section. As such, the following graphs highlight the main trends found. Figure 35 confirms the close relationship between runoff volume and % impervious surfaces in all 22 subcatchments, indicating that area imperviousness and infiltration are the primary factors affecting runoff generation at Brusdalsvatnet.

Total Runoff- Impervious surface interaction

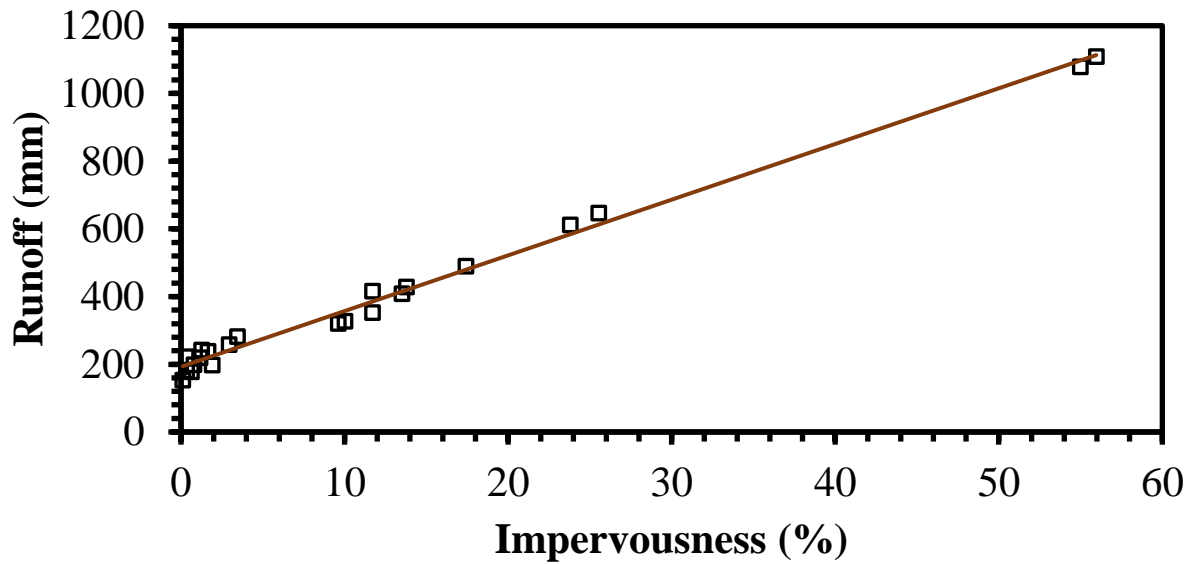


Figure 35: Total Runoff volume-% impervious surface relationship. Gage 1.

Furthermore, the Site Mean Concentration Index applied in this study is represented in Figure 36 as a stacked graph. The graph shows the trend in runoff volume and Zinc loading through all the subcatchments, accounting for Gage 1, Gage 2, and Gage 3. This trend confirms that higher runoff volume and longer dry periods lead to higher pollutant loads.

SMC Trend at Brusdalsvatnet

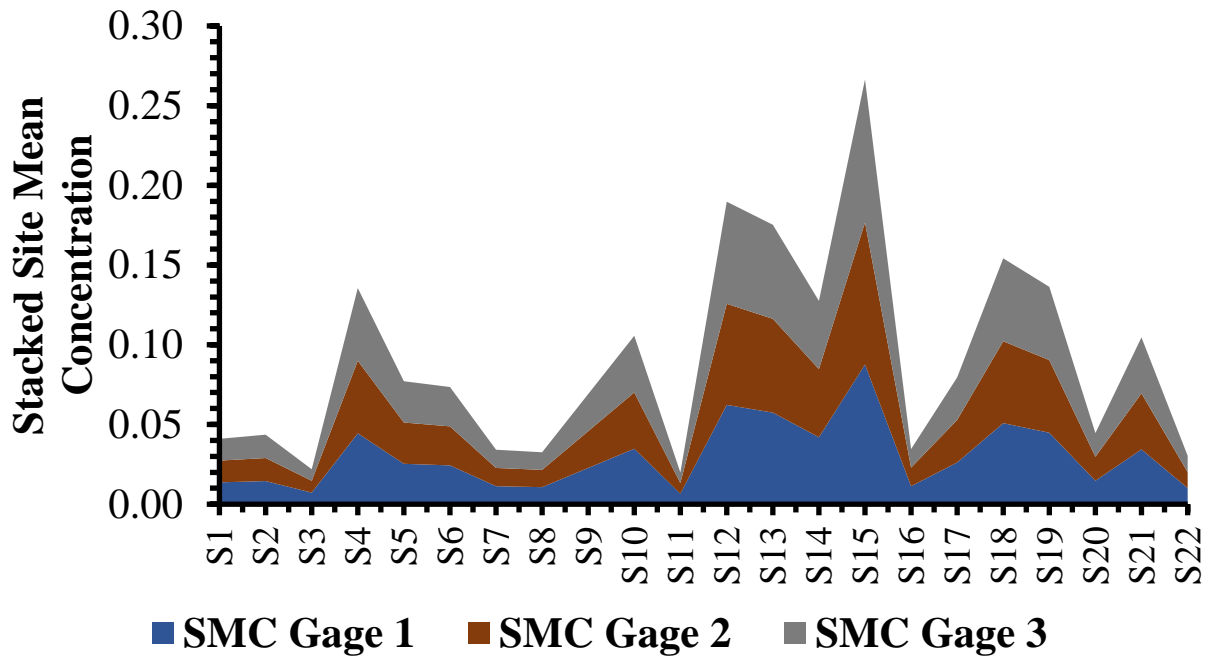


Figure 36: Runoff volume-Zinc loading trend. Gage 1, Gage 2 and Gage 3.

6. Discussion

In this section, we will discuss the geospatial map and its reliability in displaying the runoff pathways at Brusdalsvatnet, as well as the effectiveness of the tool in processing and displaying different input data. Additionally, we will examine the rainfall-runoff and runoff-washoff interactions.

6.1 Geo-spatial map at Brusdalsvatnet

The geospatial map at Brusdalsvatnet was computed using ArcGIS Pro. While the software has high accuracy, the reliability of the outcomes depends on the quality of the input dataset. In this case, the input dataset included the Pour point and DTM of Ålesund municipality, which has a 1m x 1m spatial resolution and was provided by Høydedata.no. The high-resolution input data ensures a high-quality output, but it is important to set the parameters correctly, such as correspondent tools, coordinate system, and transformations, if necessary.

The main goal of creating the Geospatial map was to identify the pathways the runoff can take on its way to the lake and gain insight into the paths that pollutants could follow. While the map provides some insight into runoff pathways, it is not as detailed as the pathways obtained through SWAT. However, due to the large study area, using SWAT for watershed delineation would have overwhelmed the data's processing and analysis. Therefore, ArcGIS Pro was chosen to delineate the watershed, as the results from ModelBuilder were deemed to be the best for displaying the entire delineated watershed. It is important to note that the accuracy and reliability of the map depend on the quality of the input dataset and the correct parameter settings, such as the correspondent tools, coordinate system, and transformations if necessary.

6.2 Runoff Flow Calculator Geo-spatial tool

ModelBuilder was utilized to compute the Runoff Flow Calculator Geo-spatial tool, where the DTM and Pour point served as the only inputs for the tool, making it accessible and user-friendly. However, it is crucial to set parameters such as the Expression of flow Accumulation correctly to display only the relevant data. Moreover, the Pour point location must be assessed correctly to obtain reliable results, and it should be placed at the lowest point of the study area. Nevertheless, other factors such as the natural course of water, channels that divert the flow of water, urbanization, and the research objectives were taken into consideration when placing the Pour point in this study. Lastly, since the Runoff Flow Calculator Geo-spatial tool uses the tool divide to account for infiltration, the outcomes of the tool may have low accuracy. To represent infiltration, Divide was used, which is a coarse way, and therefore, the results may be affected.

6.3 Precipitation-Runoff relationship

Rainfall data for the period from 01.01.2021 to 31.12.2021 was obtained from MET Norway. The analysis of the model simulation indicates high reliability in terms of both quality and quantity for present and future rainfall scenarios. It is important to note that developing a reliable model is essential for obtaining high-quality data.

The results of SWMM presented in Figure 17 Section 5.5 shows a close relationship between rainfall volume and total runoff volume. Furthermore, these results have similarities with related studies about the subject (Beldring et al., 2008; NCDEQ, 2017; Nie et al., 2009). The results of this study are mainly focused on Gage 3, the worst-case scenario, because it allows effective preventive and corrective measures, even in extreme situations. Moreover, it is a recommendation

of the Norwegian government. Table 9 shows a 4% increase in runoff volume from the period 2011-2040 to 2041-2070, while the increment from 2041-2070 to 2071-2100 is only 2%. It is impossible to provide a definitive explanation for the factors that led to this difference in runoff volume. However, it is plausible that parameters such as landuse, infiltration, and slope, which were taken into account in this study, may have contributed to these results.

According to the results presented in Table 10, subcatchments 1, 2, 3, and 7 showed the highest runoff coefficient values in the study area, indicating that these subcatchments have poor infiltration capacity. This study suggests that the main factors contributing to these results were impervious surfaces resulting from urbanization, including Highway E-39, as well as steep terrain gradients. Subcatchment S1, which is located close to the city center, had the highest impervious surface value at 60%. Similarly, subcatchments S2 and S3, which are located near the city and traversed by Highway E-39, had impervious surface values of 26% and 55%, respectively. Subcatchment S7, located in a developed area and also traversed by Highway E-39, had a high impervious surface value due to its small extension. It is important to note that Highway E-39 is not the only road that traverses the Brusdalsvatnet catchment in the study area.

Table 10 shows the extent of the impact that area imperviousness has on model results. Parameters such as Total Infiltration, Total runoff, and Impervious runoff are closely aligned with the value of impervious surface, whereas slope, which is the second most important factor, presents a lower impact on the results. It is important to mention that the infiltration rate plays a crucial role in determining the runoff volume. Therefore, in this study, its values are closely related to the applied model method, Horton, and impervious surfaces. However, it is worth noting that the impervious surfaces' computation using ArcGIS Pro does not separate roads such as Bregnevegen and Brusdalsvegen but presents the values of impervious surfaces as a whole. This thesis mainly focused on Highway E-39, but other factors, such as landuse and terrain gradient, were also considered. According to Table 10, subcatchments 1, 2, 3, and 7 showed the runoff coefficient highest values of the study area, indicating poor infiltration capacity due to impervious surfaces derived from urbanized areas and Highway E-39.

Figure 19 illustrates that S1 and S3 have the highest impervious surface values, and the results are highly accurate due to the 0.0001-meter resolution of the landuse raster provided by Georange.no. In addition, visual analysis was conducted to confirm the reliability of the results, and it was found

that the total residential impervious surface was accurately considered for all factors within the developed area. However, the fact that the surface area of Highway E-39 was not separated from the residential impervious surface values made it challenging to calculate the volume of runoff coming from the highway. In order to determine the specific value of runoff volume from Highway E-39, it was delineated in ArcGIS Pro and added to the provided landuse data. Nonetheless, delineating the highway separately does not ensure accurate results since factors such as temperature, evaporation, and sewer network were not considered during computation. Moreover, Bregnevegen road traverses S1 was not delineated separately, making it impossible to determine its impact on runoff volume. Additionally, Brusdalsvegen is a crucial road that passes through all subcatchments except S22, and its impact was not considered separately.

Figure 20 shows the slope values of the subcatchments at Brusdalsvatnet. According to the results obtained by the SWAT model, S9 and S14 have the highest slope values, with 38.1% and 43.1%, respectively. While analyzing the impact of slope on impervious surface, there is no clear correlation between impervious surface, slope, and runoff volume. This may be due to the fact that the slope results obtained from ArcGIS Pro differ from those obtained from the SWAT model, despite the use of the same DTM. Therefore, a closer inspection was required both on the field and through photos of the study area in order to assess and select the most appropriate value for each subcatchment. Hence, the results may have some degree of uncertainty.

Analyzing the impact of Highway E-39 on the runoff volume within the Brusdalsvatnet catchment is one of the main objectives of this study. Accordingly, the volume of runoff coming from the highway was calculated, and the results presented in Table 11 show the relationships between impervious surface of developed areas, impervious surface derived from Highway E-39, pervious surfaces of undeveloped areas, total runoff, and specific runoff volume derived from Highway E-39. The contribution of Highway E-39 to the total percent of the impervious area varies from 0% at S22 to 1.7% at S11. As shown in Figure 37, in general, the values of % imperviousness derived from Highway E-39 do not seem to represent a significant contribution to the total impervious area. However, subcatchments S5, S17, S18, S19, S20, and S21 are the exception as they are located in underdeveloped areas, and thus Highway E-39 has a significant contribution to % imperviousness in these areas. It is important to highlight that not all road networks are considered in this graph.

Contribution of Highway E-39 to developed areas

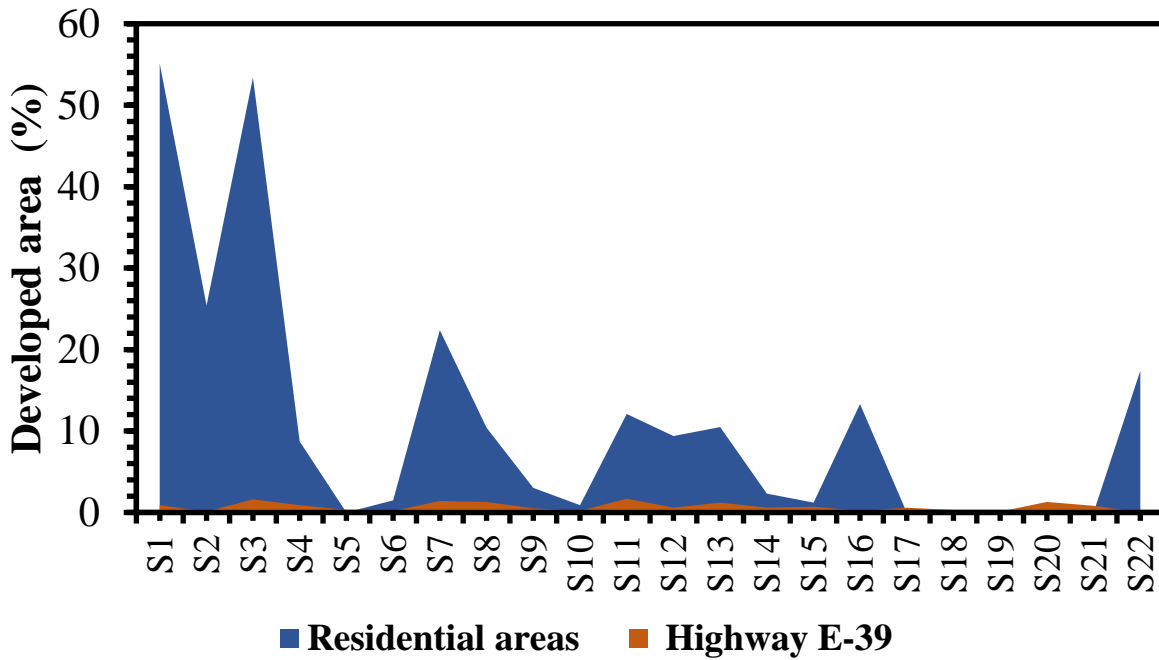


Figure 37: Impact of Highway E-39 on Impervious surfaces increase. Gage 3.

Additionally, Figure 38 shows the contribution of Highway E-39 to the runoff volume. Its contribution to the total runoff volume does not seem to be significant. However, if the entire road network is considered, there could be a larger contribution to the runoff volume.

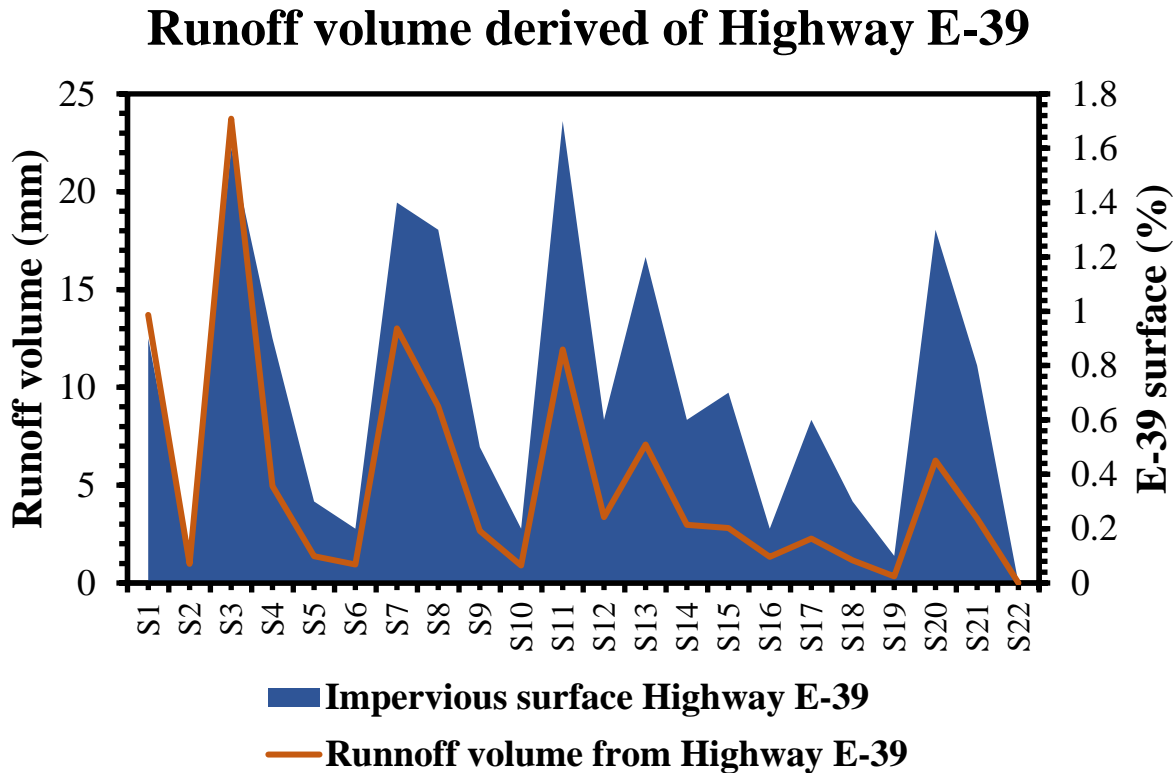


Figure 38: Impact of Highway E-39 on the total Runoff at Brusdalsvatnet. Gage 3.

Finally, as shown in Figure 22, there is a close interaction between impervious surface and total runoff. However, values may vary depending on the rainfall scenario that is taken into consideration. More details about total runoff volume can be found in Appendix C, D, and E, which contain the subcatchment runoff summary related to Gage 1, Gage 2, and Gage 3, respectively. Moreover, Figure 21 confirms the influence that impervious surfaces have on total runoff, as the subcatchments with the highest impervious surface values are the ones that present the highest runoff volumes. Nevertheless, it is important to note that in order to improve the accuracy of the results, factors such as temperature, sewer network, evaporation, and soil should be considered in future model simulations to achieve more accurate results.

6.4 Runoff-Washoff relationship

The results of the rainfall-runoff analysis were conclusive, demonstrating a close relationship between these two phenomena. Subsequently, the simulation continued by running the water quality process model to determine the pollutant load generated by the runoff volume.

According to the SWMM manual standards, the water quality process model executed has high reliability, as the results show very low values of uncertainty regarding the mass balance. The results indicate a close relationship between runoff volume and pollutant loading, as depicted in Figure 24. Impervious surface is the factor that was closely aligned with this interaction, as shown in Figure 23. However, it is important to note that in some subcatchments, such as S22 with an impervious surface of 17.4%, the value could be higher if the road Brusdalsvegen was considered, leading to a different washoff load. The subcatchments with the highest total runoff values are S1, S2, S3, and S7. The three main drivers leading to these results are impervious surfaces, infiltration, and slope. Moreover, even though the relationship between Total runoff and impervious surface is close, as shown in Figure 22, this is not the case for slope, as depicted in Figure 39.

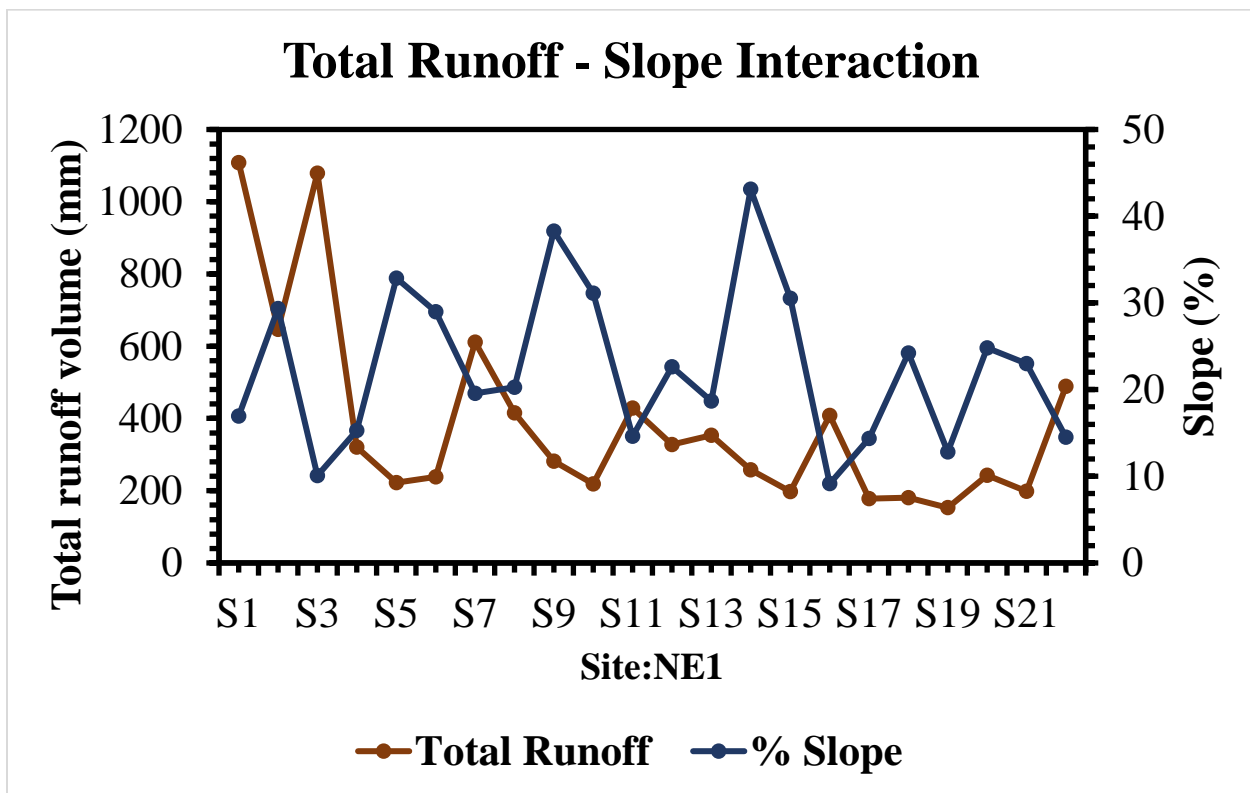


Figure 39: The impact of Slope on Total runoff volume. Gage 1

Although the slope is a factor that usually plays an important role in runoff and washoff, the results presented in Figure 39 show no close interaction between slope and runoff. Hence, this will be reflected in the washoff loading. Additionally, it is important to mention that S9 and S14 are the

subcatchments that present the highest slope values, whereas their impervious surface percentages are low at 4% and 3%, respectively. Besides, the landuse in subcatchments S9 and S14 is mainly composed of forest, with 92% and 85%, respectively. This could explain why their heavy metal loads are relatively low, given that these areas are well-vegetated with high infiltration capacity.

On the other hand, factors that led to a wide variation in pollutant loading are the sample type, area extension, and rainfall scenario projection. The values of the water samples were much lower than the soil samples, which could be due to the buildup rate of the soil samples. Hence, more washoff and thus, higher pollutant loading is generated. Likewise, area extension was crucial regarding the high zinc loading results at subcatchment 15. Even though the runoff volume was low, the loading of Zinc was high, which can be explained by the area extension. This subcatchment is the largest in the study area, with 110.6 ha. Similarly, the last factor is the projected rainfall scenario, given that the results of the three rainfall scenarios registered a continuous increment of pollutant loading for the period from 2021 to 2100. Moreover, the increase in Zinc loading for the period from 2021 to 2065-2100 was 45%.

Lastly, according to the results of SWMM, there will be an increase of up to 45% in pollutant loading, confirming climate change's impact on the environment. The equation is simple: more precipitation equals runoff volume increase, consequently leading to more pollutant transport and thus higher pollutant loading reaching water bodies. Accordingly, it represents a threat to human health, hence the importance of taking preventive and mitigating measures to break the circle.

7. Conclusion and further work

This section will summarize this thesis, its main findings, confirmation or rejection of theories, and conclusions. Additionally, suggestions will be provided for future research related to the aim of this study. Likewise, the conclusion will answer the goal and research questions.

7.1 Conclusion

In this thesis, our aim was to investigate the relationship between climate change and extreme precipitation, with a focus on analyzing links, behaviors, correlations, and interactions between precipitation, runoff, impervious surfaces, and pollutant loads at Brusdalsvatnet. To achieve this, we utilized several tools such as Geospatial analysis by ArcGIS Pro, ModelBuilder workflow, Soil and water assessment tool (SWAT), Storm Water Management Model (SWMM), and sample data.

The dataset used in this study comprised the Ålesund Municipality's entire data, which provided the foundation to configure future rainfall scenarios starting from the 2021 rainfall data. Future rainfall regimes were based on RCP 8.5 emission scenarios, representing the worst-case scenarios with a 20% and 30% rainfall increase during the periods 2031-2060 and 2060-2100, respectively. We developed three models - Gage 1 for 2021, Gage 2 for 2031-2060, and Gage 3 for 2060-2100. The models were then computed, and their results were analyzed. We tested the reliability of the model and found it to be solid and dependable.

As shown in Table 8 in Section 5.3, the Runoff Quantity Continuity analysis and Quality Routing Continuity analysis had good accuracy in Gage 1, Gage 2, and Gage 3, with an insignificant mass balance continuity error. The Runoff continuity error is -0.002% and the Routing continuity error is 0.000%. These percentages are within SWMM's manual standards, which suggest a maximum recommendable threshold of 10%. However, since the model does not consider factors such as temperature, soil, evaporation, evapotranspiration, and sewer networks, its accuracy and reliability are solely dependent on the data used. Therefore, it is essential to emphasize that introducing some of the mentioned factors could significantly improve the model's robustness.

In Section 1.2, we presented the overall aim as follows:

Goal: *This work aims to model runoff from Highway (E-39) located in the catchment of Brusdalsvatnet in Ålesund, accounting for present and future rainfall regimes.*

To answer the goal and research questions, the following conclusions were drawn: (i) There is a close relationship between rainfall intensity and runoff volume in the catchment of Brusdalsvatnet. The main factor driving the increase in runoff volume is impervious surfaces, which are potentiated by low infiltration capacity and steep gradients. (ii) Highway E-39 plays an important role in transporting pollutants through the runoff pathways to Brusdalsvatnet. (iii) A close interaction was observed between runoff volume and pollutant washoff loading, with factors related to climate change, such as antecedent dry periods and short-duration, high-intensity rainfall, potentiating the pollutants loading. (iv) The amount of pollutant loading increases significantly in subcatchments close to developed areas. (v) Future rainfall regimes are projected to result in a noticeable increase in runoff volume and pollutant loading.

7.2 Further work

The results of the model projection were capable of answering the thesis's goal. However, the robustness of the model and the reliability of the results can be improved in future research. The dataset used in this thesis lacks relevant information, such as soil, temperature, evaporation, sewer network, and wind speed. Therefore, adding these inputs to the dataset can significantly improve the results. Additionally, the sample data were not available in each subcatchment, which may have affected the computation of pollutant loading. To reduce the margin of error, it is recommended to gather several samples in each subcatchment.

Furthermore, working with different engines, as shown in this study, presents some challenges. For example, deep knowledge and expertise are required for each program, and the methods used in the programs may differ, potentially leading to different results for the same computation. Therefore, it is important to consider these factors in the early stages of the study if considering replicating this research.

References

- Åge Brabrand, T. B. o. H. P. (2013). *Status for fisk, bunndyr og elvemusling i Brusdalsvassdraget* (Rapportnr. 26). <https://www.nhm.uio.no/forskning/ressurser/publikasjoner/nhm-rapporter/nhm-rapport-026-2013.pdf>
- ArcGisPro. (2022a). *Dissolve (Data Management)*. <https://pro.arcgis.com/en/pro-app/latest/tool-reference/data-management/dissolve.htm>
- ArcGisPro. (2022b). *Fill (Spatial Analyst)*. https://pro.arcgis.com/en/pro-app/latest/tool-reference/spatial-analyst/fill.htm#L_
- ArcGisPro. (2022c). *Model parameters*. <https://pro.arcgis.com/en/pro-app/latest/help/analysis/geoprocessing/modelbuilder/model-parameters.htm>
- ArcGisPro. (2022d). *What is ModelBuilder?* <https://pro.arcgis.com/en/pro-app/latest/help/analysis/geoprocessing/modelbuilder/what-is-modelbuilder-.htm>
- Arias, P. A., N. Bellouin, E. Coppola, R.G. Jones, G. Krinner, J. Marotzke, V. Naik, M.D. Palmer, G.-K. Plattner, J. Rogelj, , M. Rojas, J. S., T. Storelvmo, P.W. Thorne, B. Trewin, K. Achuta Rao, B. Adhikary, R.P. Allan, K. Armour, G. Bala, , R. Barimalala, S. B., J.G. Canadell, C. Cassou, A. Cherchi, W. Collins, W.D. Collins, S.L. Connors, S. Corti, F. Cruz, , F.J. Dentener, C. D., A. Di Luca, A. Diongue Niang, F.J. Doblas-Reyes, A. Dosio, H. Douville, F. Engelbrecht, , V. Eyring, E. F., P. Forster, B. Fox-Kemper, J.S. Fuglestvedt, J.C. Fyfe, N.P. Gillett, L. Goldfarb, I. Gorodetskaya, , J.M. Gutierrez, R. H., E. Hawkins, H.T. Hewitt, P. Hope, A.S. Islam, C. Jones, D.S. Kaufman, R.E. Kopp, Y. Kosaka, , J. Kossin, S. K., J.-Y. Lee, J. Li, T. Mauritsen, T.K. Maycock, M. Meinshausen, S.-K. Min, P.M.S. Monteiro, , T. Ngo-Duc, F. O., I. Pinto, A. Pirani, K. Raghavan, R. Ranasinghe, A.C. Ruane, L. Ruiz, J.-B. Sallée, B.H. Samset, , S. Sathyendranath, S. I. S., A.A. Sörensson, S. Szopa, I. Takayabu, A.-M. Tréguier, B. van den Hurk, R. Vautard, , K. von Schuckmann, S. Z., X. Zhang, and K. Zickfeld, 2021: Technical Summary. In *Climate Change 2021: The , Intergovernmental, P. S. B. C. o. W. G. I. t. t. S. A. R. o. t., Panel on Climate Change [Masson-Delmotte, V., P. Zhai, A. Pirani, S.L. Connors, C. Péan, S. Berger, N. Caud, Y. Chen, , L. Goldfarb, M. I. G., M. Huang, K. Leitzell, E. Lonnoy, J.B.R. Matthews, T.K. Maycock, T. Waterfield, O. Yelekçi, R. Yu, , & and B. Zhou (eds.)]. Cambridge University Press, C., United Kingdom and New York, NY, USA, pp. 33–144. . (2021). *Technical Summary*. <https://www.ipcc.ch/report/ar6/wg1/chapter/technical-summary/>*
- B, M. (2020). Worst Climate Scenario RCP 8.5 Appears to be the Most Realistic. <https://www.sciencetimes.com/articles/26786/20200807/worst-climate-scenario-rcp-8-5-appears-realistic.htm>
- Baek, S.-S., Ligaray, M., Pyo, J., Park, J.-P., Kang, J.-H., Pachepsky, Y., Chun, J. A., & Cho, K. H. (2020). A novel water quality module of the SWMM model for assessing low impact development (LID) in urban watersheds. *Journal of hydrology (Amsterdam)*, 586, 124886. <https://doi.org/10.1016/j.jhydrol.2020.124886>
- Beldring, S., Engen-Skaugen, T., Førland, E. J., & Roald, L. A. (2008). Climate change impacts on hydrological processes in Norway based on two methods for transferring regional climate model results to meteorological station sites. *Tellus A: Dynamic Meteorology and Oceanography*, 60(3), 439-450. <https://doi.org/10.1111/j.1600-0870.2007.00306.x>
- Board, S. W. R. C. (2011). *The Clean Water Team Guidance Compendium for Watershed Monitoring and Assessment*.

- . <https://doi.org/5.1.3> FS-(RC)
- Chowdhury, S., Mazumder, M. A. J., Al-Attas, O., & Husain, T. (2016). Heavy metals in drinking water: Occurrences, implications, and future needs in developing countries. *Science of The Total Environment*, 569-570, 476-488. <https://doi.org/https://doi.org/10.1016/j.scitotenv.2016.06.166>
- Dell, T., Razzaghmanesh, M., Sharvelle, S., & Arabi, M. (2021). Development and Application of a SWMM-Based Simulation Model for Municipal Scale Hydrologic Assessments. *Water (Basel)*, 13(12), 1644. <https://doi.org/10.3390/w13121644>
- Enhuus, E. E., Riise, G., Rohrlack, T., & Heier, L. S. (2020). Mobilisering av tungmetaller i rensedammer med høy tilførsel av veisaltavrenning : studert i Fossbekken rensedam langs E18. In *Mobilization of heavy metals in stormwater ponds with substantial road salt runoff : researched in Fossbekken stormwater pond along E18, Norway*: Norwegian University of Life Sciences, Ås.
- Esri. (2023). *GIS for innovative stormwater management*. <https://www.esri.com/en-us/industries/water-utilities/segments/stormwater>
- Eva Solbjørg Flo Heggem, H. M., Jostein Frydenlund. (2019). AR50. <https://www.nibio.no/tema/jord/arealressurser/ar50>
- Folkesson, L., Bækken, T., Brenčič, M., Dawson, A., François, D., Kuřimská, P., Leitão, T., Ličbínský, R., & Vojtěšek, M. (2009). Sources and Fate of Water Contaminants in Roads. In A. Dawson (Ed.), *Water in Road Structures: Movement, Drainage and Effects* (pp. 107-146). Springer Netherlands. https://doi.org/10.1007/978-1-4020-8562-8_6
- Greipsland, I. (2016). Climate change and potential effects on agriculture and water quality. *VOL 2 4*. https://nibio.brage.unit.no/nibio-xmlui/bitstream/handle/11250/2387555/NIBIO_POP_2016_2_20.pdf?sequence=3
- Gülbaz, S. (2012). *Impact of Land Use/Cover Changes on Water Quality and Quantity in a Calibrated Hydrodynamic Model*.
- Hanssen-Bauer, I., Førland, E., Haddeland, I., Hisdal, H., Lawrence, D., Mayer, S., Nesje, A., Nilsen, J. E., Sandven, S., Sandø, A., Sorteberg, A., & Ådlandsvik, B. (2017). *Climate in Norway 2100*.
- I. Hanssen-Bauer, E. J. F., I. Haddeland, H. Hisdal, S. Mayer, A. Nesje, J.E.Ø. Nilsen, S. , & Sandven, A. B. S., A. Sorteberg og B. Ådlandsvik. (2015). *Klima i Norge 2100* (2/2015).
- IPCC, T. I. P. o. C. C. (2023). *The IPCC was created to provide policymakers with regular scientific assessments on climate change, its implications and potential future risks, as well as to put forward adaptation and mitigation options*. <https://www.ipcc.ch/>
- Kazemi Garajeh, M., Salmani, B., Zare Naghadehi, S., Valipoori Goodarzi, H., & Khasraei, A. (2023). An integrated approach of remote sensing and geospatial analysis for modeling and predicting the impacts of climate change on food security. *Scientific Reports*, 13(1), 1057. <https://doi.org/10.1038/s41598-023-28244-5>
- Lewis A. Rossman, M. A. S. (2022). *Storm Water Management Model User's Manual Version 5.2*.
- Literacy, C. (2015). *Emission Scenarios* https://www.youtube.com/watch?v=TOEEbHn_es4
- Ma, Y., McGree, J., Liu, A., Deilami, K., Egodawatta, P., & Goonetilleke, A. (2017). Catchment scale assessment of risk posed by traffic generated heavy metals and polycyclic aromatic hydrocarbons. *Ecotoxicol Environ Saf*, 144, 593-600. <https://doi.org/10.1016/j.ecoenv.2017.06.073>

- Mapscaping. (2022). Stormwater Management & GIS. <https://mapscaping.com/stormwater-management-gis/>
- Martin, C. J., Hodges, C., & Dymond, R. (2019). Geospatial Method to Map Potential Risk of Stormwater Thermal Pollution. *Journal of the American Water Resources Association*, 55(2), 511-522. <https://doi.org/10.1111/1752-1688.12732>
- Meehl, G., Stocker, T., Collins, W., Friedlingstein, P., Gaye, A. T., Jm, G., Kitoh, A., Knutti, R., Jm, M., Noda, A., Raper, S., Watterson, I. G., Weaver, A., & Zhao, Z.-C. (2007). Global Climate Projections. In (Vol. 3495).
- Mohammed, H., Tveten, A.-K., & Seidu, R. (2019). Modelling the impact of climate change on flow and E. coli concentration in the catchment of an ungauged drinking water source in Norway. *Journal of Hydrology*, 573, 676-687. <https://doi.org/https://doi.org/10.1016/j.jhydrol.2019.04.021>
- NCCS, N. C. f. C. S. (2022). *Snø, sludd og regn i fremtiden*. <https://klimaservicesenter.no/kss/framskr/sno-sludd-regn#more>
- NCDEQ. (2017). Stormwater Calculations. <https://files.nc.gov/ncdeq/Energy%20Mineral%20and%20Land%20Resources/Stormwater/BMP%20Manual/B%20%20Stormwater%20Calculations.pdf>
- Nebojsa Nakicenovic, J. A., Gerald Davis, Bert de Vries, Joergen Fenhann, , Stuart Gaffin, K. G., Amulf Griibler, Tae Yong Jung, Tom Kram, , Emilio Lebre La Rovere, L. M., Shunsuke Mori, Tsuneyuki Morita, , William Pepper, H. P., Lynn Price, Keywan Riahi, Alexander Roehrl, , Hans-Holger Rogner, A. S., Michael Schlesinger, Priyadarshi Shukla, , & Steven Smith, R. S., Sascha van Rooijen, Nadejda Victor, Zhou Dadi. (2000). *Emissions Scenarios*.
- Nexus, T. C. D. (2021). *The RCP 8.5 Cheat: Debunking the IPCC's favorite climate-change forecast*. <https://www.youtube.com/watch?v=6SOEs0LzZCg>
- Nie, L., Lindholm, O., Lindholm, G., & Syversen, E. (2009). Impacts of climate change on urban drainage systems – a case study in Fredrikstad, Norway. *Urban Water Journal*, 6(4), 323-332. <https://doi.org/10.1080/15730620802600924>
- Nikel, D. (2019). *How Climate Change Is Going To Impact Norway*. <https://www.lifeinnorway.net/how-climate-change-is-going-to-impact-norway/>
- Norway, U. F. L. (2021). *Smart Water*. <https://www.unitedfuturelab.no/en/projects/smart-water/>
- Ortiz-Bobea, A., Ault, T. R., Carrillo, C. M., Chambers, R. G., & Lobell, D. B. (2021). Anthropogenic climate change has slowed global agricultural productivity growth. *Nature Climate Change*, 11(4), 306-312. <https://doi.org/10.1038/s41558-021-01000-1>
- Pickering, N. (1996). *Physics of climate: J. P. Peixoto and A. H. Oort*. New York, USA: American Institute of Physics, 1992. 520 pp. Price: US\$ 45.00 (paperback). ISBN 0 88318 712 4. *Agricultural Systems*, 51(2), 248-250. [https://doi.org/https://doi.org/10.1016/0308-521X\(96\)86772-2](https://doi.org/https://doi.org/10.1016/0308-521X(96)86772-2)
- Rutledge, K., McDaniel, M., Teng, S., Hall, H., Ramroop, T., Sprout, E., Hunt, J., Boudreau, D., & Costa, H. (2022). *Runoff* <https://education.nationalgeographic.org/resource/runoff/>
- S.L. NEITSCH, J. G. A., J.R. KINIRY, R. SRINIVASAN, J.R. WILLIAMS. (2000). *Soil and water assessment tool SWAT User's Manual*. In
- Seidu, R. (2021). *Concentration of heavy metals in the catchment Brusdalsvatnet*.
- Senduran, C., Gunes, K., Topaloglu, D., Dede, O. H., Masi, F., & Kucukosmanoglu, O. A. (2018). Mitigation and treatment of pollutants from railway and highway runoff by

- pocket wetland system; A case study. *Chemosphere*, 204, 335-343.
<https://doi.org/10.1016/j.chemosphere.2018.03.201>
- Skaland, R. G., Herrador, B. G., Hisdal, H., Hygen, H. O., Hyllestad, S., Lund, V., White, R., Wong, W. K., & Nygård, K. (2022). Impacts of climate change on drinking water quality in Norway. *Journal of Water and Health*, 20(3), 539-550.
<https://doi.org/10.2166/wh.2022.264>
- Smith, A. H., Hopenhayn-Rich, C., Bates, M. N., Goeden, H. M., Hertz-Picciotto, I., Duggan, H. M., Wood, R., Kosnett, M. J., & Smith, M. T. (1992). Cancer Risks from Arsenic in Drinking Water. *Environmental Health Perspectives*, 97, 259-267.
<https://doi.org/10.2307/3431362>
- Steinberg, M. (2017). *Drinking water in Norway*. <https://www.fhi.no/en/op/hin/infectious-diseases/drinking-water-in-Norway/>
- SWAT. (2012). SWAT Input Data. <https://swat.tamu.edu/docs/>
- SWAT. (2023). The Soil & Water Assessment Tool (SWAT).
<https://swat.tamu.edu/#:~:text=The%20Soil%20%26%20Water%20Assessment%20Tool%20is%20a,land%20use%2C%20land%20management%20practices%2C%20and%20climate%20change.>
- Sytsma, A., Bell, C., Eisenstein, W., Hogue, T., & Kondolf, G. M. (2020). A geospatial approach for estimating hydrological connectivity of impervious surfaces. *Journal of hydrology (Amsterdam)*, 591, 125545. <https://doi.org/10.1016/j.jhydrol.2020.125545>
- Trenberth, Jones, P., Ambenje, Bojariu, R., Easterling, D., Tank, K., Parker, D., Rahimzadeh, F., Renwick, J., Rusticucci, M., Soden, B., Zhai, P., & Folland, C. (2007). Observations: Surface and Atmospheric Climate Change. In (pp. 235-336).
- Tuomela, C., Sillanpää, N., & Koivusalo, H. (2019). Assessment of stormwater pollutant loads and source area contributions with storm water management model (SWMM). *J Environ Manage*, 233, 719-727. <https://doi.org/10.1016/j.jenvman.2018.12.061>
- University, T. A. M. (2023). SWAT+. <https://swat.tamu.edu/software/plus/>
- Wang, Y., Gao, C., Yang, S., Ji, G., & Liu, X. (2016). Research on Runoff Pollution Characteristics and Countermeasures at Sensitive Highway Sites. *Polish journal of environmental studies*, 25(2), 813-821. <https://doi.org/10.15244/pjoes/61245>
- Wijesiri, B., Bandala, E., Liu, A., & Goonetilleke, A. (2020). A framework for stormwater quality modelling under the effects of climate change to enhance reuse. *Sustainability (Basel, Switzerland)*, 12(24), 1-12. <https://doi.org/10.3390/su122410463>
- Xiao, Y., Zhang, T.-t., Liang, D., & Chen, J. M. (2016). Experimental study of water and dissolved pollutant runoffs on impervious surfaces. *Journal of Hydrodynamics, Ser. B*, 28(1), 162-165. [https://doi.org/https://doi.org/10.1016/S1001-6058\(16\)60617-0](https://doi.org/https://doi.org/10.1016/S1001-6058(16)60617-0)
- Yan, M., Nie, H., Wang, W., Huang, Y., & Wang, J. (2018). Occurrence and Toxicological Risk Assessment of Polycyclic Aromatic Hydrocarbons and Heavy Metals in Drinking Water Resources of Southern China. *International Journal of Environmental Research and Public Health*, 15(7), 1422. <https://www.mdpi.com/1660-4601/15/7/1422>

Appendix A

Classification levels of heavy metals in water from Miljø-direktoratet 2020.

| Parameters | Class I | Class II | Class III | Class IV | Class V |
|------------|------------------|------------|---------------|-----------|---------------------|
| | Background level | Good Level | Moderat Level | Bad Level | Extremely Bad Level |
| Metals | µg/L | µg/L | µg/L | µg/L | µg/L |
| Lead | 0 - 0.02 | 0.02 – 1.2 | 1.2 - 14 | 14 - 57 | >85 |
| Cadmium | 0 - 0.003 | Fotnote 1 | Fotnote 2 | Fotnote 3 | >57 |
| Copper | 0 - 0.3 | 0.3 - 7.8 | | 7.8-15.6 | Footnote 3 |
| Chromium | 0 - 0.1 | 0.1 – 3.4 | | | >3.4 |
| Nickel | 0 - 0.5 | 0.5 - 4 | 4 - 34 | 34 - 67 | >67 |
| Zinc | 0 – 1.5 | 1.5 - 11 | | 11 - 60 | >60 |

1) Class II Cd values depending on the hardness of the water: ≤ 0.08 (<40 mg CaCO₃ / L); 0.08 (40 - <50 mg CaCO₃ / L); 0.09 (50 - <100 mg CaCO₃ / L); 0.15 (100 - <200 mg CaCO₃ / L); 0.25 (≥ 200 mg CaCO₃ / L).

2) Class III Cd values depending on the hardness of the water: ≤ 0.45 (<40 mg CaCO₃ / L); 0.45 (40 - <50 mg CaCO₃ / L); 0.60 (50 - <100 mg CaCO₃ / L); 0.9 (100 - <200 mg CaCO₃ / L); 1.5 (≥ 200 mg CaCO₃ / L).

3) Class IV Cd values depending on the hardness of the water: ≤ 4.5 (<40 mg CaCO₃ / L); 4.5 (40 - <50 mg CaCO₃ / L); 6.0 (50 - <100 mg CaCO₃ / L); 9.0 (100 - <200 mg CaCO₃ / L); 15 (≥ 200 mg CaCO₃ / L). Values above belong to class V.

Appendix B

Classification levels of heavy metals in soil from Miljø-direktoratet 2020.

| Parameters | Class I | Class II | Class III | Class IV | Class V |
|------------|------------------|------------|---------------|--------------|---------------------|
| | Background level | Good Level | Moderat Level | Bad Level | Extremely Bad Level |
| Metals | mg/kg TS | mg/kg TS | mg/kg TS | mg/kg TS | mg/kg TS |
| Lead | 0 - 25 | 25 - 150 | 150 - 1480 | 1480 - 2000 | 2000 - 25000 |
| Cadmium | 0 - 0.2 | 0.2 - 2.5 | 2.5 - 16 | 16 - 157 | >157 |
| Copper | 0 - 20 | 20 - 84 | | 84 - 147 | >147 |
| Chromium | 0 - 60 | 60 - 620 | 620 - 6000 | 6000 - 15500 | 15500 - 25000 |
| Nickel | 0 - 30 | 30 - 42 | 42 - 271 | 271 - 533 | >533 |
| Zinc | 0 - 90 | 90 - 139 | 139 - 750 | 750 - 6690 | >6690 |

Appendix C: Subcatchment Runoff Summary Gage 1

 Subcatchment Runoff Summary

| Subcatchment | Total Precip mm | Total Runon mm | Total Evap mm | Total Infil mm | Imperv Runoff mm | Perv Runoff mm | Total Runoff mm | Total Runoff 10 ⁶ ltr | Peak Runoff CMS | Runoff Coeff |
|--------------|--------------------|-------------------|------------------|-------------------|---------------------|-------------------|--------------------|-------------------------------------|--------------------|--------------|
| S1 | 1742.50 | 0.00 | 0.00 | 634.01 | 974.93 | 133.39 | 1108.32 | 140.42 | 0.22 | 0.636 |
| S2 | 1742.50 | 0.00 | 0.00 | 1095.53 | 445.05 | 201.95 | 647.00 | 101.84 | 0.27 | 0.371 |
| S3 | 1742.50 | 0.00 | 0.00 | 663.64 | 957.75 | 120.84 | 1078.59 | 73.67 | 0.09 | 0.619 |
| S4 | 1742.50 | 0.00 | 0.00 | 1422.06 | 167.29 | 153.17 | 320.46 | 173.69 | 0.39 | 0.184 |
| S5 | 1742.50 | 0.00 | 0.00 | 1520.48 | 5.42 | 216.62 | 222.04 | 70.94 | 0.07 | 0.127 |
| S6 | 1742.50 | 0.00 | 0.00 | 1504.16 | 28.78 | 209.59 | 238.37 | 72.27 | 0.14 | 0.137 |
| S7 | 1742.50 | 0.00 | 0.00 | 1131.29 | 414.73 | 196.50 | 611.23 | 76.16 | 0.19 | 0.351 |
| S8 | 1742.50 | 0.00 | 0.00 | 1326.78 | 203.91 | 211.85 | 415.76 | 52.76 | 0.16 | 0.239 |
| S9 | 1742.50 | 0.00 | 0.00 | 1460.93 | 60.16 | 221.45 | 281.61 | 79.27 | 0.21 | 0.162 |
| S10 | 1742.50 | 0.00 | 0.00 | 1523.46 | 20.06 | 199.00 | 219.06 | 95.86 | 0.16 | 0.126 |
| S11 | 1742.50 | 0.00 | 0.00 | 1313.85 | 240.14 | 188.54 | 428.68 | 33.14 | 0.09 | 0.246 |
| S12 | 1742.50 | 0.00 | 0.00 | 1415.11 | 174.61 | 152.79 | 327.40 | 247.65 | 0.55 | 0.188 |
| S13 | 1742.50 | 0.00 | 0.00 | 1389.39 | 203.88 | 149.24 | 353.12 | 244.50 | 0.51 | 0.203 |
| S14 | 1742.50 | 0.00 | 0.00 | 1484.42 | 51.09 | 207.02 | 258.11 | 134.84 | 0.33 | 0.148 |
| S15 | 1742.50 | 0.00 | 0.00 | 1545.30 | 33.13 | 164.09 | 197.22 | 218.09 | 0.45 | 0.113 |
| S16 | 1742.50 | 0.00 | 0.00 | 1334.33 | 235.43 | 172.76 | 408.19 | 54.82 | 0.13 | 0.234 |
| S17 | 1742.50 | 0.00 | 0.00 | 1564.36 | 10.99 | 167.17 | 178.16 | 59.13 | 0.07 | 0.102 |
| S18 | 1742.50 | 0.00 | 0.00 | 1561.94 | 5.76 | 174.81 | 180.58 | 116.24 | 0.11 | 0.104 |
| S19 | 1742.50 | 0.00 | 0.00 | 1589.65 | 1.75 | 151.11 | 152.86 | 87.62 | 0.07 | 0.088 |
| S20 | 1742.50 | 0.00 | 0.00 | 1500.23 | 21.99 | 220.31 | 242.30 | 44.61 | 0.08 | 0.139 |
| S21 | 1742.50 | 0.00 | 0.00 | 1544.13 | 13.61 | 184.79 | 198.40 | 86.32 | 0.12 | 0.114 |
| S22 | 1742.50 | 0.00 | 0.00 | 1253.27 | 303.56 | 185.69 | 489.25 | 56.31 | 0.14 | 0.281 |

Appendix D: Subcatchment Runoff Summary Gage 2

 Subcatchment Runoff Summary

| Subcatchment | Total Precip mm | Total Runon mm | Total Evap mm | Total Infil mm | Imperv Runoff mm | Perv Runoff mm | Total Runoff mm | Total Runoff 10 ⁶ ltr | Peak Runoff CMS | Runoff Coeff |
|--------------|-----------------|----------------|---------------|----------------|------------------|----------------|-----------------|----------------------------------|-----------------|--------------|
| S1 | 2091.00 | 0.00 | 0.00 | 709.18 | 1169.96 | 211.71 | 1381.66 | 175.06 | 0.29 | 0.661 |
| S2 | 2091.00 | 0.00 | 0.00 | 1230.09 | 534.08 | 326.88 | 860.96 | 135.52 | 0.36 | 0.412 |
| S3 | 2091.00 | 0.00 | 0.00 | 745.41 | 1149.36 | 195.96 | 1345.32 | 91.89 | 0.12 | 0.643 |
| S4 | 2091.00 | 0.00 | 0.00 | 1622.72 | 200.76 | 267.54 | 468.30 | 253.82 | 0.52 | 0.224 |
| S5 | 2091.00 | 0.00 | 0.00 | 1720.25 | 6.51 | 364.28 | 370.78 | 118.47 | 0.11 | 0.177 |
| S6 | 2091.00 | 0.00 | 0.00 | 1702.93 | 34.54 | 353.57 | 388.12 | 117.68 | 0.19 | 0.186 |
| S7 | 2091.00 | 0.00 | 0.00 | 1272.45 | 497.69 | 320.90 | 818.59 | 102.00 | 0.26 | 0.391 |
| S8 | 2091.00 | 0.00 | 0.00 | 1496.05 | 244.70 | 350.31 | 595.01 | 75.51 | 0.21 | 0.285 |
| S9 | 2091.00 | 0.00 | 0.00 | 1649.79 | 72.19 | 369.08 | 441.27 | 124.22 | 0.28 | 0.211 |
| S10 | 2091.00 | 0.00 | 0.00 | 1728.19 | 24.08 | 338.77 | 362.85 | 158.78 | 0.21 | 0.174 |
| S11 | 2091.00 | 0.00 | 0.00 | 1486.14 | 288.17 | 316.72 | 604.90 | 46.76 | 0.12 | 0.289 |
| S12 | 2091.00 | 0.00 | 0.00 | 1614.67 | 209.54 | 266.81 | 476.35 | 360.31 | 0.74 | 0.228 |
| S13 | 2091.00 | 0.00 | 0.00 | 1585.57 | 244.66 | 260.78 | 505.44 | 349.97 | 0.68 | 0.242 |
| S14 | 2091.00 | 0.00 | 0.00 | 1680.54 | 61.31 | 349.20 | 410.51 | 214.45 | 0.44 | 0.196 |
| S15 | 2091.00 | 0.00 | 0.00 | 1764.12 | 39.76 | 287.15 | 326.91 | 361.50 | 0.59 | 0.156 |
| S16 | 2091.00 | 0.00 | 0.00 | 1514.05 | 282.52 | 294.46 | 576.98 | 77.49 | 0.17 | 0.276 |
| S17 | 2091.00 | 0.00 | 0.00 | 1785.54 | 13.19 | 292.29 | 305.49 | 101.39 | 0.10 | 0.146 |
| S18 | 2091.00 | 0.00 | 0.00 | 1780.26 | 6.92 | 303.85 | 310.77 | 200.04 | 0.16 | 0.149 |
| S19 | 2091.00 | 0.00 | 0.00 | 1820.82 | 2.10 | 268.09 | 270.19 | 154.88 | 0.11 | 0.129 |
| S20 | 2091.00 | 0.00 | 0.00 | 1695.79 | 26.39 | 368.87 | 395.26 | 72.77 | 0.10 | 0.189 |
| S21 | 2091.00 | 0.00 | 0.00 | 1756.34 | 16.34 | 318.35 | 334.69 | 145.62 | 0.16 | 0.160 |
| S22 | 2091.00 | 0.00 | 0.00 | 1416.25 | 364.28 | 310.50 | 674.78 | 77.67 | 0.19 | 0.323 |

Appendix E: Subcatchment Runoff Summary Gage 3

 Subcatchment Runoff Summary

| Subcatchment | Total Precip mm | Total Runon mm | Total Evap mm | Total Infil mm | Imperv Runoff mm | Perv Runoff mm | Total Runoff mm | Total Runoff 10^6 ltr | Peak Runoff CMS | Runoff Coeff |
|--------------|--------------------|-------------------|------------------|-------------------|---------------------|-------------------|--------------------|--------------------------|--------------------|--------------|
| S1 | 2265.25 | 0.00 | 0.00 | 742.47 | 1267.47 | 255.15 | 1522.63 | 192.92 | 0.33 | 0.672 |
| S2 | 2265.25 | 0.00 | 0.00 | 1289.92 | 578.59 | 396.79 | 975.38 | 153.53 | 0.41 | 0.431 |
| S3 | 2265.25 | 0.00 | 0.00 | 781.82 | 1245.17 | 238.00 | 1483.17 | 101.30 | 0.14 | 0.655 |
| S4 | 2265.25 | 0.00 | 0.00 | 1714.31 | 217.49 | 333.48 | 550.97 | 298.63 | 0.59 | 0.243 |
| S5 | 2265.25 | 0.00 | 0.00 | 1809.98 | 7.05 | 448.25 | 455.30 | 145.47 | 0.13 | 0.201 |
| S6 | 2265.25 | 0.00 | 0.00 | 1792.34 | 37.42 | 435.54 | 472.96 | 143.40 | 0.21 | 0.209 |
| S7 | 2265.25 | 0.00 | 0.00 | 1335.50 | 539.17 | 390.63 | 929.80 | 115.85 | 0.30 | 0.410 |
| S8 | 2265.25 | 0.00 | 0.00 | 1571.68 | 265.10 | 428.54 | 693.64 | 88.02 | 0.24 | 0.306 |
| S9 | 2265.25 | 0.00 | 0.00 | 1734.31 | 78.21 | 452.80 | 531.01 | 149.48 | 0.31 | 0.234 |
| S10 | 2265.25 | 0.00 | 0.00 | 1820.62 | 26.09 | 418.58 | 444.67 | 194.59 | 0.24 | 0.196 |
| S11 | 2265.25 | 0.00 | 0.00 | 1563.50 | 312.19 | 389.60 | 701.79 | 54.25 | 0.13 | 0.310 |
| S12 | 2265.25 | 0.00 | 0.00 | 1705.74 | 227.00 | 332.53 | 559.53 | 423.23 | 0.83 | 0.247 |
| S13 | 2265.25 | 0.00 | 0.00 | 1675.12 | 265.05 | 325.10 | 590.15 | 408.62 | 0.78 | 0.261 |
| S14 | 2265.25 | 0.00 | 0.00 | 1768.75 | 66.42 | 430.14 | 496.56 | 259.40 | 0.49 | 0.219 |
| S15 | 2265.25 | 0.00 | 0.00 | 1864.06 | 43.07 | 358.15 | 401.22 | 443.67 | 0.66 | 0.177 |
| S16 | 2265.25 | 0.00 | 0.00 | 1595.24 | 306.07 | 363.98 | 670.05 | 89.99 | 0.20 | 0.296 |
| S17 | 2265.25 | 0.00 | 0.00 | 1886.52 | 14.30 | 364.46 | 378.76 | 125.71 | 0.12 | 0.167 |
| S18 | 2265.25 | 0.00 | 0.00 | 1879.70 | 7.50 | 378.08 | 385.58 | 248.20 | 0.19 | 0.170 |
| S19 | 2265.25 | 0.00 | 0.00 | 1926.97 | 2.28 | 336.01 | 338.29 | 193.91 | 0.13 | 0.149 |
| S20 | 2265.25 | 0.00 | 0.00 | 1783.46 | 28.59 | 453.25 | 481.84 | 88.71 | 0.12 | 0.213 |
| S21 | 2265.25 | 0.00 | 0.00 | 1852.65 | 17.70 | 394.93 | 412.63 | 179.54 | 0.18 | 0.182 |
| S22 | 2265.25 | 0.00 | 0.00 | 1489.29 | 394.64 | 381.36 | 776.00 | 89.32 | 0.21 | 0.343 |